Robust H∞/ μ Control and Uncertainty Description of Mechatronic Systems

メタデータ	言語: eng
	出版者:
	公開日: 2017-10-05
	キーワード (Ja):
	キーワード (En):
	作成者:
	メールアドレス:
	所属:
URL	http://hdl.handle.net/2297/30579

Robust H_∞/μ Control and Uncertainty Description of Mechatronic Systems

Toru Namerikawa

October, 1996

(1)

博 士 論 文

メカトロニクスシステムの不確かさの記述と
ロバストH∞/μ制御に関する研究

金沢大学大学院自然科学研究科

滑川 徹

Contents

Acknowledgment

Chapter 1

Introduction

1.1 Background

The field of control engineering has developed over this century from its origins in the investigation of feedback amplifiers, into a broad discipline concerning various issues of modeling, dynamics, optimization and feedback control. On one side lie complex engineering problems, such as regulation in chemical processes, trajectory tracking for robot manipulators, stabilization of high performance aircraft and magnetic suspension systems, or dynamics of queueing systems. On the other side lie tools from virtually every mathematical discipline, from dynamical systems and differential geometry to stochastic processes and operator theory. In the middle of this, the task of the control theorist is to abstract a problem of significance in engineering, cast it in an appropriate mathematical setting, and derive a solution, by which is meant a practically computable method of evaluation of the problem at hand. This eclectic mix of disciplines has made control theory the home of people who have found it difficult to choose between the fascinating worlds of engineering and mathematics.

While engineers are mainly concerned with real-world problems, and mathematicians with the logical consistency of their abstractions, it is the job of those who attempt to apply mathematics to the real world to deal with the fundamental gaps between theory and practice, which reflect themselves in uncertainty about the behavior of a real system when one is given a mathematical prediction. This is particularly the case for control theory, which treats the question of feedback, a technique used by both natural and artificial systems to obtain reliability in spite of faulty predictions. A property of design feedback compensator will effectively reduce the sensitivity of the systems to certain sources of

uncertainty, but at the expense of increased sensitivity to order unmodeled effects, e.g., in another frequency band. Consequently, a theory of feedback must provide means to quantify these tradeoffs, which can only be achieved if in addition to a mathematical model, one utilizes some form of quantification of model uncertainty.

This thesis is concerned with the robust H_∞/μ control of real mechatronic systems from the point of view of the effect of uncertainty. The fundamental challenge in this area has been to refine as much as possible the uncertainty description in a model of a complex system, compatible with the possibility of a tractable evaluation of its effect. I describe a set of models and perform worst-case analysis by using H_∞/μ synthesis and analysis, and evaluate its effects by mechatronic experiments.

1.1.1 Control of Real Physical System

No mathematical system can exactly model a real physical system. For this reason we must be aware of how modeling errors might adversely affect the stability and performance of a control system. In the physical sciences, very accurate models in themselves are the objective. To obtain these physical laws, one often distills the phenomenon to its simplest form. In this context, uncertainty is interpreted in a narrow sense as referring to the limits in the predictive power of the best available models.

Models play a different role in engineering science; they are tools employed in analysis, simulation and design of complex, artificial systems. Consequently, models fidelity must be traded off with the complexity of the modeling process and the tractability of the resulting mathematical and computational problems. From this point of view the best model is the simplest summary of the main aspects of the physical system which are relevant to the engineering question at hand.

The issue of uncertainty is at the main theme of control engineering, since a feedback configuration can significantly affect the sensitivity of the system behavior to uncertainty at the component level. This is the main motivation for the construction of feedback systems, but also the main potential danger as unmodeled effects can. Consequently, to perform good designs, the control engineer must be furnished with rich descriptions of uncertainty and tools to assess their impact in a complex system.

It is very important and difficult to treat various models of plant uncertainty. H_∞/μ control has a good structure to treat uncertainty. In this paper robust stability, stability in the face of plant uncertainty, in studied using the small-gain theorem and Nyquist stability

criterion. Further robust performance, guaranteed tracking in the face of plant uncertainty is also discussed.

1.1.2 Uncertainty and Robustness

A fundamental problem in the design of control systems is to control accurately the outputs of a system(plant) whose dynamics contain significant uncertainties. For example, characteristic of magnetic force is so complex that analysis of this force is very difficult and no mathematical models can express the exact behavior of it. In the latest few decades there have been great advances in the theory for the design of robustly uncertainty-tolerant feedback control systems [9]. The problem in robust feedback control system design is to synthesize a control law which maintains system stability and performance and error signals to within pre-specified tolerances despite the effects of uncertainty of the system [11].

Uncertainty may take a lot of forms but among the most significant are

- Parametric Uncertainty

- Disturbance Signals

- Unmodeled Linear Dynamics

- Unmodeled Nonlinear Dynamics

Uncertainty in any form is no doubt the major issue in most control system designs. This motivates researchers to seek a quantitative measure for the size of the uncertainty, e.g., the H_2 and H_∞ norm, the real/complex structured singular value μ, and so on.

1.1.3 Previous Work

It is a few decades since H_∞/μ control theory has been studied extremely as a design tool [6] for the robust controlled system. H_∞/μ control theory provides a direct and reliable procedure for synthesizing controller which optimally satisfies the H_∞ norm/ structured singular value μ specifications. This method has an advantage to quantify the effects of unmodeled dynamics and to clarify the stability margin.

There are so many theoretical results and papers in robust control fields. Nowadays the most challenging issue is its application to real physical systems. Applications of H_∞ control to industry is now expected.

Many application papers have been published, but almost of them employ poor control problems and groundless generalized plants. Just a few papers focus on real uncertainties/perturbations.

Doyle and Balas applied H_∞/μ control theory to a flexible structure[5], and they introduced the large-scaled and complicated interconnection structures for the plant. Hyde and Glover also controlled a VSTOL by using H_∞ control law [29][30][31]. Steinbuch used μ-synthesis for control of a compact disc player [75].

In order to design a H_∞/μ control system, it is very important to choose suitable design parameters for each control problem and a plant. The problem is how to construct the generalized plant and how to select design parameters. In the previous research, even as the above papers, tuning of the design parameters depended on experimental/simulated trial and error. Tuning of design parameters, especially frequency weighing functions is very heavy burden for control design engineers. Development of systematic tuning method of design parameter is now expected.

Further, in the previous works, physical limit of allowable perturbation for robust stability/performance was not clear. Weightings for uncertainties were just design parameters, but physical stability and performance margins against perturbations were not considered.

The second problem is that there are just a few application papers of H_∞/μ control theory in real nonlinear mechatronic systems, as robot manipulators. Robot dynamics is highly interfered, nonlinear, and complicated. Experimental evaluation is now expected. Hashimoto and Asai treated H_∞ control or μ synthesis of a robot manipulator, but dynamic couplings between joints were not considered, and the uncertainties caused by modeling errors was treated the external disturbance[27][4].

1.2   Goal and contribution of this paper

The goal/contributions of this paper is as following three items.

- As described in the last subsection, in order to design a H_∞/μ control system with better properties, it is very important to choose design parameters suitably, and we expect them to be selected more systematically and meaningfully.

  The first goal of this thesis is a proposal of a more systematic quantification of the model uncertainty.

We make a set of plant model and quantify the model uncertainties, and clarify the limit of allowable class of perturbation for robust stability and performance.

- There are just a few papers of H_∞/μ application in real robot manipulator control field, because robot dynamics is highly interfered, nonlinear, and complicated. Experimental evaluation is now extremely expected.

  The second goal of this thesis is a robust control of robot manipulators by using H_∞ control theory.

  We guarantee the robust stability of the robot manipulator control system against model perturbations and dynamic couplings.

  Further we apply the robust H_∞/μ control theory to a robot manipulator in order to evaluate its effectiveness for nonlinear systems.

  Our approaches taken here are as follows.

  - μ-synthesis with exact linearization

  - constant scaled H_∞ control considering structured uncertainties

  - μ-synthesis using linear parameter varying representation

- Third, we apply the advanced H_∞/μ control theory to real mechanical systems, then evaluate the performance of the control theme and expressive ability of LFT against various forms of uncertainties.

  We experimentally show that H_∞/μ control theory has a very good framework to treat uncertainties, in order to guarantee robust stability and robust performance.

  Our mechatronic plants employed to evaluate robust control theory are as follows.

  - magnetic bearing: linear, MIMO, unstable

  - pantograph system with linear DC motor: linear, SISO, stable, but highly oscillatory

  - robot manipulator: nonlinear, MIMO, stable

1.3   Organization of the thesis

Organization of the thesis is represented in the diagram of Fig.1.1

This thesis has a small hierarchy.
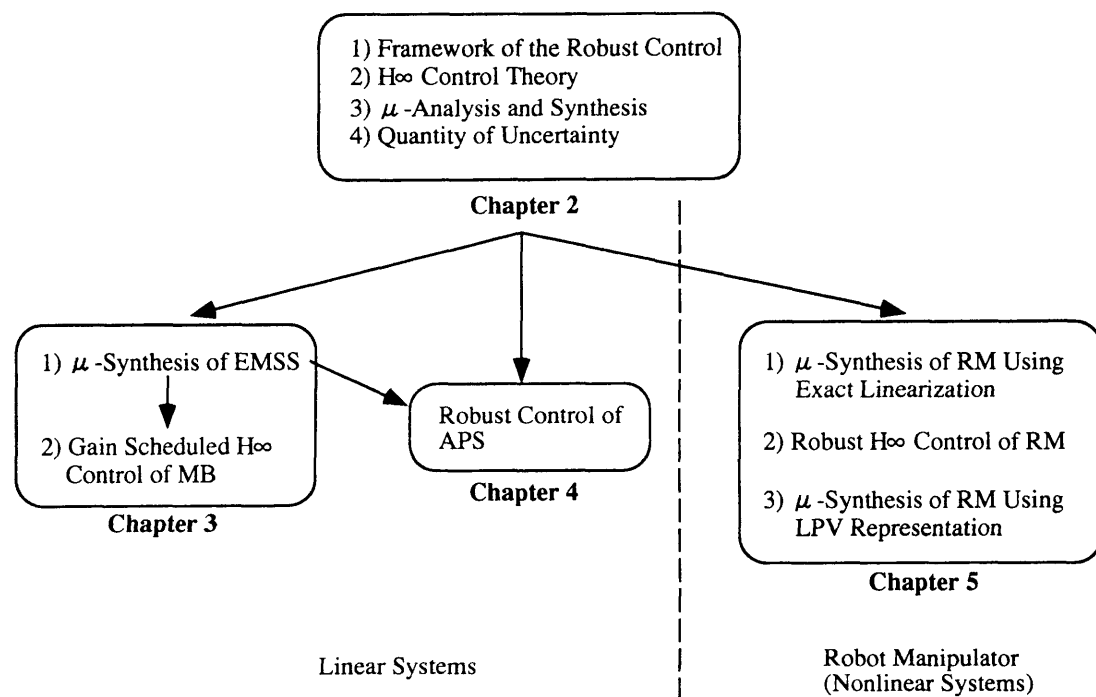
Figure 1.1: Organization of the thesis

Chapter 2 explains a general robust control problem and asserts a main approach to quantify uncertainties. In this chapter, at first, framework of the robust control is described, especially about modeling, uncertainty, and uncertainty descriptions. Then H_∞ control problem/theory, and μ-analysis and synthesis approach is introduced. Mathematical definitions and theorems are also given in Chapter 2. The article entitled "Quantity of uncertainty" is written in section 2.4, which is a main assertion and concept of this thesis.

Then we apply this methodology proposed in section 2.4 to three mechatronic systems, and results are presented in chapter 3, 4, and 5, respectively.

In chapter 3, robust control of magnetic suspension systems is described. Section 3.1 is entitled with "μ-Synthesis of an Electromagnetic Suspension System". And section 3.2 is entitled with "Application of Gain Scheduled H_∞ Robust Controllers to a Magnetic Bearing ". In section 3.1, we show a result of μ-synthesis approach with a simple SISO magnetic suspension system. Section 3.2 is an extension version of section 3.1. Here the controlled plant is a MIMO(four inputs, four outputs) multivariable magnetic bearing system. We derive an advanced gain scheduled H_∞ control method by utilizing free parameter of the controller, and applied the method to this magnetic bearing system.

In chapter 4, robust control of active pantograph system by using linear DC motor, is

described. Here we considered both parametric uncertainties and dynamical uncertainty which is an unmodeled uncertainty of the plant in the modeling process, and construct the interconnection structure by LFT. For controller design, we employ μ-synthesis approach. The experimental results show the effectiveness of the proposed modeling and design by a comparison with a conventional modeling and H_∞ method.

In Chapter 5, robust H_∞ control of robot manipulators is discussed. This chapter is constructed with three main sections, and the following approaches are taken in this chapter.

- μ-synthesis with exact linearization

- constant scaled H_∞ control

- linear parameter varying representation approach

Robot manipulator dynamics is written with nonlinear ordinary differential equation. This makes robot manipulator control complicated.

In the first approach, we employ the exact linearization, and then for the obtained linearized plant, we apply the linear μ-synthesis method. In the second approach, we divide the original nonlinear dynamics with linear nominal model and nonlinear perturbation. Then we used constant H_∞ problem and small gain theory to guarantee the robust stability for nonlinear perturbation. The third approach utilize the recent advanced topics, gain scheduling for linear parameter varying system. Dynamics of robot manipulator with flexible links is written as linear parameter varying system. We derive the LPV equation of the plant and μ-synthesis approach is used for control system design.

In chapter 3 and 4, we treat linear systems and in chapter 5 our plant is a robot manipulator, which is a typical nonlinear system. From section 3.1 to 3.2, complexity of the plant is extended from SISO to MIMO. From section 3.1 to chapter 4, description of the model uncertainty is extended from the unstructured one to the structured.

Finally, we conclude this thesis in Chapter 6.

Chapter 2

Robust Control and Uncertainty Description

Recently H_∞ and μ-synthesis theories have been developed [12] [13]. The H_∞ theory provides a direct, reliable procedure for synthesizing controller which optimally satisfies singular value loop shaping specifications. Robust stability in the H_∞ control framework is guaranteed by the small gain theorem, this theorem provides reliable results for unstructured uncertainties, but it is well known that it gives conservative evaluations for structured uncertainties as robust performance problems.

To improve this property, by using the multivariable Nyquist stability criterion, the μ-analysis and synthesis method provides a less conservative valuation for a structured uncertainty.

2.1 Framework of the Robust Control

2.1.1 Modeling and Uncertainty

Any mathematical models can not exactly express a behavior of the real physical system. For this reason we must be aware of how modeling errors might adversely affect the stability and performance of a control system.

Fig. 2.1 shows an usual framework of the control system design and real-time control. Generally we derive a model for the real plant and by using the obtained model, a controller is designed. We implement this controller and apply it to the original real plant. But the controller was just optimized for the 'model' and not for the real system. The

uncertainty between the real physical system and the nominal model depresses the stability and performance of the closed-loop system.

In the physical sciences, very accurate models are the objective in themselves. To obtain these physical laws, one often distills the phenomenon to its simplest form. In this context, uncertainty is interpreted in a narrow sense as referring to the limits in the predictive power of the best available models. For example, the uncertainty associated with prediction in a chaotic systems, or the uncertainty principle in quantum mechanics refer to fundamental limitations in predictability.

Models play a different role in engineering science; they are tools employed in analysis, simulation and design of complex, artificial systems. Consequently, models fidelity must be traded off with the complexity of the modeling process and the tractability of the resulting mathematical and computational problems. From this point of view the best model is the simplest summary of the main aspects of the physical system which are relevant to the engineering question at hand. Correspondingly, the term "uncertainty" is used here in a broader sense: is not only describes what one is fundamentally unable to predict, but also, and often predominantly, many aspects of the system which one has chosen to neglect or simplify. For uncertainty in this broad sense, there is by definition no detailed model, but often the modeling process yields a crude description which allows one to assess its implications on the overall system. There descriptions of uncertainty appear commonly and in various forms in engineering models, whatever they result from "black box" system identification techniques, from "first principles" models obtained by application and simplification of physical laws, or a combination thereof.

As remarked in Introduction, the issue of uncertainty is at the heart of control engineering, since a feedback configuration can significantly affect the sensitivity of the system behavior to uncertainty at the component level. This is the main motivation for the construction of feedback systems, but also the main potential danger as unmodeled effects can, for example, lead to instability. Consequently, to perform good designs, the control engineer must be furnished with rich descriptions of uncertainty and tools to assess their impact in a complex system. It should be clear from the nature of these descriptions that no hard "guarantees" can result from this assessment; ultimately, the control engineer must be the final mediator between the mathematics and the real system.

In Fig. 2.1, the uncertainty Δ causes various problems when we design a controller and control of a real physical system. We know Δ is a gap between the real physical system and the model, but we have to discuss the Δ in detail. Our problems are as follows.
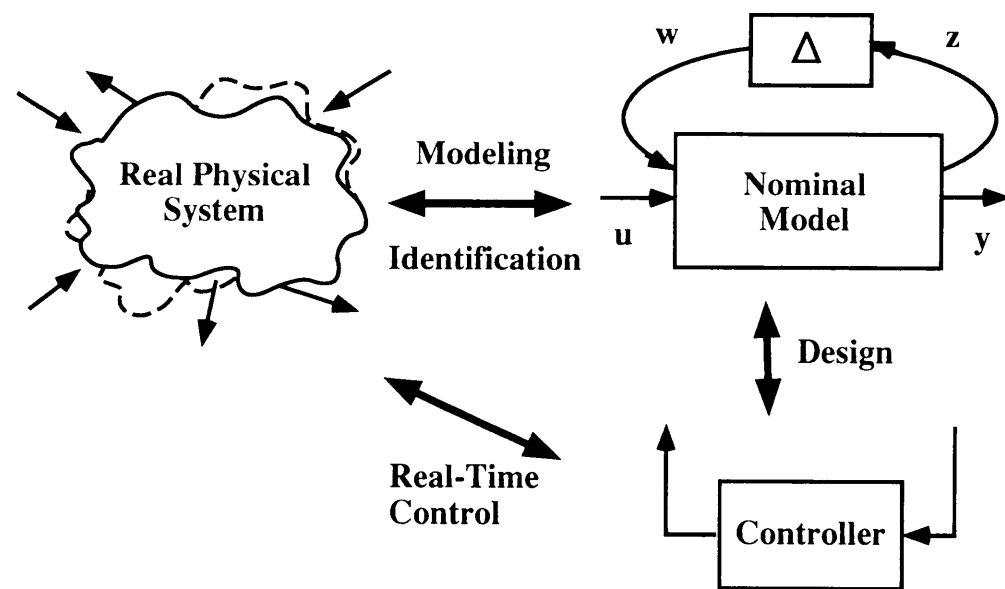
Figure 2.1: General framework of design and real-time control

- What is physically included in Δ ?

- How is Δ expressed?

- How can we measure/quantify Δ?

These problems are discussed in the following sessions.

2.1.2   Uncertainty Descriptions

Traditional methods for uncertainty characterization in dynamical systems include parametric uncertainty, disturbance signals, and system perturbations to account for unmodeled dynamics. We now describe how these typically arise in modeling. For more motivation we refer to [14].

Parametric Uncertainty

Parameters are present in most engineering models, representing a real physical quantity which can be assumed to be a real constant within the range of validity of the model. The following are some reasons for uncertainty in the value of a parameter.

- It could be obtained indirectly from experimental data, which leads to statistical deviations.

- It could represent a standardized component (e.g., electrical resistor) subject to manufacturing tolerances.

- It could represent an operation condition which varies in an unforeseen way. A constant parameter is a reasonable model when this variation is very slow (e.g., ambient temperature). In other cases the rate of variation of the operation condition is comparable to the modeled dynamics (e.g., aerodynamic efficient of an airplane executing a sharp maneuver). In this case a time-varying parameter may be preferred.

The most straightforward representation of parametric uncertainty is in terms of an interval of the real line, such as

$$p = p_0 + k_p\delta, \quad \delta \in [-1,\ 1].$$

In models of linear dynamical systems, it is common to encounter rational dependence of a transfer function on an uncertain parameter.

Disturbance Signals

Another commonly used method to account for model uncertainty is the injection of disturbances, which are thought of as generated by an external process. Some ways in which they arise are

- To account for microscopic fluctuations which are not included in a large scale model(e.g., wind turbulence, thermal noise in a circuit).

- To describe more systematic effects which are neglected in a simplified model (e.g., ripple in a voltage source, quantization error in an A/D converter).

- In identified models, frequently used as an error signal needed to account for the data.

The two standard choices for characterization of disturbances are in terms of a stochastic process, or in terms of a set of signals.

Unmodeled Linear Dynamics

The most commonly used dynamical system model for purposes of control is linear, finite dimensional time invariant system, which is equivalent to a set of linear ODEs, preferably of

low order. Assuming for now that nonlinear effects are negligible, a low order approximation amounts to neglecting linear dynamics, in particular distributed effects.

This uncertainty is expressed as follows

- Additive Uncertainty:

$$\Pi = P + W_1 \Delta W_2.$$

- Multiplicative Uncertainty:

$$\Pi = (I + W_1 \Delta W_2)P.$$

- Coprime Factor Uncertainty:

$$\Pi = (\tilde{M} + \tilde{\Delta}_M)^{-1}(\tilde{N} + \tilde{\Delta}_N).$$

Unmodeled Nonlinear Dynamics

If nonlinear are very significant in the range of operation, the model itself must be chosen to be nonlinear. Uncertainty descriptions for nonlinear models are not very well developed, and are one of the main open challenges for a satisfactory theory of robust nonlinear control.

2.2 H_∞ Control Theory

Robust stability against unstructured uncertainty in H_∞ control framework is guaranteed by small gain theorem. Detailed definition and proof are written in [87].

In this section, the results by Keith Glover and John C. Doyle[25] is introduced.

There are so many other state-space formulae for all stabilizing controllers that satisfy an H_∞ norm bound, but this one is the original and the most famous and typical characterization, which is employed by MATLAB and MATRIXx.

2.2.1   Problem Formulation

The most general block diagram of a control system is shown in Figure 2.2 . Where P is the generalized plant and K is the controller.

Since the work of Zames[86], there has been much interest in the design of feedback controllers for linear systems that minimize the H_∞ norm of a specified closed-loop transfer function. Let a linear system $P(s)$ be described by the state equation

$$\dot{x}(t) = Ax(t) + B_1 w(t) + B_2 u(t), \tag{2.1}$$

$$z(t) = C_1 x(t) + D_{11} w(t) + D_{12} u(t), \tag{2.2}$$

$$y(t) = C_2 x(t) + D_{21} w(t) + D_{22} u(t). \tag{2.3}$$

where

$$x(t) \in \mathbf{R}^n, \ w(t) \in \mathbf{R}^{m_1}, \ u(t) \in \mathbf{R}^{m_2}, \ z(t) \in \mathbf{R}^{p_1}, \ y(t) \in \mathbf{R}^{p_2}$$

The generalized plant P contains what is usually called the plant in a control system plus all any frequency-dependent weighting functions.

The signals, $w(t)$, $z(t)$, $y(t)$, and $u(t)$ are vector-valued functions of time. $x(t)$ is the state vector. The components of

w :   are all the exogenous input: reference, disturbances, sensor noises, and so on.

z :   are all the signals we wish to control: tracking errors between reference signals and plant output, actuator signals whose values must be kept between certain limits, and so on.
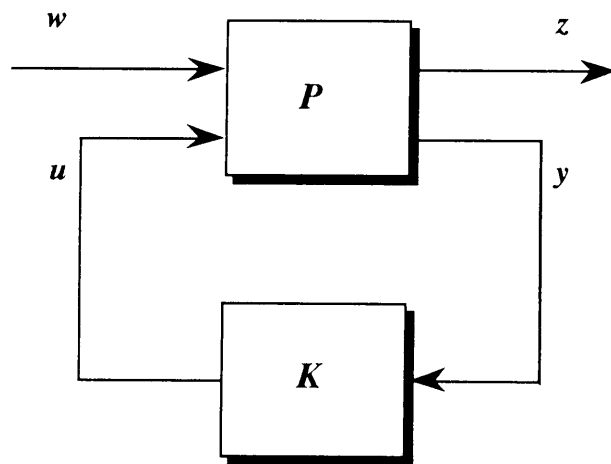
Figure 2.2: Most general Control System

y :   contains the outputs of all sensors.

u :   contains all controlled inputs to the generalized plant.

The transfer functions will be denoted as follows

$$P(s) \; := \; \begin{pmatrix} P_{11} & P_{12} \\ P_{21} & P_{22} \end{pmatrix} \tag{2.4}$$

$$= \begin{pmatrix} D_{11} & D_{12} \\ D_{21} & D_{22} \end{pmatrix} + \begin{bmatrix} C_{12} \\ C_{12} \end{bmatrix} (sI - A)^{-1} \begin{bmatrix} B_1 & B_2 \end{bmatrix} \tag{2.5}$$

$$\stackrel{s}{=} \left[\begin{array}{c|cc} A & B_1 & B_2 \\ \hline C_1 & D_{11} & D_{12} \\ C_2 & D_{12} & D_{22} \end{array} \right] \tag{2.6}$$

$$=: \left[\begin{array}{c|c} A & B \\ \hline C & D \end{array} \right] \tag{2.7}$$

The diagram is also referred to as a linear fractional transformation(LFT; see subsection 2.3.2) on K and P is called the coefficient matrix for the LFT. The resulting closed-loop transfer function from w to z is denoted by $T_{zw} = \mathcal{F}_l(P, K)$, where

$$\mathcal{F}_l(P, K) := P_{11} + P_{12}K(I - P_{22}K)^{-1}P_{21}. \tag{2.8}$$

The H_∞ control problem is then to choose a controller $K(s)$, that makes the closed-loop system internally stable (see [25]) and minimize $\|\mathcal{F}_l(P, K)\|_\infty$,

where

$$\|G\|_\infty = \sup_\omega \bar{\sigma} \left(G(j\omega) \right) \quad (\bar{\sigma} := \text{maximum singular value}). \tag{2.9}$$

We will in fact be considering the closely-related problem of finding all stabilizing K such that

$$\|\mathcal{F}_l(P, K)\|_\infty \leq \gamma \tag{2.10}$$

for some prespecified $\gamma \in \mathbf{R}$

It is the purpose of the present note to give a state-space parametrization of all controllers that satisfy (2.10); this solution will only involve two algebraic game-type Riccati equations, each of degree n[25] [12].

2.2.2   Characterizing all solutions

This section will give a state-space characterization of all stabilizing controllers $K(s)$ such that $\|\mathcal{F}_l(P, K)\|_\infty < \gamma$. We will make the following assumptions that are also typically made in the corresponding LQG problems.

Assumption 2.1

- (A1) (A, B_2) is stabilizable

- (A2) (C_2, A) is detectable.

- (A3)   rank $D_{12} = m_2$ (D_{12} is full column rank.)

- (A4)   rank $D_{21} = p_2$ (D_{21} is full row rank.)

- (A5)   rank $\begin{bmatrix} A - j\omega I & B_2 \\ C_1 & D_{12} \end{bmatrix} = n + m_2 \quad \forall \omega \quad$ (full column rank)

  $\Updownarrow$

  P_{12} does not have any zeros on the imaginary axis.

  $\Updownarrow$

  There are no unobservable poles of $(A - B_2 D_{12}^\dagger C_1, \; D_{12}^\perp C_1)$ on the imaginary axis.

- (A6)   rank $\begin{bmatrix} A - j\omega I & B_1 \\ C_2 & D_{21} \end{bmatrix} = n + p_2 \quad \forall \omega \quad$ (full row rank)

  $\Updownarrow$

  P_{21} does not have any zeros on the imaginary axis.

  $\Updownarrow$

  There are no uncontrollable poles of $(A - B_1 D_{21}^\dagger C_2, \; B_1 D_{21}^\perp)$ on the imaginary axis.

- (A7)   A scaling of u and y, together with a unitary transformation of w and z, enables us to assume without loss of generality,

$$D_{12} = \begin{bmatrix} 0 \\ I_{m_2} \end{bmatrix}, \quad D_{21} = [\, 0 \quad I_{p_2} \,], \quad D_{22} = 0$$

Assumptions (A1) and (A2) are required for the existence of a stabilizing K. These assumptions are equivalent that the real plant is stabilizable and detectable, and the weighting functions are stable.

(A3) and (A4) are sufficient to ensure that the controllers are proper, but there are sensible problems when it is violated. $D_{12} = P_{12}(\infty)$, $D_{21} = P_{21}(\infty)$, then these assumptions mean P_{12} and P_{21} do not have any zeros at $j = \infty$. If these would be deleted, expansion of equations are more complicated.

(A5) and (A6) are need for spectral factorizations.

(A7) ensure that the solution to the corresponding LQG problem is closed-loop asymptotically stable, and is also convenient for the present problem.

The main result is now stated as follows.

Theorem 2.1

For the system described by (2.1)-(2.3) and satisfying the assumptions (A1)-(A7), There exists an internally stabilizing controller $K(s)$ such that $||\mathcal{F}_l(P, K)||_\infty < \gamma$ if and only if

(i) $\gamma > \max(\bar{\sigma}[D_{1111}, D_{1112}], \bar{\sigma}[D_{1111}^\star, D_{1121}^\star])$,
where

$$D_{11} = \begin{bmatrix} D_{1111} & D_{1112} \\ D_{1121} & D_{1122} \end{bmatrix},$$

$D_{1111} \in R^{(p_1-m_2) \times (m_1-p_2)}, D_{1112} \in R^{(p_1-m_2) \times p_2}, D_{1121} \in R^{m_2 \times (m_1-p_2)}, D_{1122} \in R^{m_2 \times p_2}$.

and
(ii) there exist $X_\infty \geq 0$ and $Y_\infty \geq 0$ satisfying (2.11) and (2.12) respectively and such that $\lambda_{\max}(X_\infty Y_\infty) < \gamma^2$,
where

$$X_\infty = \mathrm{Ric}\left\{ \begin{bmatrix} A & 0 \\ -C_1^\star C_1 & -A^\star \end{bmatrix} - \begin{bmatrix} B \\ -C_1^\star D_{1\bullet} \end{bmatrix} R^{-1}[D_{1\bullet}^\star C_1 \quad B^\star] \right\}, \quad (2.11)$$

$$Y_\infty = \mathrm{Ric}\left\{ \begin{bmatrix} A^\star & 0 \\ -B_1 B_1^\star & -A \end{bmatrix} - \begin{bmatrix} C^\star \\ -B_1 D_{\bullet 1}^\star \end{bmatrix} \tilde{R}^{-1}[D_{\bullet 1} B_1^\star \quad C] \right\}, \quad (2.12)$$

$$R = D_{1\bullet}^\star D_{1\bullet} - \begin{bmatrix} \gamma^2 I_{m_1} & 0 \\ 0 & 0 \end{bmatrix}, \quad D_{1\bullet} = [\, D_{11} \quad D_{12} \,] \quad (2.13)$$

$$\tilde{R} = D_{\bullet 1} D_{\bullet 1}^\star - \begin{bmatrix} \gamma^2 I_{p_1} & 0 \\ 0 & 0 \end{bmatrix}, \quad D_{\bullet 1} = \begin{bmatrix} D_{11} \\ D_{21} \end{bmatrix} \quad (2.14)$$

The solution X_∞ and Y_∞ to an algebraic Riccuti equation (ARE) are denoted via its Hamiltonian matrix as (2.11) and (2.12).

Theorem 2.2

Given that the conditions of Theorem 2.1 are satisfied, then all rational internally stabilizing controllers $K(s)$ satisfying $||\mathcal{F}_l(P, K)||_\infty < \gamma$ are given by

$$K := \mathcal{F}_l(K_a, \Phi) = K_{11} + K_{12}\Phi(I - K_{22}\Phi)^{-1}K_{21}, \quad (2.15)$$

$$\Phi \in RH_\infty, \quad s.t. \ ||\Phi||_\infty < \gamma,$$

where

$$K_a := \begin{bmatrix} K_{11} & K_{12} \\ K_{21} & K_{22} \end{bmatrix} \overset{s}{\equiv} \left[\begin{array}{c|cc} \hat{A} & \hat{B}_1 & \hat{B}_2 \\ \hline \hat{C}_1 & \hat{D}_{11} & \hat{D}_{12} \\ \hat{C}_2 & \hat{D}_{12} & 0 \end{array} \right], \quad (2.16)$$

$$\hat{A} = A + HC + \hat{B}_2 \hat{D}_{12}^{-1} \hat{C}_1, \quad (2.17)$$

$$\hat{B}_1 = -H_2 + \hat{B}_2 \hat{D}_{12}^{-1} \hat{D}_{11}, \quad (2.18)$$

$$\hat{B}_2 = (B_2 + H_{12}) \hat{D}_{12}, \quad (2.19)$$

$$\hat{C}_1 = F_2 Z + \hat{D}_{11} \hat{D}_{21}^{-1} \hat{C}_2, \quad (2.20)$$

$$\hat{C}_2 = -\hat{D}_{21}(C_2 + F_{12}) Z, \quad (2.21)$$

$$\hat{D}_{11} = -D_{1121} D_{1111}^\star (\gamma^2 I - D_{1111} D_{1111}^\star)^{-1} D_{1112} - D_{1122}, \quad (2.22)$$

$\hat{D}_{12} \in R^{m_2 \times m_2}$ and $\hat{D}_{21} \in R^{p_2 \times p_2}$ are any matrices (e.g., Cholesky factors) satisfying

$$\hat{D}_{12} \hat{D}_{12}^\star = I - D_{1121}(\gamma^2 I - D_{1111}^\star D_{1111})^{-1} D_{1121}^\star, \quad (2.23)$$

$$\hat{D}_{21}^\star \hat{D}_{21} = I - D_{1121}^\star(\gamma^2 I - D_{1111} D_{1111}^\star)^{-1} D_{1121}, \quad (2.24)$$

$$F = \begin{bmatrix} F_{11} \\ F_{12} \\ F_2 \end{bmatrix} = -R^{-1}[D_{1\bullet}^\star C_1 + B^\star X_\infty], \quad (2.25)$$

$$H = [\, H_{11} \quad H_{12} \quad H_2 \,] = -[B_1 D_{\bullet 1}^\star + Y_\infty C^\star] \tilde{R}^{-1}, \quad (2.26)$$

$$Z = (I - \gamma^{-2} Y_\infty X_\infty)^{-1}, \quad (2.27)$$

$F_{11} \in R^{(m_1-p_2)\times n}$, $F_{12} \in R^{p_2 \times n}$, $F_2 \in R^{m_2 \times n}$, $H_{11} \in R^{n\times(p_1-m_2)}$, $H_{12} \in R^{n\times m_2}$, $H_2 \in R^{n\times p_2}$. F and H are called the 'state feedback' and 'output injection' matrices, respectively. In (2.16), $\Phi(s)$ is called free parameter. And if $\Phi(s) = 0$, then controller $K(s)$ should be $K_{11}(s)$ from (2.16). $K_{11}(s)$ is generally called 'central controller'. The central controller is formulated as

$$K_{11}(s) = \left[\begin{array}{c|c} \hat{A} & \hat{B}_1 \\ \hline \hat{C}_1 & \hat{D}_{11} \end{array}\right] \qquad (2.28)$$

2.3 μ-Analysis and Synthesis

The small gain theorem provides reliable results for unstructured uncertainties, but it is well known that it gives conservative evaluations for structured uncertainties as robust performance problems. To improve this property, by using the multivariable Nyquist stability criterion[41], the μ-analysis and synthesis method provides a less conservative valuation for a structured uncertainty.

2.3.1 Structured Singular Value μ

In this section I devote to defining the structured singular value, a matrix function denoted by μ [13]. Consider matrices $M \in \mathbf{C}^{n\times n}$. In the definition of $\mu(M)$, there is an underlying structure $\mathbf{\Delta}$, (a prescribed set of block diagonal matrices) on which everything in the sequel depends. For each problem, this structure is in general different; it depends on the uncertainty and performance objectives of the problem. Defining the structure involves specifying three things; the type of each block, the total number of blocks, and their dimensions.

There are two types of blocks-repeated scalar and full blocks. Two nonnegative integers, S and F, represent the number of repeated scalar blocks and the number of full blocks, respectively. To bookkeep their dimensions, we introduce positive integers $r_1,...,r_S$; $m_1,...,m_F$. The i'th repeated scalar block is $r_i \times r_i$, while the j'th full block is $m_j \times m_j$. With those integers given, we define $\mathbf{\Delta} \subset \mathbf{C}^{n\times n}$ as

$$\mathbf{\Delta} = \{\mathrm{diag}[\delta_1 I_{r_1},\ldots,\delta_S I_{r_S},\Delta_1,\ldots,\Delta_F] : \delta_i \in \mathbf{C}, \ \Delta_j \in \mathbf{C}^{m_j \times m_j}\} \qquad (2.29)$$

For consistency among all dimensions, we must have

$$\sum_{i=1}^{S} r_i + \sum_{j=1}^{F} m_j = n \qquad (2.30)$$

We will often need norm bounded subsets of $\mathbf{\Delta}$, and we introduce the following notation

$$\mathbf{B\Delta} = \{\Delta \in \mathbf{\Delta} : \bar{\sigma}(\Delta) \le 1\} \qquad (2.31)$$

Note that in (2.29) all of the repeated scalar blocks appear first. This is just to keep the notation as simple as possible, in fact they can come in any order. Also, the full blocks do not have to be square, but restricting them as such saves a great deal in terms of notation.

Definition 2.1 [13]

For $M \in \mathbf{C}^{n \times n}$, $\mu_{\mathbf{\Delta}}(M)$ is defined

$$\mu_{\mathbf{\Delta}}(M) := \frac{1}{\min\{\bar{\sigma}(\Delta) : \Delta \in \mathbf{\Delta}, \det(I - M\Delta) = 0\}} \qquad (2.32)$$

unless no $\Delta \in \mathbf{\Delta}$ makes $I - M\Delta$ singular, in which case $\mu_{\mathbf{\Delta}}(M) := 0$.

An alternative expression for $\mu_{\mathbf{\Delta}}(M)$ follows from the definition (2.32).

$$\mu_{\mathbf{\Delta}}(M) := \max_{\Delta \in \mathbf{B}\mathbf{\Delta}} \rho(M\Delta) \qquad (2.33)$$

From (2.33) continuity of the function $\mu : \mathbf{C}^{n \times n} \to \mathbf{R}$ is apparent. In general, though, the function $\mu : \mathbf{C}^{n \times n} \to \mathbf{R}$ is not a norm, since it doesn't satisfy the triangle inequality. However, for any $\alpha \in \mathbf{C}$, $\mu(\alpha M) = |\alpha| \mu(M)$, so in some sense, it is related to how "big" the matrix is in a norm sense.

We can relate $\mu(\alpha M)$ to familiar linear algebra quantities when $\mathbf{\Delta}$ is one of two extreme sets.

- If $\mathbf{\Delta} = \{\delta I : \delta \in \mathbf{C}\}$ ($S = 1$, $F = 0$, $r_1 = n$), then $\mu(M) = \rho(M)$, the spectral radius of M.

- If $\mathbf{\Delta} = \mathbf{C}^{n \times n}$ ($S = 0$, $F = 1$, $m_1 = n$), then $\mu(M) = \bar{\sigma}(M)$.

For a general $\mathbf{\Delta}$ as in (2.29) we must have

$$\{\delta I_n : \delta \in \mathbf{C}\} \subset \mathbf{\Delta} \subset \mathbf{C}^{n \times n} \qquad (2.34)$$

Hence directly from the definition of μ, and the two special cases above, we conclude that

$$\rho(M) \leq \mu_{\mathbf{\Delta}}(M) \leq \bar{\sigma}(M) \qquad (2.35)$$

These bounds alone are not sufficient for our own purposes, because the gap between ρ and $\bar{\sigma}$ can be arbitrarily large. They are refined by considering transformations on M that do not affect $\mu_{\mathbf{\Delta}}(M)$, but do affect ρ and $\bar{\sigma}$. To do this, define the following two subsets of $\mathbf{C}^{n \times n}$

$$\mathbf{Q} = \{Q \in \mathbf{\Delta} : Q^*Q = I_n\} \qquad (2.36)$$

$$\mathbf{D} = \left\{ \begin{array}{l} \operatorname{diag}[D_1, \ldots, D_S, d_1 I_{m_1}, \ldots, d_{F-1} I_{m_{F-1}}, I_{m_F}] : \\ D_i \in \mathbf{C}^{r_i \times r_i}, D_i = D_i^* > 0, d_j \in \mathbf{R}, d_j > 0 \end{array} \right\} \qquad (2.37)$$

Note that for any $\Delta \in \mathbf{\Delta}$, $Q \in \mathbf{Q}$, and $D \in \mathbf{D}$,

$$Q^* \in \mathbf{Q}, \quad Q\Delta \in \mathbf{\Delta}, \quad \Delta Q \in \mathbf{\Delta}$$

$$\bar{\sigma}(Q\Delta) = \bar{\sigma}(\Delta Q) = \bar{\sigma}(\Delta) \qquad (2.38)$$

$$D\Delta = \Delta D \qquad (2.39)$$

Consequently

Theorem 2.3:

For all $Q \in \mathbf{Q}$ and $D \in \mathbf{D}$

$$\mu_{\mathbf{\Delta}}(MQ) = \mu_{\mathbf{\Delta}}(QM) = \mu_{\mathbf{\Delta}}(M) = \mu_{\mathbf{\Delta}}\left(DMD^{-1}\right) \qquad (2.40)$$

Therefore, the bounds in (2.35) can be tightened to

$$\max_{Q \in \mathbf{Q}} \rho(QM) \leq \max_{\Delta \in \mathbf{B}\mathbf{\Delta}} \rho(\Delta M) = \mu_{\mathbf{\Delta}}(M) \leq \inf_{D \in \mathbf{D}} \bar{\sigma}\left(DMD^{-1}\right) \qquad (2.41)$$

where the equality comes from (2.33). Note that the last element in the D matrices in (2.37) is normalized to 1 since for any nonzero scalar γ, $DMD^{-1} = (\gamma D)M(\gamma D)^{-1}$.

Bounds

Here I will concentrate on the μ bounds. From (2.41)

$$\max_{Q \in \mathbf{Q}} \rho(QM) \leq \mu_{\mathbf{\Delta}}(M) \leq \inf_{D \in \mathbf{D}} \bar{\sigma}\left(DMD^{-1}\right) \qquad (2.42)$$

The lower bound is always an equality. Unfortunately, the quantity $\rho(QM)$ can have multiple local maxima which are not global. Thus local search cannot be guaranteed to obtain μ, but can only yield a lower bound. So we use a slightly different formulation

of the lower bound as a power algorithm which is reminiscent of power algorithms for eigen values and singular values. While there are open questions about convergence, the algorithm usually works quite well and has proven to be an effective method to compute μ.

2.3.2   Linear Fractional Transformations

Using only the definition of μ, some simple theorems about a class of general matrix transformations called Linear Fractional Transformations can be proven. To introduce these, consider a complex matrix M partitioned as

$$M = \begin{bmatrix} M_{11} & M_{12} \\ M_{21} & M_{22} \end{bmatrix} \tag{2.43}$$

and suppose there is a defined block structure $\mathbf{\Delta_2}$ which is compatible in size with M_{22} (for any $\Delta_2 \in \mathbf{\Delta_2}$, $M_{22}\Delta_2$ is square). For $\Delta_2 \in \mathbf{\Delta_2}$, consider the following loop equations,

$$\begin{bmatrix} e \\ z \end{bmatrix} = M \begin{bmatrix} d \\ w \end{bmatrix}$$

$$w = \Delta_2 z \tag{2.44}$$

These equations (2.44) are called **well posed** if for any vector d, there exist unique vectors w, z, and e satisfying the loop equations. It is easy to see that the set of equations is well posed if and only if the inverse of $I - M_{22}\Delta_2$ exists. If not, then depending on d and M, there is either no solution to the loop equations, or there are an infinite number of solutions. When the inverse does indeed exist, the vectors e and d must satisfy $e = \mathcal{F}_l(M, \Delta_2)d$, where

$$\mathcal{F}_l(M, \Delta_2) = M_{11} + M_{12}\Delta_2 \left(I - M_{22}\Delta_2\right)^{-1} M_{21} \tag{2.45}$$

$\mathcal{F}_l(M, \Delta_2)$ is called a **Linear Fractional Transformation** on M by Δ_2, and in a feedback diagram appears in Figure 2.3 .

The subscript l on $\mathcal{F}_l$ pertains to the "lower" loop of M is closed by Δ_2. An analogous formula describes $\mathcal{F}_u(M, \Delta_1)$, which is the resulting matrix obtained by closing "the upper" loop of M with a matrix $\Delta_1 \in \mathbf{\Delta_1}$.

In (2.45) , the matrix M_{11} is assumed to be something nominal, and $\Delta_2 \in \mathbf{B\Delta_2}$ is viewed as a norm bounded perturbation from an allowable perturbation class, $\mathbf{\Delta_2}$. The matrices M_{12}, M_{21} and M_{22} and the formula $\mathcal{F}_l$ reflect prior knowledge on how the unknown perturbation affects the nominal map, M_{11}.
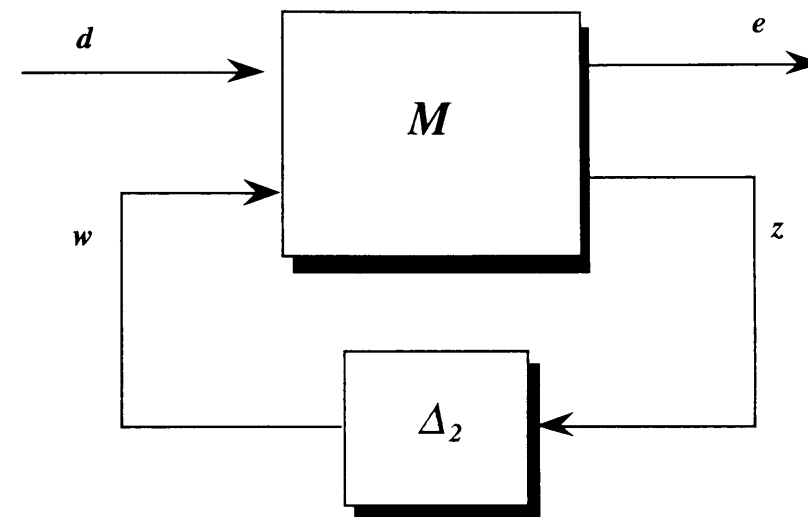
Figure 2.3: Lower Linear Fractional Transformation

The constant matrix problem to solve is:

- determine whether the LFT is well posed for all $\Delta_2 \in \mathbf{\Delta_2}$. with $\bar{\sigma}(\Delta_2) \leq \beta$, and,

- if so, them determine how "large" $\mathcal{F}_l(M, \Delta_2)$ can get for this norm-bounded set of perturbations.

The next section has simple theorems which answer this problem.

2.3.3   Well posedness and Performance for LFT's

Let M be a complex matrix partitioned as (2.43) and suppose there are two defined block structures, $\mathbf{\Delta_1}$ and $\mathbf{\Delta_2}$, which are compatible in size with M_{11} and M_{22} respectively. Define a third structure $\mathbf{\Delta}$ as

$$\mathbf{\Delta} = \left\{ \begin{bmatrix} \Delta_1 & 0 \\ 0 & \Delta_2 \end{bmatrix} : \Delta_1 \in \mathbf{\Delta_1}, \Delta_2 \in \mathbf{\Delta_2} \right\}. \tag{2.46}$$

Now there are three structures with which we may compute μ with respect to. The notation we use to keep track of this is as follows: $\mu_1(\cdot)$ is with respect to $\mathbf{\Delta_1}$, $\mu_2(\cdot)$ is with respect to $\mathbf{\Delta_2}$,: $\mu_{\mathbf{\Delta}}(\cdot)$ is with respect to $\mathbf{\Delta}$. In view of this, $\mu_1(M_{11})$, $\mu_2(M_{22})$ and $\mu_{\mathbf{\Delta}}(M)$ all make sense, though for instance, $\mu_1(M)$ does not.

Let $\Delta_2 \in \mathbf{\Delta_2}$. The linear fractional transformation, $\mathcal{F}_l(M, \Delta_2)$ is well posed if $I - M_{22}\Delta_2$ is invertible, and in that case is defined as

$$\mathcal{F}_l(M, \Delta_2) = M_{11} + M_{12}\Delta_2 \ (I - M_{22}\Delta_2)^{-1} M_{21} \qquad (2.47)$$

The first theorem is nothing more than a restatement of the definition of μ.

Theorem 2.4:

The linear fractional transformation $\mathcal{F}_l(M, \Delta_2)$ is well posed for all $\Delta_2 \in \mathbf{B\Delta_2}$ if and only if $\mu_2(M_{22}) < 1$.

As the "perturbation" Δ_2 deviates from zero, the matrix $\mathcal{F}_l(M, \Delta_2)$ deviates from M_{11}. The range of values that $\mu_1(\mathcal{F}_l(M, \Delta_2))$ takes on is intimately related to $\mu_\Delta(M)$, as follows:

Theorem 2.5:

The following are equivalent:

$$\mu_\Delta(M) \leq 1 \quad \Longleftrightarrow \quad \begin{cases} \mu_2(M_{22}) < 1, \text{ and} \\ \displaystyle\max_{\Delta_2 \in \mathbf{B\Delta_2}} \mu_1(\mathcal{F}_l(M, \Delta_2)) < 1 \end{cases} \qquad (2.48)$$

This theorem forms the basis for all uses of μ in linear system robustness analysis, whether from a state-space, frequency domain, or Lyapunov approach. The frequency domain μ tests play a key role in robustness analysis.

2.3.4   Robust Stability

The most well-known use of μ as a robustness analysis tool is in the frequency domain. Suppose $\hat{P}(s)$ is a stable, multi-input, multi-output transfer function of a linear system. For clarity, assume $\hat{P}(s)$ has n_z inputs and n_w outputs. Let $\mathbf{\Delta}$ be a block structure, as in (2.29), and assume that the dimensions are such that $\mathbf{\Delta} \subset \mathbf{C}^{n_z \times n_w}$. We want to consider feedback perturbations to $\hat{P}$ which are themselves dynamical systems, with the block-diagonal structure of the set $\mathbf{\Delta}$. To do so, first let $\mathcal{M}_S$ denote the entire set of real-rational, proper, stable, transfer matrices. Associated with any block structure $\mathbf{\Delta}$, let $\mathcal{M}(\mathbf{\Delta})$ denote the set of all block diagonal, stable rational transfer functions, with block structure like $\mathbf{\Delta}$.

$$\mathcal{M}(\mathbf{\Delta}) := \{\Delta(\cdot) \in \mathcal{M}_S : \Delta(s_o) \in \mathbf{\Delta} \text{ for all } s_o \in \mathbf{C}_+\} \qquad (2.49)$$

Theorem 2.6:

Let $\beta > 0$. The loop shown below is well-posed and internally stable for all $\Delta(\cdot) \in \mathcal{M}(\mathbf{\Delta})$ with $||\Delta||_\infty < \frac{1}{\beta}$ if and only if

$$||P||_\mathbf{\Delta} := \sup_{\omega \in \mathbf{R}} \mu_\Delta\left(\hat{P}(j\omega)\right) \leq \beta \qquad (2.50)$$

The peak value on the μ plot of the frequency response that the perturbation sees determines the size of perturbations that the loop is robustly stable against.

2.3.5   Robust Performance

Often times, stability is not the only property of a closed-loop system that must be robust to perturbations. Typically there are exogenous disturbances acting on the system (wind gusts, sensor noise) which result in tracking and regulation errors. Under perturbation, the effect that these disturbances have on error signals can greatly increase. In most cases, long before the onset of instability, the closed-loop performance will degrade to the point of unacceptability. Hence the need for a "robust performance" test. Such a test will indicate the worst-case level of performance degradation associated with a given level of perturbations.

Assume $\hat{P}$ is stable, real-rational, proper transfer function, with $n_z + n_d$ inputs, and $n_w + n_e$ outputs. Partition $\hat{P}$ in the obvious manner, so that $\hat{P}_{11}$ has n_z inputs and n_w outputs, and so on. Let $\mathbf{\Delta} \subset \mathbf{C}^{n_w \times n_z}$ be a block structure, as in (2.29). Define an augmented block structure [13]

$$\mathbf{\Delta}_P := \left\{ \begin{bmatrix} \Delta & 0 \\ 0 & \Delta_F \end{bmatrix} : \Delta \in \mathbf{\Delta}, \Delta_F \in \mathbf{C}^{n_d \times n_e} \right\} \qquad (2.51)$$

The setup is to theoretically address the robust performance questions about the loop shown as Figure 2.4
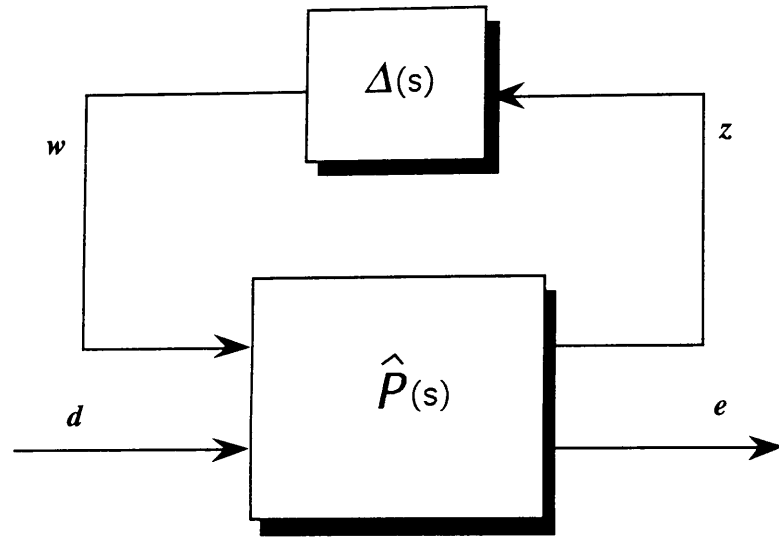
Figure 2.4: Upper Linear Fractional Transformation

The perturbed transfer function from d to e is denoted by $\mathcal{F}_u(\hat{P}, \Delta)$.

Theorem 2.7:

Let $\beta > 0$. For all $\Delta(s) \in \mathcal{M}(\Delta)$ with $||\Delta||_\infty < \frac{1}{\beta}$, the loop shown above is well-posed, internally stable, and $||\mathcal{F}_u(\hat{P}, \Delta)||_\infty \leq \beta$ if and only if

$$||P||_{\Delta_P} := \sup_{\omega \in \mathbf{R}} \mu_{\Delta_P}\left(\hat{P}(j\omega)\right) \leq \beta \qquad (2.52)$$

2.4 Quantity of Uncertainty

In the previous research, tuning of the design parameters depended on experimental/ simulated trial and error. Tuning of design parameters, especially frequency weighing functions is very heavy burden for control design engineers. Development of systematic tuning method of design parameter is now expected. Further, physical limit of allowable perturbation for robust stability/performance was not clear. Weightings for uncertainties were just design parameters, but physical stability and performance margins against perturbations were not considered.

Hence, we expect design parameters to be selected more systematically and meaningfully. In this section, I make a set of plant model and quantify the model uncertainties by iterative design method, and clarify the limit of allowable class of perturbation for robust stability and performance.

2.4.1 Iterative Design

Our approach taken here is to treat quantization of uncertainty as one of control system design process. The problem of uncertainty quantization cannot be separated from control system design. These two parts are correlate closely with each other.

We would like to make the closed-loop system possess robustness. If the system has an over-robustness property, however, the performance of the system would be deteriorated. Hence a balance of robustness and performance is a matter of great importance to a control system design. Quantization of uncertainty depends on the synthesis.

The following items are interrelated.

- quantization of uncertainty

- performance specification

- construction of interconnection structure

- design(synthesis)

Our proposal is iteration of uncertainty quantization, which is as follows. As a result of this iteration, the class/quantity of uncertainty which is guaranteed robust stability/performance should be obtained.

Iterative Design Procedure

Step1: make a set G: Construct a plant model set G which involves the nominal linear model G. This set should be represented by a matrix function: linear fractional transformations(LFT) as $G := \mathcal{F}_l(\hat{G}, \Delta)$, where $\hat{G}$ involves a nominal model G and weighting functions for uncertainties, and Δ is given by

$$\Delta = \{\mathrm{diag}[\delta_1 I_{r_1}, \ldots, \delta_S I_{r_S}, \Delta_1, \ldots, \Delta_F] : \delta_i \in \mathbf{C}, \ \Delta_j \in \mathbf{C}^{m_j \times m_j}\}. \quad (2.53)$$

Step2: set a performance spec: Set a performance specification by using weighting function W_{perf}, e.g., integral property for disturbance elimination, and tracking to the reference signal.

Step3: construct the interconnection structure: First, construct the generalized plant $\tilde{G}$ from $\hat{G}$ and W_{perf}, then put Δ together with Δ_{perf} as

$$\Delta_P := \left\{ \begin{bmatrix} \Delta & 0 \\ 0 & \Delta_{perf} \end{bmatrix} : \Delta \in \Delta, \Delta_{perf} \in \mathbf{C}^{n_d \times n_e} \right\} \quad (2.54)$$

Step4: synthesis: Solve H_∞/μ Control Problem to achieve H_∞ norm, or the structured singular value μ test, and obtain the controller K.

Step5: judgement: The upper bound γ of the $||\mathcal{F}_l(\tilde{G}, K)||_\infty$, or $\mu_{\Delta_P}(\mathcal{F}_l(\tilde{G}, K))$ is obtained in Step4. If $\gamma < 1$, then go to Step6, but if $\gamma \geq 1$, return to Step1 and reselect a set of plant model G.

Step6: experimental evaluation: By experiments, the stability and performance of the obtained closed-loop system are evaluated for a set G.

In the above iteration, making a set G performs a key role. The method to make a set G is described in the next subsection.

2.4.2 How to make a set G

Our approaches to make a set G are following three items. For the simplicity, in this section I explain just SISO systems, but it can be extended to MIMO systems.
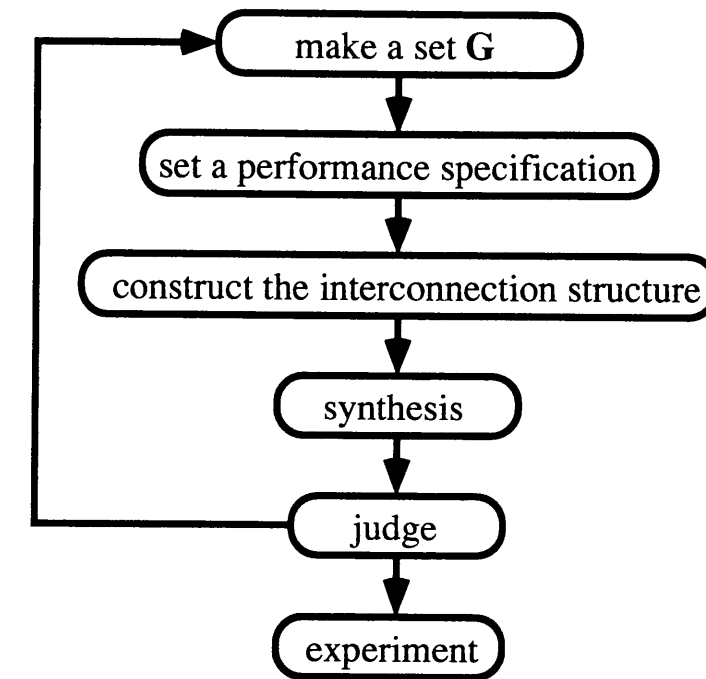
Figure 2.5: Flow Chart of Iterative Design

(1) **set of parameters:**

This set is used in order to take the parametric uncertainty into account. According as the state $x(t)$ of the system, parametric numerical value changes. Usually, the nominal values of the parameters are decided as the value when the state $x(t) \in R^n$ is on the equilibrium point, and the obtained values are employed around the equilibrium point. But, at the neighborhood of the equilibrium point, numerical values of parameters should be perturbed.

First, select the k state variables $x_i(i = 1, .., k) \subset x$ which are expected most to be regulate, then set the range (the upper and lower bound) which is guaranteed robust stability/performance.

$$x_{i_{\min}} \leq x_i \leq x_{i_{\max}}, \quad i = 1, \ldots k. \quad (2.55)$$

By these change of state variables, the m model parameters $p_j(j = 1, \ldots m)$ which are included in A, B matrices are perturbed as

$$p_{j_{\min}} \leq p_j(x_i) \leq p_{j_{\max}}, \quad (x_{i_{\min}} \leq x_i \leq x_{i_{\max}}, \ i = 1, \ldots, k, \ j = 1, \ldots, m) \quad (2.56)$$

Then the nominal value of p_j and the weighting of parametric uncertainty should be decided as follows.

$$p_{j_{nom}} = p_j|_{x_j = x_{j_{nom}}} \qquad (2.57)$$

$$w_{p_j} = \max(p_{j_{max}} - p_{j_{nom}}, p_{j_{nom}} - p_{j_{min}}) \qquad (2.58)$$

Hence the set of parameter is written as,

$$p_j := \{p_{j_{nom}} + \delta w_{p_j} : \ |\delta| < 1.\}, \quad j = 1, \dots, m. \qquad (2.59)$$
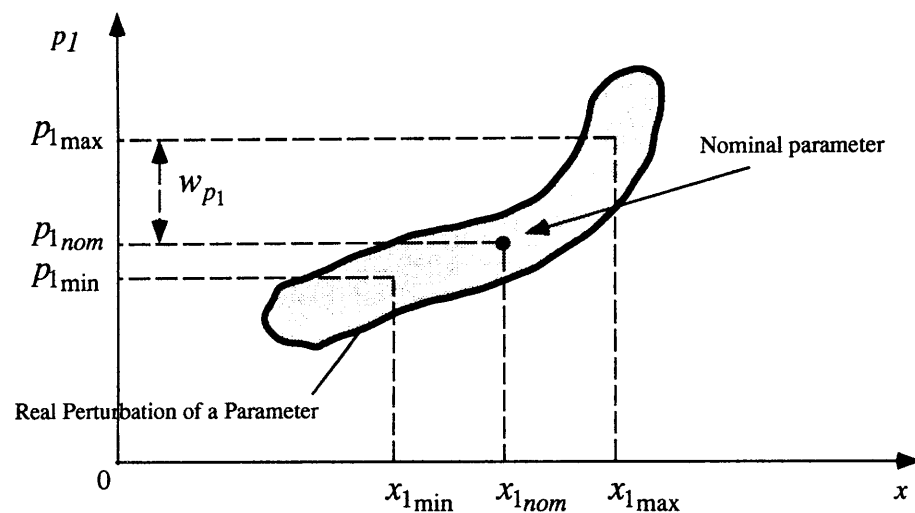
Figure 2.6: Parametric Uncertainty

(2) **set of linear models:**

This set is used in order to take the neglected linear dynamics into account. Here we assume that the plant can be represented as a following linear model.

$$
\begin{aligned}
x &= Ax + Bu, \\
y &= Cx, \qquad (2.60)
\end{aligned}
$$

where $A \in R^{n \times n}$, $B \in R^{n \times 1}$, and $C \in R^{1 \times n}$.

Prepare the $(k+1)$ combinations $(A_i, B_i), (i = 0, \dots, k)$, which are system matrices, and these are derived according to the precision/assumption of modeling. And we define that (A_0, B_0) represents a combination of nominal model. Hence the nominal

transfer function $G_{nom}(s)$ and the k magnitudes of perturbed dynamics are as follows.

$$G_{nom}(s) := C(sI - A_0)^{-1}B_0 \qquad (2.61)$$

$$\|W(j\omega)\|_\infty \geq \|C(j\omega I - A_i)^{-1}B_i - C(j\omega I - A_0)^{-1}B_0\|_\infty, \quad (i = 1, \dots, k) \qquad (2.62)$$

Hence the set of linear dynamics is written as,

$$G_i(s) := \{G_{i_{nom}}(s) + \Delta W(s) : \ \|\Delta\|_\infty \leq 1.\}. \qquad (2.63)$$

(3) **linear dynamics with nonlinear perturbations:** This set is employed in order to take the neglected nonlinear dynamics into account. Here we assume that the plant can be represented as a following nonlinear model.

$$
\begin{aligned}
\dot{x} &= f(x)x + Bu, \\
&= \{A + (f(x) - A)\}x + Bu, \\
&:= \{A + D(x)\}x + Bu, \qquad (2.64)
\end{aligned}
$$

where $f(x), D(x) \in R^{n \times n}$. If we put the bound of perturbation as follows.

$$|w_{ij}| = \max |d(x)_{ij}|, \quad i, j = 1, \dots, n, \qquad (2.65)$$

where w_{ij} is ij-element of the matrix $W \in R^{n \times n}$, and W is calculated by equation (2.65).

Then the set is written as

$$\dot{x} := \{(A + \sum_{i=1}^{k} \delta_i \hat{W}_i)x + Bu : \ |\delta_i| \leq 1\}, \qquad (2.66)$$

where $\hat{W}_i \in R^{n \times n}$.

The parametric uncertainty in the nominal system is reflected by the k scalar uncertain parameters $\delta_1, \dots, \delta_k$, and we can specify them, say by $\delta_i \in [-1, 1]$. The structural knowledge about the uncertainty is contained in the matrices $\hat{W}_i$. They reflect how the i'th uncertainty, δ_i, affects the state space model.

I apply this proposed iterative design procedure to robust control systems design in the following chapters, and evaluate this method.

Chapter 3

Robust Control of Magnetic Suspension Systems

Since magnetic suspension systems are unstable by nature, feedback control is always necessary. In order to synthesis a feedback controller, a precise mathematical model for the plant is required, however uncertainty is inevitable between the plant and the model. The controller is required to have robustness for stability against model uncertainties.

This chapter deals with two magnetic suspension systems. One is a simple SISO electromagnetic suspension system, and the other is a complicated MIMO magnetic bearing, the latter is an expansion and application of the former in a sense.

3.1 μ-Synthesis of an Electromagnetic Suspension System

This section deals with μ-synthesis of an electromagnetic suspension system. First, an issue of modeling a real physical electromagnetic suspension system is discussed. We derive a nominal model as well as a set of models in which the real system is assumed to reside. Different model structures and possible model parameter values are fully employed to determine unstructured additive plant perturbations, which directly yield uncertainty frequency weighting function. Second, based on the set of plant models, we setup robust performance control objectives. Third, we make use of the $D - K$ iteration approach for the controller design. Finally, implementing the controller with a digital signal processor, experiments are carried out. With these experimental results, we show robust performance of the designed control system.

3.1.1 Introduction

Electromagnetic suspension systems can suspend objects without any contact. The increasing use of this technology in its various forms makes the research extremely active. The electromagnetic suspension technology has already applied to magnetically levitated vehicles, magnetic bearings, and so on. Recent advances on this field are shown in [1], [32].

Feedback control is indispensable for magnetic suspension systems, since they are essentially unstable systems. In order to synthesis a feedback control system, a precise mathematical model for the plant is required. However it is known that a design model can not always express the behavior of the real physical plant. An ideal mathematical model has various uncertainties such as parameter identification errors, unmodeled dynamics, neglected nonlinearities. The controller is required to have robustness for stability and performance against uncertainties on the model.

Recently, μ-synthesis which is constructed with both H_∞ synthesis and μ-analysis, has been developed for the design of robust control systems [61], [74]. Beyond the singular value specifications, the μ-synthesis technique can put both robust stability and robust performance problems in a unified framework. Applications of the μ-synthesis method have been reported in [19]-[24], [75][78][79][34]. In the case of applications of H_∞/μ control to real physical systems, it is quite important to select appropriate design parameters. These parameters construct some parts of the generalized plant, e.g., uncertainty and performance weightings.

In this section, we evaluate μ-synthesis methodology experimentally with a real electromagnetic suspension system. We model the additive uncertainties and decide the frequency weighting function for uncertainty accurately and reasonably. Experimental results show that the closed-loop system with a μ controller achieves robust performance.

3.1.2 Experimental Setup

Electromagnetic Suspension System

The structure of the electromagnetic suspension system is shown schematically in Figure 3.1. The objective of our control experiments is to suspend an iron ball stably and firmly without any contact by controlling the attractive forces of an electromagnet. Note that this system is essentially unstable.

In Figure 3.1, a cylindrical electromagnet as an actuator is located at the upper part

of the experimental system. Mass of the iron ball is 1.75 kg, and it has a diameter of 77 mm. A gap sensor of our own producing is placed at the bottom of the system to measure the gap length between the iron ball and the electromagnet. The sensor is scaled for a gap of 2.4 mm per volt. It is a standard induction probe of eddy-current type. Physical parameters of this experimental machine are shown in Table 3.1.
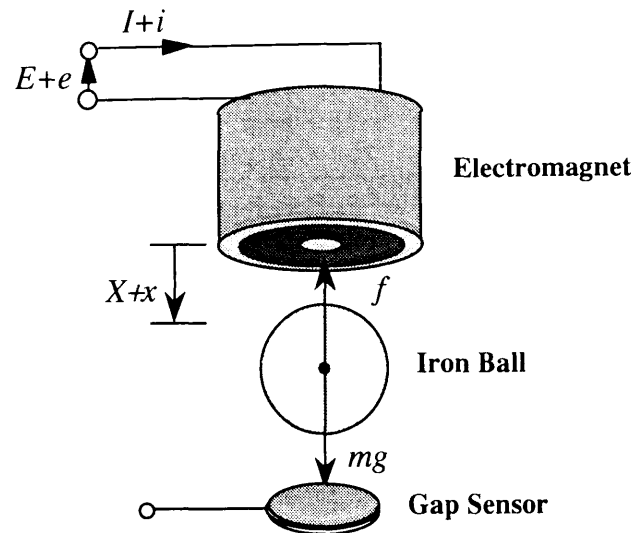

Figure 3.1: Schematic diagram of the Electromagnetic Suspension System

Digital Controller

The experimental machine is controlled by a digital controller using a DSP (Digital Signal Processor). The experimental setup basically consists of the DSP which is sandwiched between A/D and D/A converters. Real-time control is implemented with a processor NEC μPD77230, which can execute one instruction in 150 ns with 32-bit floating point arithmetic. This device has enough fast processing speed to stabilize a relatively simple magnetic suspension system in Figure 3.1. The control algorithm is written in the assembly language for the DSP and a software development is assisted by a host personal computer NEC PC-9801 under the MS-DOS environment. The data acquisition board MSP-77230 consists of a 12-bit A/D converter and a 12-bit D/A converter with the maximum conversion speed of 10.5 μs and 1.5 μs, respectively.

The sensor outputs are filtered through an analog low-pass circuit, and then converted to digital signals by A/D converters. The DSP calculates the control input signals. These digital signals are converted to analog signals by D/A converters with a range of ±5 V.

The converted signals and the steady current signals are added and amplified by 10 times to actuate the electromagnet. Steady state voltage of the electromagnet is 24.6 V and the maximum voltage of a regulated DC power supply is 70.0 V.

3.1.3   Model of Electromagnetic Suspension System

Our purpose in this section is to introduce an ideal mathematical model and an uncertainty weighting function for the system. See [23] for details.

Model Structures

We employ four different model structures for the system depicted in Figure 3.1. All of the models are finite-dimensional, linear, and time-invariant of the following state space form:

$$\dot{\boldsymbol{x}} = A\boldsymbol{x} + Bu, \quad y = C\boldsymbol{x} \tag{3.1}$$

$$\boldsymbol{x} = \begin{bmatrix} x & \dot{x} & i \end{bmatrix}^T, \quad u = e, \quad y = x,$$

First, we introduce ideal mathematical models for the real electromagnetic suspension system. Due to the idealizing assumptions that we make, two types of ideal mathematical models can be derived hereafter, which are composed of nonlinear differential equations. We define them as Type[A] and Type[B], respectively.

Since the behavior of the electromagnetic force is nonlinear, we then employ the linearization procedure around an operating point. In order to account for the neglected nonlinearity, we derive two types of linear model, respectively. Thus, we derive four linear models according to the following manners:

- **Model[A1]:** L =CONSTANT; and the nonlinearity of the electromagnetic forces are approximated up to the **first-order** term in the Taylor series expansion.

- **Model[A2]:** L =CONSTANT; and the nonlinearity of the electromagnetic forces are approximated up to the **second-order** term in the Taylor series expansion.

- **Model[B1]:** $L = L(x)$; and the nonlinearity of the electromagnetic forces are approximated up to the **first-order** term in the Taylor series expansion.

- **Model[B2]:** $L = L(x)$; and the nonlinearity of the electromagnetic forces are approximated up to the **second-order** term in the Taylor series expansion.

Ideal Mathematical Model: Type[A]

We derive ideal mathematical models for the real electromagnetic suspension system, where the following assumptions on the electromagnet are considered.

- **(A.1)** Magnetic permeability of the electromagnet is infinity.

- **(A.2)** Magnetic flux density and magnetic field have not hysteresis, and they are not saturated.

- **(A.3)** Eddy current in the magnetic pole can be neglected.

Using **(A.1)** and **(A.2)**, we can treat the coil inductance L as a function of variable x. Then, the system can be written by the following nonlinear differential equations

$$m\frac{d^2x}{dt^2} = mg - f, \quad f = k\left(\frac{i}{x+x_0}\right)^2, \quad e = Ri + \frac{d}{dt}\left\{L\left(x\right)i\right\}, \tag{3.2}$$

where the coefficients k and x_0 in (3.2) are constants determined by identification experiments. Further, we introduce another assumption for Type[A].

- **(A.A)** The coil inductance is constant near an operating point. Furthermore, the electromotive forces due to the differential of gap can be neglected.

Then from (3.2), we get

$$e = Ri + L_c\frac{di}{dt}. \tag{3.3}$$

The ideal mathematical model: Type[A] is represented by (3.2) and (3.3) .

Model[A1]

In view of (3.2) and (3.3), we can obtain the linear model (3.4); Model[A1]

$$A = \begin{bmatrix} 0 & 1 & 0 \\ \frac{2kI^2}{m(X+x_0)^3} & 0 & -\frac{2kI}{m(X+x_0)^2} \\ 0 & 0 & -\frac{R}{L} \end{bmatrix}, \quad B = \begin{bmatrix} 0 \\ 0 \\ \frac{1}{L} \end{bmatrix}, \quad C = \begin{bmatrix} 1 \\ 0 \\ 0 \end{bmatrix}^T. \tag{3.4}$$

Model[A2]

We can further obtain another linear model (3.5); Model[A2].

$$A = \begin{bmatrix} 0 & 1 & 0 \\ \frac{2kI^2}{m(X+x_0)^3}\Delta y & 0 & -\frac{2kI}{m(X+x_0)^2}\Delta y \\ 0 & 0 & -\frac{R}{L} \end{bmatrix}, \quad B = \begin{bmatrix} 0 \\ 0 \\ \frac{1}{L} \end{bmatrix}, \quad C = \begin{bmatrix} 1 \\ 0 \\ 0 \end{bmatrix}^T, \tag{3.5}$$

$$\Delta x = \frac{x}{X+x_0}, \quad \Delta i = \frac{i}{I}, \quad \Delta y = 1 - \frac{3}{2}\Delta x + \frac{1}{2}\Delta i.$$

In this way, we deal with the deviation x and i as fixed numbers, at the second-order term in the Taylor series expansion and include them in the matrix A as Δx, Δi and Δy.

Ideal Mathematical Model: Type[B]

For the ideal mathematical model Type[B], we also consider the assumptions; (A.1), (A.2), (A.3) and here in addition to them, we introduce the next assumption (A.B) instead of (A.A). Using this assumption, we can obtain more accurate model than one of Type[A].

- **(A.B)**   The coil inductance L is a function of a gap x, and written as follows.

$$L\left(x\right) = \frac{Q}{x+X_\infty} + L_0 \tag{3.6}$$

where the coefficients Q, X_∞ and L_0 are also the constants determined by identification experiments. For any given current i in a coil with inductance L, the magnetic co-energy is shown as $\frac{1}{2}Li^2$. Hence electromagnetic forces between the electromagnet and the iron ball in (3.2) is equal to the change rate of co-energy with respect to the distance x, i.e.,

$$f = \frac{\partial}{\partial x}\left\{\frac{1}{2}L\left(x\right)i^2\right\} = \frac{1}{2}i^2\frac{\partial L\left(x\right)}{\partial x} = \frac{Q}{2}\left(\frac{i}{x+X_\infty}\right)^2. \tag{3.7}$$

Comparing (3.2) with (3.7)

$$X_\infty = x_0, \quad Q = 2k \tag{3.8}$$

Then from (3.2), (3.6) and (3.8), we get

$$e = Ri - \frac{2ki}{(x+x_0)^2}\frac{dx}{dt} + \left(\frac{2k}{x+x_0} + L_0\right)\frac{di}{dt}. \tag{3.9}$$

Now we obtained the ideal mathematical model: Type[B] which is constructed with (3.2) and (3.9).

Model[B1]

From (3.2) and (3.9), the linear model (3.10); Model[B1] is derived.

$$A = \begin{bmatrix} 0 & 1 & 0 \\ \frac{2kI^2}{m(X+x_0)^3} & 0 & -\frac{2kI}{m(X+x_0)^2} \\ 0 & \frac{2kI}{(X+x_0)\{2k+L_0(X+x_0)\}} & -\frac{R(X+x_0)}{2k+L_0(X+x_0)} \end{bmatrix}, \quad B = \begin{bmatrix} 0 \\ 0 \\ \frac{X+x_0}{2k+L_0(X+x_0)} \end{bmatrix}, \quad C = \begin{bmatrix} 1 \\ 0 \\ 0 \end{bmatrix}^T. \tag{3.10}$$

Model[B2]

Moreover, the linear model (3.11); Model[B2] can be derived.

$$A = \begin{bmatrix} 0 & 1 & 0 \\ \frac{2kI^2}{m(X+x_0)^3}\Delta y & 0 & -\frac{2kI}{m(X+x_0)^2}\Delta y \\ 0 & \frac{2kI(1-2\Delta x+\Delta i)}{(X+x_0)\{2k(1-\Delta x)+L_0(X+x_0)\}} & -\frac{R(X+x_0)}{2k(1-\Delta x)+L_0(X+x_0)} \end{bmatrix}, \tag{3.11}$$

$$B = \begin{bmatrix} 0 \\ 0 \\ \frac{X+x_0}{L_0(X+x_0)+2k(1-\Delta x)} \end{bmatrix}, \quad C = \begin{bmatrix} 1 \\ 0 \\ 0 \end{bmatrix}^T.$$

Thus, now we obtained four linear model structures: **Model[A1]**, **Model[A2]**, **Model[B1]**, and **Model[B2]**.

Model Parameters

In order to account for unpredictable perturbations in the model parameters, we set the nominal value as well as the possible max./min. value of each parameter in every linear model. To obtain the possible max./min. value of each parameter, consider the steady-state gap $X=5.0$ mm (nominal). Now let us perturb it with $X=4.5$ mm and $X=5.5$ mm (perturbed ± 0.5 mm). And, for these cases, we measured the three sets of the parameter values. The results of measurements are shown in Table 3.1.

Nominal Model

We derive the nominal model using the simplest Model[A1] structure and the nominal model parameter ($X=5.0$ mm case). Its state space form is then of the following form

$$A_{nom} = \begin{bmatrix} 0 & 1 & 0 \\ 4481 & 0 & -18.43 \\ 0 & 0 & -45.69 \end{bmatrix}, \quad B_{nom} = \begin{bmatrix} 0 \\ 0 \\ 1.969 \end{bmatrix}, \quad C_{nom} = \begin{bmatrix} 1 \\ 0 \\ 0 \end{bmatrix}^T. \tag{3.12}$$

And the corresponding nominal transfer function is as follows.

$$G_{nom} = \frac{-36.27}{(s+66.94)(s-66.94)(s+45.69)}. \tag{3.13}$$

Modeling Unstructured Uncertainty

In order to account for unstructured uncertainties, we should consider not only a nominal model but also a set of plant models in which the real system is assumed to reside. Considering only unstructured uncertainties, we get all unstructured uncertainties together into 1-full block uncertainty.

In order to estimate the quantities of additive model perturbations, we employ differences of gain between the nominal transfer function and the perturbed transfer function with only one parameter changed and the others fixed, where we did not consider that plural parameters change together. In such a way, 24 perturbed models have been employed.

They are shown in Table 3.2. With these notations, we can define the corresponding perturbed transfer functions $\hat{G}_{ij}$ in an obvious way.

$$\Delta_{ij} := \hat{G}_{ij} - G_{nom} \quad (1 \leq i \leq 12, \ j = a, b). \tag{3.14}$$

Frequency responses of these additive perturbations $|\Delta_{ij}(j\omega)|$ are plotted in Figure 3.2, with 24 dotted lines. Now let us consider the set of plant models. Here we assume the following form

$$\mathbf{G} := \{ G_{nom} + \Delta_{add} W_{add} : \|\Delta_{add}\|_\infty \leq 1 \}. \tag{3.15}$$

in which the real plant is assumed to reside. All of the uncertainties are captured in the normalized, unknown transfer function Δ_{add}. It is natural to choose the uncertainty weighting W_{add} as follows (shown in Figure 3.2). Here it should be noted that the magnitude of the uncertainty weighting W_{add} covers all the model perturbations shown in Figure 3.2.

$$W_{add} = \frac{1.4 \times 10^{-5} (1+s/8)(1+s/170)(1+s/420)}{(1+s/30)(1+s/35)(1+s/38)} \tag{3.16}$$

Table 3.1: **Parameters of Electromagnetic Suspension System**

Parameter	Max. value	Nominal value	Min. value
m [kg]	- - -	1.75	- - -
X [m]	5.50×10^{-3}	5.00×10^{-3}	4.50×10^{-3}
I [A]	1.18	1.06	0.93
x [m]	5.00×10^{-4}	0.00	-5.00×10^{-4}
i [A]	1.18×10^{-1}	0.00	-1.26×10^{-1}
L [H]	5.57×10^{-1}	5.08×10^{-1}	4.65×10^{-1}
R [Ω]	2.37×10^{1}	2.32×10^{1}	2.27×10^{1}
k [Nm^2/A^2]	3.35×10^{-4}	2.90×10^{-4}	2.53×10^{-4}
x_0 [m]	-3.32×10^{-4}	-6.41×10^{-4}	-9.42×10^{-4}
Q [Hm]	6.70×10^{-4}	5.79×10^{-4}	5.06×10^{-4}
x_∞ [m]	-3.32×10^{-4}	-6.41×10^{-4}	-9.42×10^{-4}
L_0 [H]	3.96×10^{-1}	3.75×10^{-1}	3.54×10^{-1}
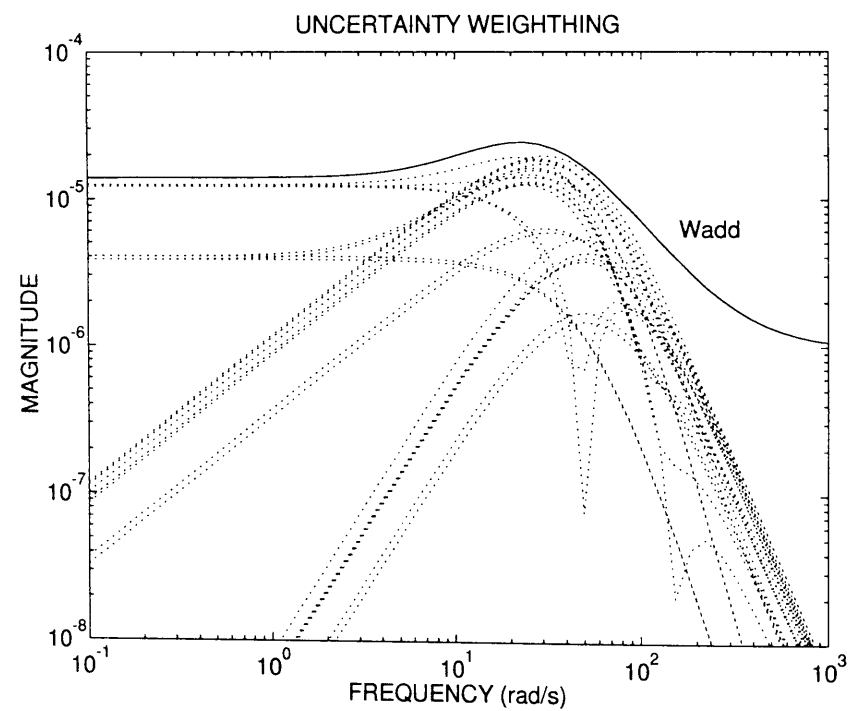
Figure 3.2: Uncertainty Weighting

Table 3.2: **Definition of Perturbed Models**

Perturbed Model	Model Structure	Parameter Change
model(1a)	Model[A1]	$k \rightarrow k_{max}$
model(1b)	Model[A1]	$k \rightarrow k_{min}$
model(2a)	Model[A1]	$x_0 \rightarrow x_{0max}$
model(2b)	Model[A1]	$x_0 \rightarrow x_{0min}$
model(3a)	Model[A1]	$R \rightarrow R_{max}$
model(3b)	Model[A1]	$R \rightarrow R_{min}$
model(4a)	Model[A1]	$L \rightarrow L_{max}$
model(4b)	Model[A1]	$L \rightarrow L_{min}$
model(5a)	Model[A2]	$x' \rightarrow x'_{max}$
model(5b)	Model[A2]	$x' \rightarrow x'_{min}$
model(6a)	Model[A2]	$i' \rightarrow i'_{max}$
model(6b)	Model[A2]	$i' \rightarrow i'_{min}$
model(7a)	Model[B1]	$k \rightarrow k_{max}$
model(7b)	Model[B1]	$k \rightarrow k_{min}$
model(8a)	Model[B1]	$x_0 \rightarrow x_{0max}$
model(8b)	Model[B1]	$x_0 \rightarrow x_{0min}$
model(9a)	Model[B1]	$R \rightarrow R_{max}$
model(9b)	Model[B1]	$R \rightarrow R_{min}$
model(10a)	Model[B1]	$L_0 \rightarrow L_{0max}$
model(10b)	Model[B1]	$L_0 \rightarrow L_{0min}$
model(11a)	Model[B2]	$x' \rightarrow x'_{max}$
model(11b)	Model[B2]	$x' \rightarrow x'_{min}$
model(12a)	Model[B2]	$i' \rightarrow i'_{max}$
model(12b)	Model[B2]	$i' \rightarrow i'_{min}$

3.1.4   Design

Control Objectives

Electromagnetic suspension system is essentially unstable. We must design a robust controller to stabilize the closed loop system, furthermore, we would like to design a controller to maintain the performance against unpredictable disturbances and the uncertainties.

Let us consider the feedback structure shown in Figure 3.3. The box represents the set of the models: **G** of the real system.
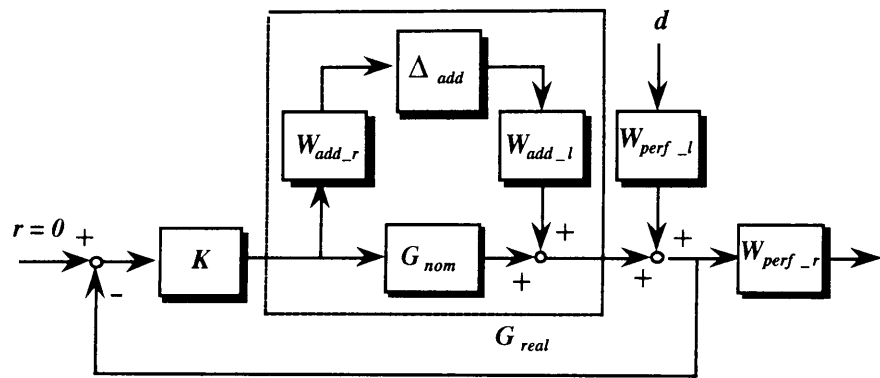
Figure 3.3: Feedback Structure

Robust stability requirement for the additive uncertainty can be evaluated using the closed-loop transfer function KS, where $S := (I + GK)^{-1}$. Hence robust stability test for $G \in \mathbf{G}$ is equivalent to

$$\left\| W_{add_r} K \left(I + G_{nom} K \right)^{-1} W_{add_l} \right\|_\infty < 1. \tag{3.17}$$

It is noted in Figure 3.3 that we factor the uncertainty weighting as $W_{add} = W_{add_l} \times W_{add_r}$, where

$$W_{add_l} = 1.0 \times 10^{-5}, \quad W_{add_r} = \frac{1.4 \times (1 + s/8)(1 + s/170)(1 + s/420)}{(1 + s/30)(1 + s/35)(1 + s/38)}. \tag{3.18}$$

In order to reject the disturbances at low frequency band, the performance weighting function W_{perf} is now chosen as follows.

$$W_{perf} = \frac{200.0}{1 + s/0.1} \tag{3.19}$$

We also factor the performance weighting as $W_{perf} = W_{perf_l} \times W_{perf_r}$, where

$$W_{perf_l} = 1.0 \times 10^{-5}, \quad W_{perf_r} = \frac{2.0 \times 10^7}{1 + s/0.1}. \tag{3.20}$$

In practical situation, however, we would like to achieve this performance specification for all the possible plant $G \in \mathbf{G}$. A necessary and sufficient condition for this robust performance is

$$\left\| W_{perf_r} \left(I + GK \right)^{-1} W_{perf_l} \right\|_\infty < 1, \ \forall G \in \mathbf{G}. \tag{3.21}$$

Now the control objective is to find a stabilizing controller K which achieves the following two conditions

- The closed-loop system remains internally stable for every plant model $G \in \mathbf{G}$,

- The weighted sensitivity function satisfies the performance test (3.21) for every plant $G \in \mathbf{G}$.

The design objectives have been specified as the requirements for particular closed loop transfer functions with the frequency weighting functions W_{add} and W_{perf}. The above control objectives exactly fit in the μ-synthesis framework by introducing a fictitious uncertainty block Δ_{perf}. Rearranging the feedback structure in Figure 3.3, we can build the interconnection structure shown in Figure 3.4.

Figure 3.4: Interconnection Structure

μ-Synthesis

We first define a block structure $\boldsymbol{\Delta}_P$ as

$$\boldsymbol{\Delta}_P := \left\{ \begin{bmatrix} \Delta_{add} & 0 \\ 0 & \Delta_{perf} \end{bmatrix} : \Delta_{add} \in \mathbf{C}, \Delta_{perf} \in \mathbf{C} \right\}. \tag{3.22}$$

Next, consider a generalized plant P partitioned as

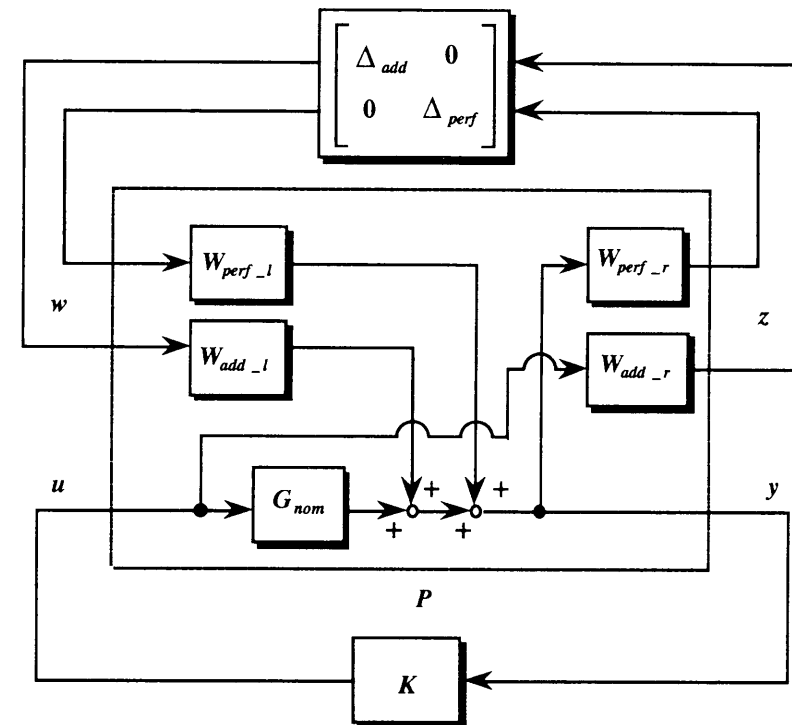$$P = \begin{bmatrix} P_{11} & P_{12} \\ P_{21} & P_{22} \end{bmatrix}. \tag{3.23}$$

Obviously in Figure 3.4, we can get a lower linear fractional transformation $\mathcal{F}_l(P,K)$ on P by K

$$\mathcal{F}_l(P,K) := P_{11} + P_{12}K \left(I - P_{22}K \right)^{-1} P_{21}. \tag{3.24}$$

Finally, **robust performance condition** is equivalent to the following structured singular value μ test

$$\sup_{\omega \in \mathbf{R}} \mu_{\boldsymbol{\Delta}_P} \left(\mathcal{F}_l(P,K)(j\omega) \right) < 1. \tag{3.25}$$

The complex structured singular value $\mu_{\boldsymbol{\Delta}_P}$ is defined as

$$\mu_{\boldsymbol{\Delta}_P}(M) := \frac{1}{\min \{ \bar{\sigma}(\Delta) : \Delta \in \boldsymbol{\Delta}, \, \det(I - M\Delta) = 0 \}}, \tag{3.26}$$

unless no $\Delta \in \boldsymbol{\Delta}$ makes $I - M\Delta$ singular, in which case $\mu_{\boldsymbol{\Delta}}(M) := 0$. In this case a matrix M in (3.26) belongs to $\mathbf{C}^{2 \times 2}$

D-K iteration

Unfortunately, it is not known how to obtain a controller K achieving the structured singular value test (3.25) directly. But we can obtain the lower and upper bounds of μ. Our approach taken here is the so-called $D - K$ iteration procedure.

The $D - K$ iteration involves a sequence of minimizations over either K or D while holding the other fixed, until a satisfactory controller is constructed. First, for $D = I$ fixed, the controller K_1 is synthesized using the well-known state space H_∞ optimization method. Let $P_1 = P$ denote the given open-loop interconnection structure in Figure 3.4, and $\mathcal{F}_l(P,K)$ be the closed-loop transfer function from the disturbances w to the errors z.

Then, solving the following H_∞ control problem

$$\|\mathcal{F}_l(P_1,K_1)\|_\infty < \gamma_1, \qquad \gamma_1 = 1.3. \tag{3.27}$$

The problem (3.27) yields the central controller K_1 below

$$
\begin{aligned}
K_1 \;=\; & \frac{-5.22 \times 10^8 (s + 12.46)(s + 30.0)(s + 35.0)(s + 38.0)}{(s + 0.10)(s + 31.6 - j5.12)(s + 31.6 + j5.12)(s + 39.77)} \\
& \times \frac{(s + 45.69)(s + 66.94)}{(s + 315.2 - j329.6)(s + 315.2 + j329.6)(s + 734.7)}.
\end{aligned}
\tag{3.28}
$$

Here we try to assess robust performance of this closed-loop system using μ-analysis associated with the block structure (3.22). The maximum singular value and μ upper bound of the closed-loop transfer function $\mathcal{F}_l(P_1, K_1)$ are plotted in Figure 3.5. It is noteworthy to point out that the peak value of the upper bound μ plot is not less than 1. This reveals that the closed-loop system with this H_∞ controller K_1 does not achieve robust performance condition.

Next, the above calculations of μ produce a scaling matrix at each frequency In this design, we try to fit the curve using a **1st order** transfer function.

Now, let P_2 denote the new open-loop interconnection structure absorbing the scaling matrix D. This time, from the following H_∞ control problem

$$\|\mathcal{F}_l(P_2, K_2)\|_\infty < \gamma_2, \qquad \gamma_2 = 1.0, \tag{3.29}$$

we can calculate the controller K_2 as follows.

$$
\begin{aligned}
K_2 \;=\; & \frac{-8.01 \times 10^9 (s + 10.54)(s + 15.75)(s + 30.0)(s + 35.0)(s + 38.0)}{(s + 0.10)(s + 19.59 - j5.32)(s + 19.59 + j5.32)(s + 38.48 - j2.70)(s + 38.48 + j2.70)} \\
& \times \frac{(s + 45.69)(s + 66.94)(s + 169.6)}{(s + 176.6)(s + 420.1 - j272.8)(s + 420.1 + j272.8)(s + 8180)}.
\end{aligned}
\tag{3.30}
$$

The maximum singular value and μ upper bound of this closed-loop system are plotted in Figure3.6. Since the value of μ is less than 1 in Figure 3.6, robust performance condition is now achieved.
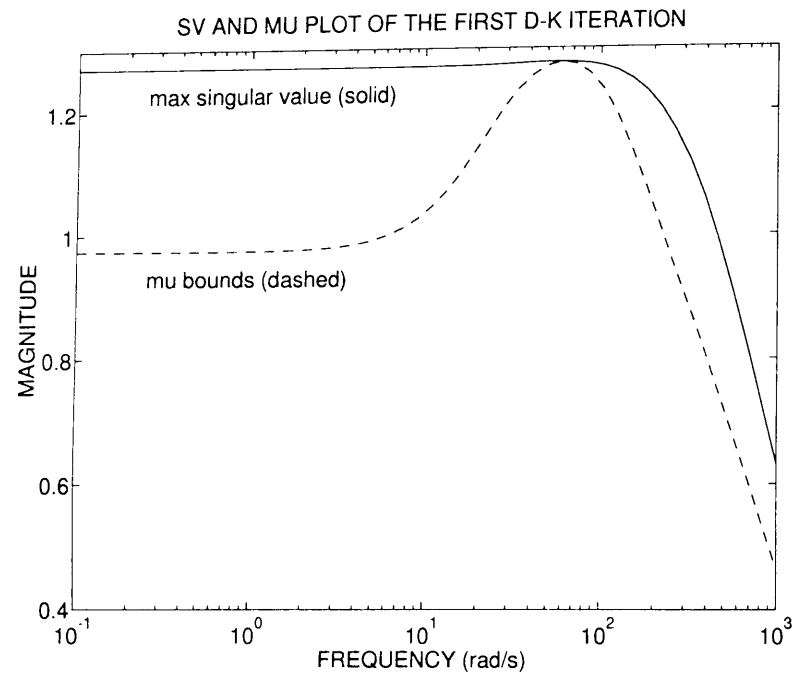
Figure 3.5: $\bar{\sigma}$ and μ plot of the first $D - K$ iteration
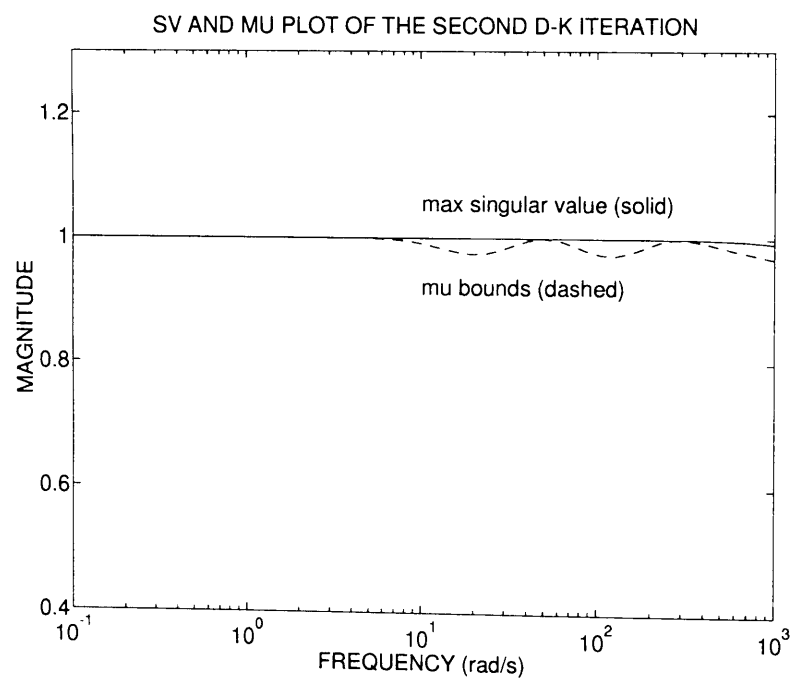
Figure 3.6: $\bar{\sigma}$ and μ plot of the second $D - K$ iteration

3.1.5 Experimental Results

The designed controllers K_1 and K_2 are continuous-time systems. In order to implement these two controllers with the digital controller, we discretized them via the well known Tustin transform. The controllers K_1 and K_2 are discretized at the sampling period of $45\mu s$ and $60\mu s$, respectively.

We succeeded in the stable suspension of the iron ball using both of the controllers K_1 and K_2. In the Section 4, robust stability and robust performance objectives were considered as the control problems. The obtained H_∞ controller K_1 achieves robust stability condition, and μ controller K_2 achieves not only robust stability but also robust performance specification. Hence, we evaluate robust performance as well as robust stability of the closed-loop systems with responses against various external disturbances.

There the disturbances are added to the experimental system as an applied voltage in the electromagnet. It is noted that there are four types of disturbances. Taking account that the steady-state force of the electromagnet is equal to 17.15 N, we added the following disturbance forces to the floating iron ball:

$$\text{downward } 17.15 \text{ N}, \quad \text{downward } 34.30 \text{ N},$$

These disturbances are large enough to evaluate the robustness of both these two controllers. Experimental results are shown in Figure 3.7 through Figure 3.10.
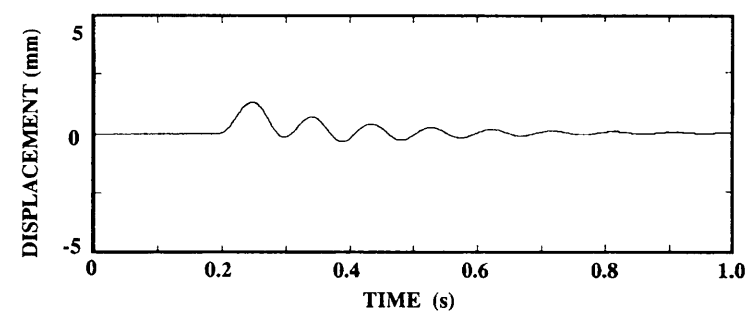
Figure 3.7: Response to step disturbance with $\mathbf{K_1}$ (-17.15N)
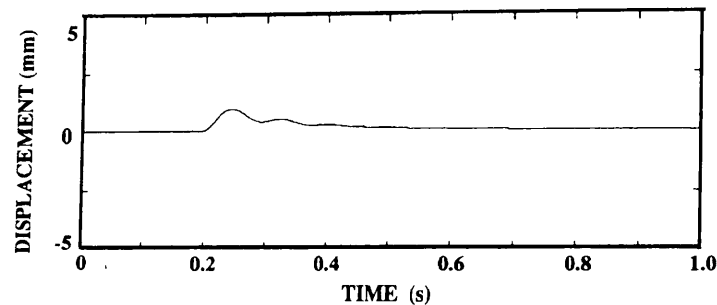
Figure 3.8: Response to step disturbance with **K₂** (-17.15N)
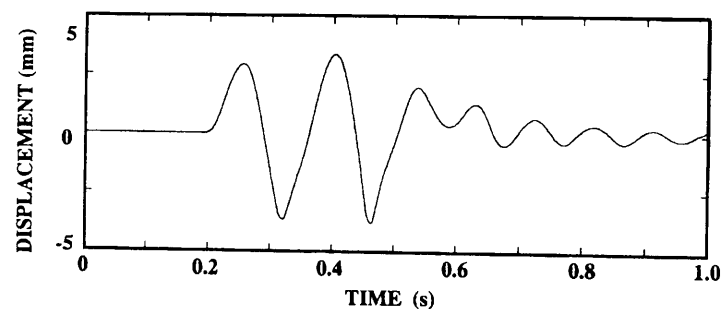
Figure 3.9: Response to step disturbance with **K₁** (-34.30N)
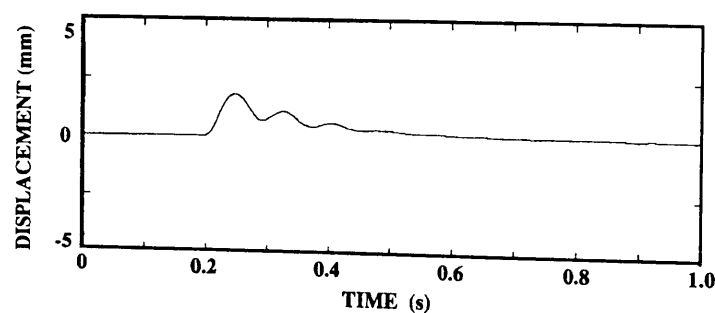
Figure 3.10: Response to step disturbance with **K₂** (-34.30N)

First of all, these experimental results in Figure 3.7 through Figure 3.10 show that the iron ball is suspended. Responses in Figure 3.9 are vibrating extremely, however, their vibration get on the decrease. This shows the closed-loop systems with both the controllers K_1 and K_2 remain stable against these disturbances. Comparing Figure 3.7 with Figure 3.9, the responses with K_1 deteriorate extremely against relatively large disturbances. While in Figure 3.8 and Figure 3.10, the responses with the controller K_2 maintain good transient responses against these disturbances. Now we can see the following observation.

- **The closed-loop system with the μ controller K_2 achieves robust performance, while the closed-loop system with the H_∞ controller K_1 does not.**

3.1.6   Conclusions

In this section, we experimentally evaluated a controller designed by μ-synthesis methodology with an electromagnetic suspension system. We have obtained a nominal mathematical model as well as a set of plant models in which the real system is assumed to reside. With this set of the models we designed the control system to achieve robust performance objective utilizing μ-synthesis method.

First, four types of different model structures were derived based on the several idealizing assumptions for the real system. Second, for every model, the nominal value as well as the possible maximum and minimum values of each model parameter was determined by measurements and/or experiments. Third, a nominal model was naturally chosen. This model has the simplest model structure of all four models and makes use of nominal parameter values. Then, model perturbations were defined to account for additive unstructured uncertainties from such as neglected nonlinearities and model parameter errors. Fourth, we defined a family of plant models where the unstructured additive perturbation was employed. The method to model the plant as belonging to a family or set plays a key role for systematic robust control design. Fifthly, we setup robust performance objective as a structured singular value test. Next, for the design, the $D - K$ iteration approach was employed. Finally, the experimental results showed that the closed-loop system with the μ-controller achieves not only nominal performance and robust stability, but in addition robust performance.

3.2   Gain Scheduled H_∞ Robust Control of a Magnetic Bearing

This section deals with the problem of an unbalance vibration of the magnetic bearing system. We design a control system achieving the elimination of the unbalance vibration, using a loop shaping design procedure (LSDP). After the introduction of our experimental setup, a mathematical model of the magnetic bearing is shown. Then, the gain scheduled H_∞ robust controllers with free parameters are designed, based on the LSDP, so as to reject the disturbances caused by unbalance on the rotor asymptotically even if the rotational speed of the rotor varies. Finally, several simulation and experimental results show the effectiveness of this proposed methodology.

3.2.1   Introduction

This section proposes a gain scheduled robust control scheme for a rotating active magnetic bearing (AMB) system. By using magnetic bearings, a rotor is supported without any contact. The technique of contact-less support for rotors becomes more important in the wide industrial application fields[50].

Imbalance in the rotor mass causes vibration in rotating machines. Balancing in the rotor is very difficult, there is often a residual imbalance. But, this imbalance problem can be conquered by active control. It is well known there are two methods to solve the above imbalance problem of magnetic bearings. The first method is to compensate for the unbalance forces by generating electro-magnetic forces that cancel these forces. The other method is to make the rotor rotate around its axis of inertia (automatic balancing). In this case no unbalance forces are produced. There are several effective methods in the literature to achieve automatic balancing in the magnetic bearings [65][33][55]. If the magnetic bearings should be applied to precision machines, however, the rotor would be expected to rotate around its geometrical axis, hence our approach taken here is the first method.

This section is concerned with the problems of the interference caused by gyroscopic effect and the problem of the vibration caused by unbalance on the rotor. In [19], the control system has been designed by using the Loop Shaping Design Procedure (LSDP) [44], and we have experimentally demonstrated their attenuating effect of the unbalance vibration. The attenuation was only achieved at the fixed-regular rotational speed of the

rotor in [19], however, the elimination of the variable unbalance vibration caused by the variable rotational speed is expected in the next step. The vibrations caused by unbalance of the rigid rotor can be modeled as frequency-varying sinusoidal disturbances. Hence, in this section, we propose the gain scheduled H_∞ controllers with the free parameter as a function of rotational speed to eliminate frequency-varying sinusoidal disturbances. This gain-scheduling approach is very simple and utilizes the free parameter of the H_∞ controller [76],[77]. The other gain-scheduling approaches for H_∞ control are reported in references [3][59][60][83].

Outline of this section is as follows. First, we introduce the magnetic bearing system, and derive the mathematical model of the system [18][47]. Next, we adopt the H_∞ problem with boundary constraints to the normalized Left Coprime Factor robust stabilization H_∞ problem [76][77], the conditions for existing of controller are derived with LSDP. Thirdly, we design the controllers that achieve asymptotic disturbance rejection and robust stability. Finally, we present simulation and experimental results with the obtained H_∞ controllers, and indicate the effectiveness of this proposed approach.

3.2.2   Modeling

Magnetic Bearing System

The magnetic bearing system employed in this research is a 4-axis controlled horizontal shaft magnetic bearing with symmetric structure, the axial motion is not controlled actively. The diagram of experimental machine is shown in Fig. 3.11. The diameter of the rotor is 96 mm and its span is equal 660 mm. A three-phase induction motor (1kW,four poles) is located at the center of the rotor. Around a rotor, four pairs of electromagnets are arranged radially on both sides. And four pairs of eddy-current type gap sensors are located on outside of the electromagnets. Further this system employs a tachometer in order to measure the rotational speed of the rotor. The experimental machine is controlled by a digital control system that consists of a 32-bit floating point Digital Signal Processor (DSP) DSP32C(AT&T), 12-bit A/D converters and 12-bit D/A converters. Using these systems, the final discrete-time controllers including a free parameter are computed on the DSP. The diagram of digital control system is shown in Fig. 3.12.
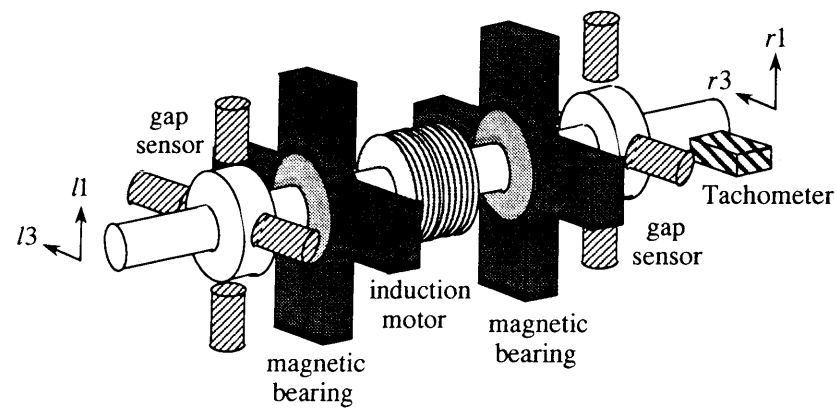
Figure 3.11: Diagram of Experimental Machine

Mathematical Model of the Magnetic Bearing

In this section, we derive the state equation of a magnetic bearing system with the following assumptions:

1. The rotor is rigid and has no unbalance.

2. All electromagnets are identical.

3. Attractive force of an electromagnet is in proportion to (electric current / gap length)^2.

4. The resistance and the inductance of the electromagnet coil are constant and independent of the gap length.

5. Small deviations from the equilibrium point are treated.

Based on the above assumptions, a mathematical model of a magnetic bearing has been derived in reference [47] [49], and the obtained result is as follows.

$$\begin{bmatrix} \dot{x}_v \\ \dot{x}_h \end{bmatrix} = \begin{bmatrix} A_v & pA_{vh} \\ -pA_{vh} & A_h \end{bmatrix} \begin{bmatrix} x_v \\ x_h \end{bmatrix} + \begin{bmatrix} B_v & 0 \\ 0 & B_h \end{bmatrix} \begin{bmatrix} u_v \\ u_h \end{bmatrix} + p^2 \begin{bmatrix} E_v \\ E_h \end{bmatrix} w \qquad (3.31)$$

$$\begin{bmatrix} y_v \\ y_h \end{bmatrix} = \begin{bmatrix} C_v & 0 \\ 0 & C_h \end{bmatrix} \begin{bmatrix} x_v \\ x_h \end{bmatrix} \qquad (3.32)$$

where the subscripts 'v' and 'h' in the vectors and the matrices stand for the vertical motion and the horizontal motion of the magnetic bearing, respectively. In addition, the subscript
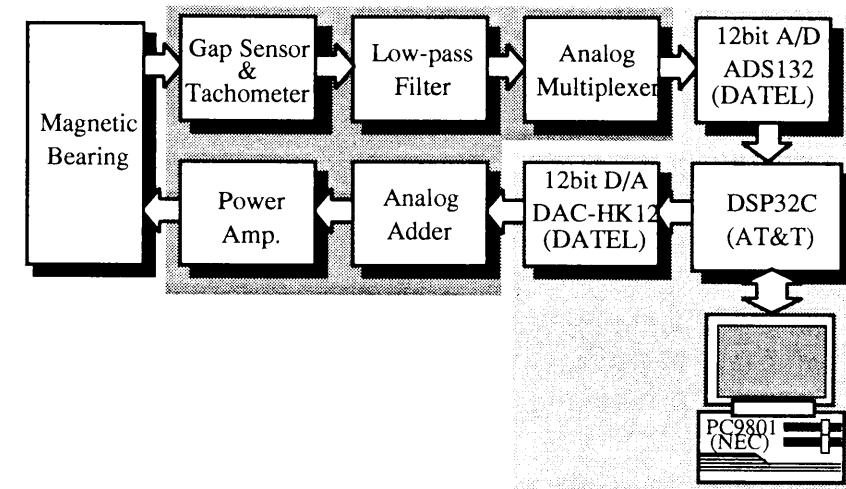
Figure 3.12: Digital Control System

'vh' stands for the interference term between the vertical motion and the horizontal motion, and p denotes the rotational speed of the rotor. Each vector in (3.31) and (3.32) can be defined as

$$\begin{aligned} x_v &= \begin{bmatrix} g_{l1} & g_{r1} & \dot{g}_{l1} & \dot{g}_{r1} & i_{l1} & i_{r1} \end{bmatrix}^T, \\ x_h &= \begin{bmatrix} g_{l3} & g_{r3} & \dot{g}_{l3} & \dot{g}_{r3} & i_{l3} & i_{r3} \end{bmatrix}^T, \\ u_v &= \begin{bmatrix} e_{l1} & e_{r1} \end{bmatrix}^T, \quad u_h = \begin{bmatrix} e_{l3} & e_{r3} \end{bmatrix}^T, \\ w &= \begin{bmatrix} \epsilon \sin(pt + \kappa) \\ \tau \cos(pt + \lambda) \\ \epsilon \cos(pt + \kappa) \\ \tau \sin(pt + \lambda) \end{bmatrix} \end{aligned} \qquad (3.33)$$

where

g_j : deviations from the steady gap lengths between the electromagnets and the rotor

i_j : deviations from the steady currents of the electromagnets

e_j : deviations from the steady voltages of the electromagnets

$\epsilon, \tau, \kappa, \lambda$: unbalance parameters [47][49]

$(j = l1, r1, l3, r3.)$

The subscripts $'l'$ and $'r'$ denote the left-hand side and the right-hand side of the magnetic bearing respectively, and the subscripts '1' and '3' denote one of the vertical directions and one the horizontal directions of the rotor respectively. Each matrix in (3.31) and (3.32) can be defined as follows.

$$A_v := \begin{bmatrix} 0 & I & 0 \\ A_1 + A_2 A_{4v} & 0 & A_2 A_{5v} \\ 0 & 0 & -(R/L)I \end{bmatrix},$$

$$A_h := \begin{bmatrix} 0 & I & 0 \\ A_1 + A_2 A_{4h} & 0 & A_2 A_{5h} \\ 0 & 0 & -(R/L)I \end{bmatrix},$$

$$A_{vh} := \begin{bmatrix} 0 & 0 & 0 \\ 0 & A_3 & 0 \\ 0 & 0 & 0 \end{bmatrix}, \qquad B_v = B_h := \begin{bmatrix} 0 \\ 0 \\ (1/L)I \end{bmatrix},$$

$$C_v = C_h := \begin{bmatrix} I & 0 & 0 \end{bmatrix}, \qquad E_v := \begin{bmatrix} 0 \\ E_{1v} \\ 0 \end{bmatrix}, \qquad E_h := \begin{bmatrix} 0 \\ E_{1h} \\ 0 \end{bmatrix},$$

$$A_1 := \frac{\alpha}{l_l + l_r} \begin{bmatrix} (l_r - l_m)\left(\frac{1}{m} - \frac{l_l l_m}{J_y}\right) & (l_l - l_m)\left(\frac{1}{m} - \frac{l_l l_m}{J_y}\right) \\ (l_r - l_m)\left(\frac{1}{m} + \frac{l_r l_m}{J_y}\right) & (l_l - l_m)\left(\frac{1}{m} + \frac{l_r l_m}{J_y}\right) \end{bmatrix},$$

$$A_2 := \begin{bmatrix} -\frac{1}{m} - \frac{l_l^2}{J_y} & -\frac{1}{m} + \frac{l_l l_r}{J_y} \\ -\frac{1}{m} + \frac{l_l l_r}{J_y} & -\frac{1}{m} - \frac{l_r^2}{J_y} \end{bmatrix},$$

$$A_3 := \frac{J_x}{J_y(l_l + l_r)} \begin{bmatrix} -l_l & l_l \\ l_r & -l_r \end{bmatrix},$$

$$A_{4v} := -\frac{2}{W} diag[F_{l1} + F_{l2}, \; F_{r1} + F_{r2}],$$

$$A_{4h} := -\frac{2}{W} diag[F_{l3} + F_{l4}, \; F_{r3} + F_{r4}],$$

$$A_{5v} := 2 diag\left[\frac{F_{l1}}{I_{l1}} + \frac{F_{l2}}{I_{l2}}, \; \frac{F_{r1}}{I_{r1}} + \frac{F_{r2}}{I_{r2}}\right],$$

$$A_{5h} := 2 diag\left[\frac{F_{l3}}{I_{l3}} + \frac{F_{l4}}{I_{l4}}, \; \frac{F_{r3}}{I_{r3}} + \frac{F_{r4}}{I_{r4}}\right],$$

$$E_{1v} := \begin{bmatrix} -1 & l_l\left(1 - \frac{J_x}{J_y}\right) & 0 & 0 \\ -1 & -l_r\left(1 - \frac{J_x}{J_y}\right) & 0 & 0 \end{bmatrix},$$

$$E_{1h} := \begin{bmatrix} 0 & 0 & 1 & l_l\left(1 - \frac{J_x}{J_y}\right) \\ 0 & 0 & 1 & -l_r\left(1 - \frac{J_x}{J_y}\right) \end{bmatrix}.$$

For the notations, as well as the parameter values, see Table 3.3. In the above equations,

Table 3.3: **Parameters of Experimental Machine**

Parameter	Symbol	Value	Unit
Mass of the Rotor	m	1.39×10^1	kg
Moment of Inertia about X	J_x	1.348×10^{-2}	kg $\cdot$ m^2
Moment of Inertia about Y	J_y	2.326×10^{-1}	kg $\cdot$ m^2
Distance between Center of Mass and Left Electromagnet	l_l	1.30×10^{-1}	m
Distance between Center of Mass and Right Electromagnet	l_r	1.30×10^{-1}	m
Distance between Center of Mass and Motor	l_m	0	m
Steady Attractive Force	$F_{l1,r1}$	9.09×10	N
	$F_{l2\sim l4}$	2.20×10	N
	$F_{r2\sim r4}$	2.20×10	N
Steady Current	$I_{l1,r1}$	6.3×10^{-1}	A
	$I_{l2\sim l4}$	3.1×10^{-1}	A
	$I_{r2\sim r4}$	3.1×10^{-1}	A
Steady Gap	W	5.5×10^{-4}	m
Resistance	R	1.07×10	Ω
Inductance	L	2.85×10^{-1}	H

α denotes the coefficient of the force which occurs when the rotor eccentrically deviates, and hence we set $\alpha = 0$. The numerical values of these matrices can be easily obtained with Table 3.3, and the result is written in reference [18].

3.2.3 H_∞ Gain Scheduling

In order to attenuate the unbalance vibration of the rotor, we design the robust H_∞ controllers which achieve the sinusoidal disturbance rejection asymptotically. As is well known, the controllers must have the imaginary poles at the frequencies corresponding to the rotational speed to possess high stiffness. For such a control system design, the LSDP based on the normalized Left Coprime Factor (LCF) robust stabilization method [44] is employed. Using the free parameter method which have been proposed in the reference [19], it is possible to obtain the gain scheduled controllers by the free parameter as the

function of rotational speed. We therefore show the condition for existing of controllers, by adopting the control problem with boundary constraints [76][77] to the normalized LCF robust stabilization problem, and we design a robust controller which satisfies the derived specifications using the LSDP.

Let (N, M) represent a normalized left coprime factorization of a plant G. Let these coprime factors be assumed to have uncertainties Δ_N, Δ_M and let G_Δ represent the plant with these uncertainties.

$$
\begin{aligned}
G_\Delta &= M_\Delta^{-1} N_\Delta \\
&= (M + \Delta_M)^{-1}(N + \Delta_N)
\end{aligned}
\tag{3.34}
$$

where N_Δ and M_Δ represent a left coprime factorization of G_Δ, and

$$
\Delta = \{[\,\Delta_N, \quad \Delta_M\,] \in RH_\infty \,;\, \|[\,\Delta_N, \quad \Delta_M\,]\|_\infty < \varepsilon\}.
\tag{3.35}
$$

G_Δ can be written in the form of an Upper Linear Fractional Transformation (ULFT) as follows.

$$
\begin{aligned}
G_\Delta &= F_U(P, \Delta) \\
&= P_{22} + P_{21}\Delta(I - P_{11}\Delta)^{-1}P_{12},
\end{aligned}
\tag{3.36}
$$

where

$$
P = \left[\begin{array}{c|c} P_{11} & P_{12} \\ \hline P_{21} & P_{22} \end{array}\right] = \left[\begin{array}{c|c} 0 & I \\ \hline M^{-1} & G \\ \hline M^{-1} & G \end{array}\right].
\tag{3.37}
$$

The robust stabilization problem for the *perturbed* plant G_Δ can be treated as the next H_∞ control problem:

$$
\left\| \begin{bmatrix} K \\ I \end{bmatrix} (I - GK)^{-1}M^{-1} \right\|_\infty \le \varepsilon^{-1} := \gamma
\tag{3.38}
$$

It is known that the solution of this problem and the largest number of ε ($= \epsilon_{\max} := \gamma_{\min}$) can be obtained by solving two Riccati equations without iterative procedure. All controllers K satisfying (3.38) are given by

$$
K = F_L(K_a, \Phi) := K_{11} + K_{12}\Phi(I - K_{22}\Phi)^{-1}K_{21},
\tag{3.39}
$$

where

$$
K_a = \left[\begin{array}{c|c} K_{11} & K_{12} \\ \hline K_{21} & K_{22} \end{array}\right],
\tag{3.40}
$$

$$
\|\Phi\|_\infty \le 1.
\tag{3.41}
$$

For the calculation of K_a and $\epsilon_{\max}$, see [44]. In order to eliminate the unbalance vibration of the rotor, which can be modeled as sinusoidal disturbances [47], the robust controller should be designed to achieve sinusoidal disturbance rejection asymptotically. In this case, as is well known, the controller must have the imaginary poles at the frequencies corresponding to the rotational speed of the rotor [76][77]. Hence, for the achievement of sinusoidal disturbance rejection whose frequency is ω_0 [rad/s], $K(s)$ is required to satisfy

$$
K(\pm j\omega_0) = \infty \iff \{I - G(\pm j\omega_0)K(\pm j\omega_0)\}^{-1} = 0.
\tag{3.42}
$$

We then derive the conditions, by adopting the H_∞ problem with boundary constraints [77] shown in Appendix to this problem, whereby there exist the controllers satisfying both (3.38) and (3.42). The boundary constraint $\{L, \Pi, \Psi\}$ corresponding to (3.42) is given by

$$
L = [\,0 \quad I\,], \quad \Pi = M(\pm j\omega_o), \quad \Psi = 0.
\tag{3.43}
$$

The basic constraint $\{L_B, \Psi_B\}$ in (3.66) (Appendix) is described by

$$
L_B = P_{12}^\perp(\pm j\omega_0) = [\,-G(\pm j\omega_0) \quad I\,],
\tag{3.44}
$$

$$
\Psi_B = P_{12}^\perp(\pm j\omega_0)P_{11}(\pm j\omega_0) = M^{-1}(\pm j\omega_0).
\tag{3.45}
$$

It is obvious that $\{L, \Pi, \Psi\}$ is satisfying condition (b) in Theorem A, and the extended boundary constraint $\{\hat{L}, \hat{\Psi}\}$ in (3.67) (Appendix) is given by

$$
\hat{L} = \begin{bmatrix} -G(\pm j\omega_0) & I \\ 0 & I \end{bmatrix}, \quad \hat{\Psi} = \begin{bmatrix} I \\ 0 \end{bmatrix}.
\tag{3.46}
$$

After some straightforward calculation, we have

$$
\gamma\bar{\sigma}\,(N(\pm j\omega_0)) > 1,
\tag{3.47}
$$

where

$$
\bar{\sigma}\,(N(\pm j\omega_0)) = \left(\frac{\bar{\sigma}^2\,(G(\pm j\omega_0))}{1 + \bar{\sigma}^2\,(G(\pm j\omega_0))}\right)^{1/2},
$$

$\bar{\sigma}\,(\bullet)$: the maximum singular value.

from the condition (c) of Theorem A.

If we choose free parameter $\Phi(s)$ such that

$$
\Phi(\pm j\omega_o) = K_{22}^{-1}(\pm j\omega_o)
\tag{3.48}
$$

under the conditions (3.41) and (3.47) , it can be seen that we obtain the controller with the imaginary poles at $\pm j\omega_0$ from (3.39) . Based on it, we design the control system using the Loop Shaping Design Procedure (LSDP) [44]. The procedure is briefly outlined below:

Loop Shaping Design Procedure (LSDP)

< Step 1> Loop Shaping

Selecting shaping function W_1 and W_2, the singular values of the nominal plant G are shaped to have a desired open loop shape. Let G_S represent this shaped plant

$$G_S = W_2 G W_1 \tag{3.49}$$

W_1 and W_2 should be selected such that G_S has no hidden unstable modes.

< Step 2 > Robust Stabilization

The maximum stability margin $\epsilon_{\max}$ is calculated. If $\epsilon_{\max} << 1$, return to Step 1, then W_1 and W_2 should be selected again. Otherwise, γ is appropriately selected as $\gamma \geq \gamma_{\min} = \epsilon_{\max}$ and K_a is calculated. The free parameter Φ is selected such as (3.48) under the conditions, then the H_∞ controller: $K_\infty(s)$ is synthesized for G_S from (3.39) .

< Step 3 > Final Controller

The final controller K can be obtained by the combination of W_1, W_2 and K_∞

$$K = W_1 K_\infty W_2 \tag{3.50}$$

In this procedure, $\epsilon_{\max}$ is treated as a design indicator rather than the maximum stability margin of G_S. Thus, we can design the robust controllers achieving sinusoidal disturbance rejection asymptotically using the LSDP. Moreover, utilizing the free parameter for such design, it is possible to obtain the gain scheduled controllers by scheduling the free parameter as the function of rotational speed of the rotor, which achieve the elimination of the unbalance vibration even if the rotational speed of the rotor varies.

The H_∞ controller: $K_\infty(s)$ with the free parameter Φ is shown as follows.

$$K_\infty = F_L(K_a, \Phi) \tag{3.51}$$

where

$$K_a = \left[\begin{array}{c|cc} A_{K_a} & B_{K_a 1} & B_{K_a 2} \\ \hline C_{K_a 1} & D_{K_a 11} & D_{K_a 12} \\ C_{K_a 2} & D_{K_a 21} & D_{K_a 22} \end{array}\right], \qquad \Phi = \left[\begin{array}{c|c} A_\Phi & C_\Phi \\ \hline B_\Phi & D_\Phi \end{array}\right]$$

Hence

$$K_\infty := \left[\begin{array}{cc|c} A_{K_\infty 11} & A_{K_\infty 12} & B_{K_\infty 1} \\ A_{K_\infty 21} & A_{K_\infty 22} & B_{K_\infty 2} \\ \hline C_{K_\infty 1} & C_{K_\infty 2} & D_{K_\infty} \end{array}\right]$$

$$= \left[\begin{array}{cc|c} A_{K_a} + B_{K_a 2} Z_0 C_{K_a 2} & B_{K_a 2} X_0 & B_{K_a 1} + B_{K_a 2} Z_0 D_{K_a 21} \\ Y_0 C_{K_a 2} & A_\Phi + Y_0 D_{K_a 22} C_\Phi & Y_0 D_{K_a 21} \\ \hline C_{K_a 1} + D_{K_a 12} Z_0 C_{K_a 2} & D_{K_a 12} X_0 & D_{K_a 11} + D_{K_a 12} Z_0 D_{K_a 21} \end{array}\right] \tag{3.52}$$

where

$$X_0 = (I - D_\Phi D_{K_a 22})^{-1} C_\Phi, \qquad Y_0 = B_\Phi (I - D_{K_a 22} D_\Phi)^{-1}, \qquad Z_0 = (I - D_\Phi D_{K_a 22})^{-1} D_\Phi.$$

Therefore the final H_∞ controller K is as

$$K = W_1 K_\infty W_2$$

where we define the weighting functions W_1 and W_2 as

$$W_1 = \left[\begin{array}{c|c} A_{W1} & C_{W1} \\ \hline B_{W1} & D_{W1} \end{array}\right], \qquad W_2 : \text{diagonal constant matrix}, \tag{3.53}$$

then

$$K = \left[\begin{array}{ccc|c} A_{W1} & B_{W1} C_{K_\infty 1} & B_{W1} C_{K_\infty 2} & B_{W1} D_{K_\infty} W_2 \\ 0 & A_{K_\infty 11} & A_{K_\infty 12} & B_{K_\infty 1} W_2 \\ 0 & A_{K_\infty 21} & A_{K_\infty 22} & B_{K_\infty 2} W_2 \\ \hline C_{W1} & D_{W1} C_{K_\infty 1} & D_{W1} C_{K_\infty 2} & D_{W1} D_{K_\infty} W_2 \end{array}\right]$$

$$= \left[\begin{array}{ccc|c} A_{W1} & B_{W1}(C_{K_a 1} + D_{K_a 12} Z_0 C_{K_a 2}) & B_{W1} D_{K_a 12} X_0 & B_{W1}(D_{K_a 11} + D_{K_a 21} Z_0 D_{K_a 21}) W_2 \\ 0 & A_{K_a} + B_{K_a 2} Z_0 C_{K_a 2} & B_{K_a 2} X_0 & (B_{K_a 1} + B_{K_a 2} Z_0 D_{K_a 21}) W_2 \\ 0 & Y_0 C_{K_a 2} & A_\Phi + Y_0 D_{K_a 22} C_\Phi & Y_0 D_{K_a 21} W_2 \\ \hline C_{W1} & D_{W1}(C_{K_a 1} + D_{K_a 12} Z_0 C_{K_a 2}) & D_{W1} D_{K_a 12} X_0 & D_{W1}(D_{K_a 11} + D_{K_a 12} Z_0 D_{K_a 21}) W_2 \end{array}\right].$$

$$\tag{3.54}$$

The block diagram of this final controller is shown in Fig. 3.13.

3.2.4   Controller Design

In this section, the feedback controllers are designed with the LSDP. We assume rotational speed $p = 0$ in the nominal plant G. In this case, we can see that there is no coupling
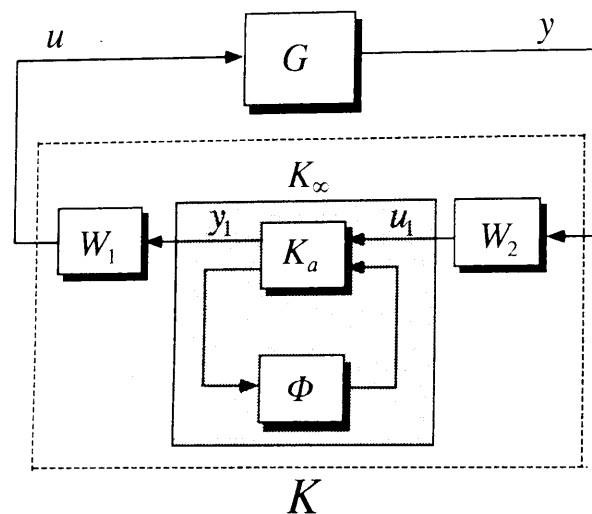
Figure 3.13: The gain scheduled H_∞ controller with the free parameter Φ

between the vertical motion and horizontal motion in (3.31). Therefore, the plant model can be separated into the vertical plant $G_v(s) := C_v(sI - A_v)^{-1}B_v$ and the horizontal plant $G_h(s) := C_h(sI - A_h)^{-1}B_h$, respectively.

$$G = \begin{bmatrix} G_v & 0 \\ 0 & G_h \end{bmatrix} \tag{3.55}$$

Then, two controllers are designed for the each plant, respectively. The final controller K for the entire plant G is constructed with the combination of these two controllers.

$$K = \begin{bmatrix} K_v & 0 \\ 0 & K_h \end{bmatrix} \tag{3.56}$$

where K_v denotes the controller for the vertical plant, and K_h denotes the controller for the horizontal plant. The shaping functions and the design parameters are selected as follows.

(v) Design for vertical motion

$$W_{1v}(s) = \frac{1300(1 + s/(2\pi \cdot 5))(1 + s/(2\pi \cdot 35))(1 + s/(2\pi \cdot 50))}{(1 + s/(2\pi \cdot 0.01))(1 + s/(2\pi \cdot 700))(1 + s/(2\pi \cdot 1200))} \begin{bmatrix} 1 & 0 \\ 0 & 1 \end{bmatrix} \tag{3.57}$$

$$W_{2v}(s) = 10000 \begin{bmatrix} 1 & 0 \\ 0 & 1 \end{bmatrix} \tag{3.58}$$

$$\epsilon_{v\_max} = 0.19944, \quad \epsilon_v^{-1} = \gamma_v = 5.25 \tag{3.59}$$

(h) Design for horizontal motion

$$W_{1h}(s) = \frac{1100(1 + s/(2\pi \cdot 5))(1 + s/(2\pi \cdot 25))(1 + s/(2\pi \cdot 40))}{(1 + s/(2\pi \cdot 0.01))(1 + s/(2\pi \cdot 700))(1 + s/(2\pi \cdot 1200))} \begin{bmatrix} 1 & 0 \\ 0 & 1 \end{bmatrix} \tag{3.60}$$

$$W_{2h}(s) = 10000 \begin{bmatrix} 1 & 0 \\ 0 & 1 \end{bmatrix} \tag{3.61}$$

$$\epsilon_{h\_max} = 0.27432, \quad \epsilon_h^{-1} = \gamma_h = 3.75. \tag{3.62}$$

In this design, verifying the condition (3.47), it can be seen that it is possible to design the controllers below $\omega_0 = 324.63$ [rad/s] ($p = 3100$ [rpm]) from Fig. 3.14.
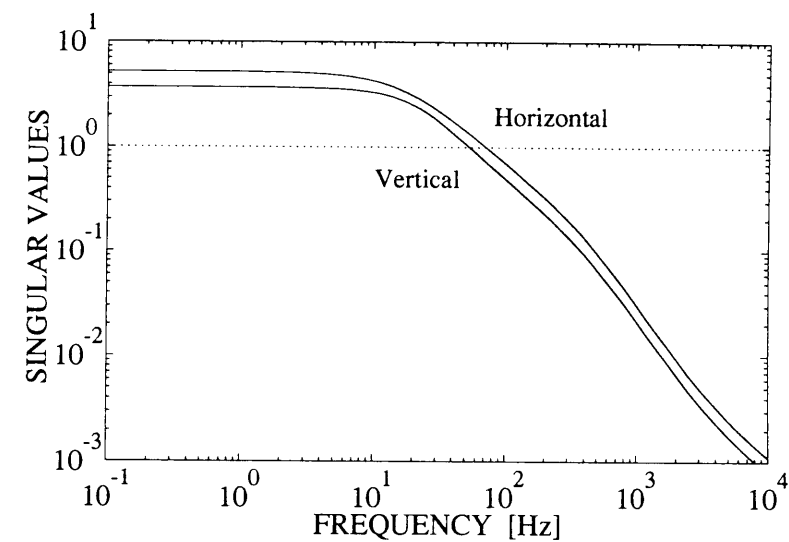
Figure 3.14: Magnitude of $\gamma\sigma(N_S)$

Hence we design the controllers within the above bound. In order to satisfy the conditions (3.41), the free parameters are selected as

$$\Phi_d(s) = C_{\Phi d}(sI - A_{\Phi d})^{-1}B_{\Phi d} \tag{3.63}$$

where

$$A_{\Phi d} = \begin{bmatrix} -a_d & 0 \\ 0 & -b_d \end{bmatrix}, \quad B_{\Phi d} = \begin{bmatrix} I \\ I \end{bmatrix}, \quad C_{\Phi d} = \begin{bmatrix} C_{\Phi 1 d} & C_{\Phi 2 d} \end{bmatrix}$$

$$C_{\Phi 1 d} = \frac{(a_d^2 + \omega_0^2)}{\omega_0(a_d - b_d)} \left\{ \omega_0 \Re(K_{22d}^{-1}(j\omega_0)) + b_d \Im(K_{22d}^{-1}(j\omega_0)) \right\}$$

$$C_{\Phi_2 d} = \frac{(b_d^2 + \omega_0^2)}{\omega_0(b_d - a_d)} \left\{ \omega_0 \Re(K_{22d}^{-1}(j\omega_0)) + a_d \Im(K_{22d}^{-1}(j\omega_0)) \right\}$$
$$(d = v, \ r)$$

Furthermore, in order to satisfy the condition (3.41), the parameters a_d, b_d of $A_{\Phi d}$ and $C_{\Phi d}$ are respectively adjusted as Table 3.2.4.

Table 3.4: **Parameters a_d, b_d of Free parameters**

Rotational speed (rpm)	a_v	b_v	a_h	b_h
1000 ~ 1600	2800	8	2800	8
1600 ~ 2200		16		16
2200 ~ 2600	2500	25	2500	27
2600 ~ 2900		37		36
2900 ~ 3100				40

When we obtain the shaped plants, a model reduction technique has been employed. The procedure of the model reduction is 'The Nominal Plant Model Reduction Procedure' as shown in [44, Procedure 5.5]. The order of the each shaped plant has been reduced from 12 states to 8. As a consequence, the final controller has 36 states. For an example, we show the frequency responses of the designed controller, which is denoted by K_{1300}, with $\omega_0 = 136.14$ [rad/s]$(p = 1300$ [rpm]). The singular values of the shaped plants and the open loop transfer functions are shown in Fig. 3.15. And Fig. 3.16 shows the singular values of the sensitivity functions. From these figures, we can see that sensitivity approaches zero at the frequency ω_0.

In this design, we ignored the interference terms, which express the gyroscopic effect, as $p = 0$. We therefore verify the robust stability of this system against changes in the rotational speed of the rotor. Let the perturbed plant $(p \neq 0)$ be denoted by G_p and the additive perturbation Δ_p of from G is as follows.

$$\Delta_p = G_p - G \tag{3.64}$$

Then the robust stability is guaranteed within the the following inequality (3.65).

$$\bar{\sigma}(\Delta_p) < \frac{1}{\bar{\sigma}(K(I - GK)^{-1})} \tag{3.65}$$

In Fig. 3.17, the singular values $1/\bar{\sigma}(K(I - GK)^{-1})$ and $\sigma(\Delta_p)$ at $\omega_0 = 1675.5$ [rad/s] $(p = 16000$ [rpm]) are plotted. From this analysis, we can see the closed-loop system is stable at $\omega_0 \leq 1675.5$ [rad/s].
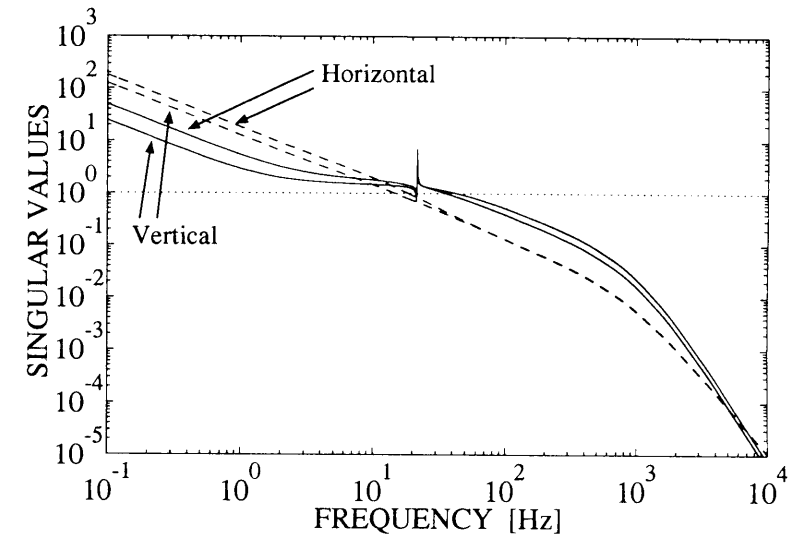
Figure 3.15: Open loop transfer functions $GK[$—$]$ and the shaped plant $G_S[--]$
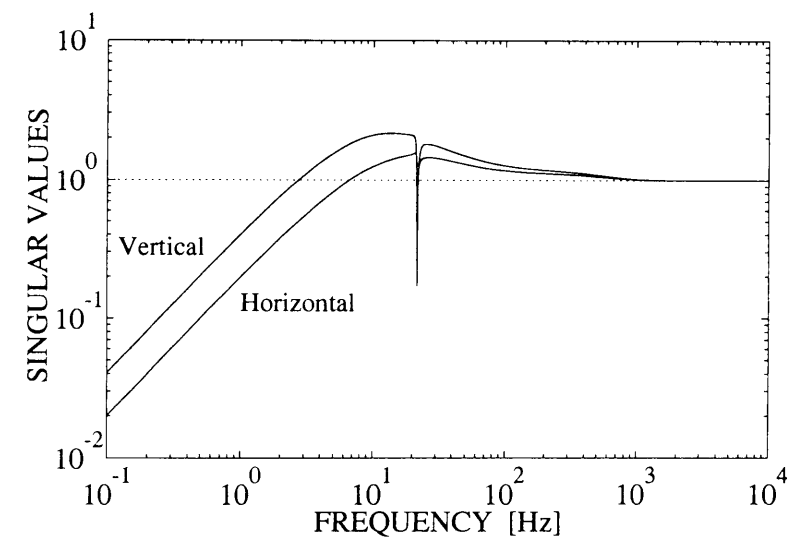
Figure 3.16: $\sigma((I - GK)^{-1})$
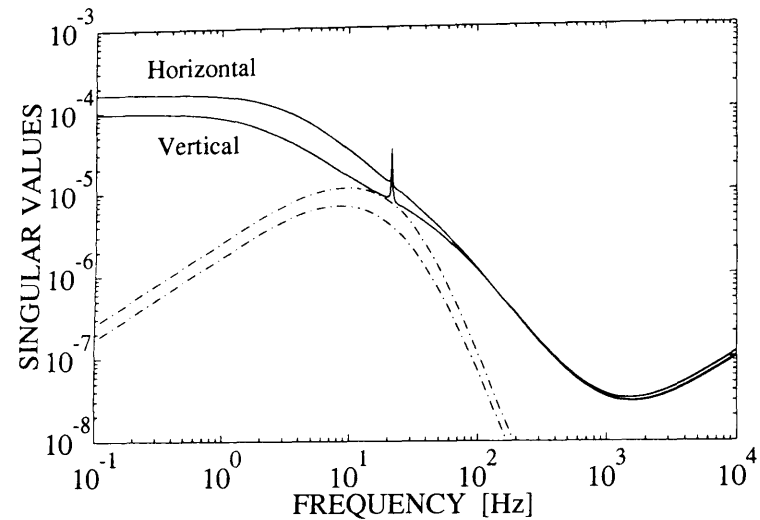
Figure 3.17: $1/\sigma(K(I - GK)^{-1})$ [——] and $\sigma(\Delta_p)[- \cdot -]$

3.2.5   Simulation Results

The simulation results based on the derived nominal mathematical model, which are carried out by using SIMULINK [8], are shown in Fig. 3.18 and Fig. 3.19. These figures show the displacement on the left side of the rotor when the rotational speed is varied at the rate of 2 rpm a second. For the comparison, the linear time invariant H_∞ controller K_{1300} was employed, where, the controller K_{1300} has the fixed pole at $f_0 = 1300/60 = 21.7$Hz, and no gain-scheduling is adopted.

The results with the time-invariant H_∞ controller: K_{1300} are shown in Fig. 3.18(a) and Fig. 3.18(b), which indicate the response of the rotor when the rotational speed is varied from 1200 rpm to 1400 rpm. And the corresponding results with the Gain Scheduled H_∞ controller K are shown in Fig. 3.19(a) and Fig. 3.19(b), respectively.

Fig. 3.18(a) and 3.19(a) show the vertical rotor displacement with the variable rotating speed, and Fig. 3.18(b) and 3.19(b) show the horizontal rotor displacement. From these simulation results, it can be seen that even if the rotational speed of the rotor varies, the unbalance vibration of the rotor is eliminated by the proposed Gain Scheduled H_∞ robust controllers.
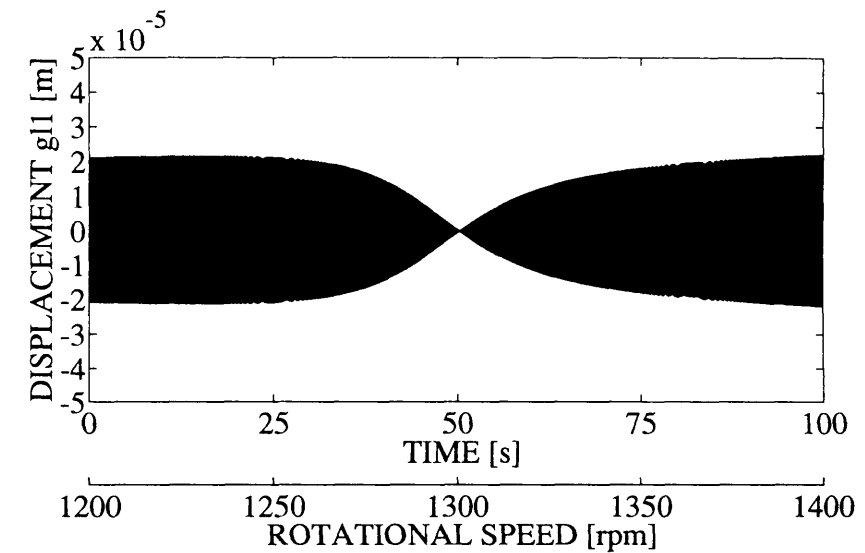
(a) Vertical case
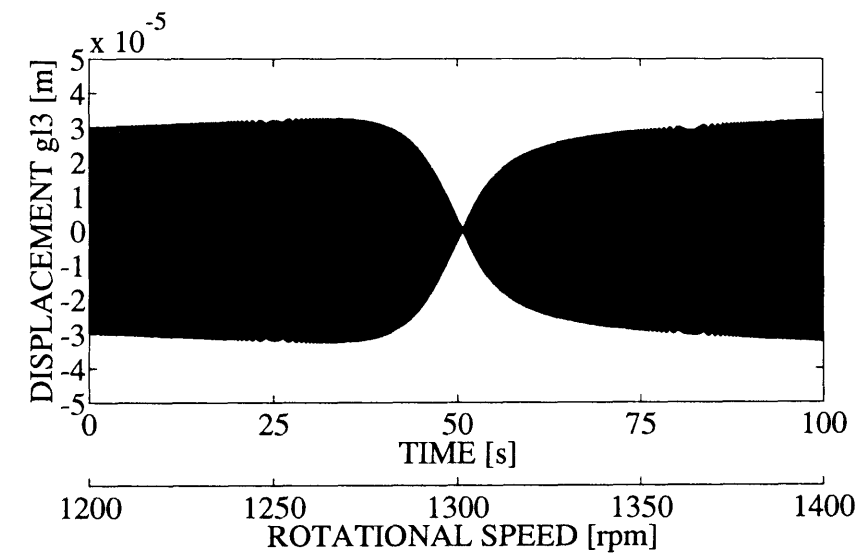
(b) Horizontal case

Figure 3.18: Displacement versus rotational speed with the controller K_{1300}
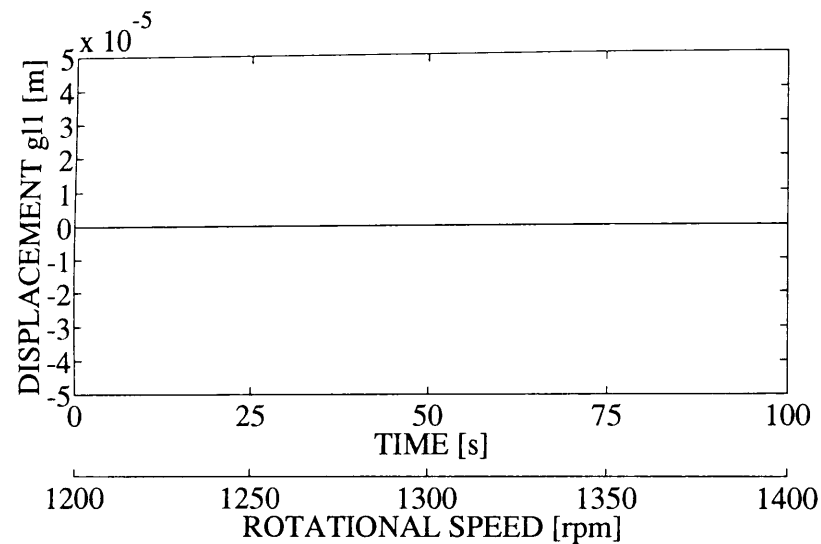
(a) **Vertical case**
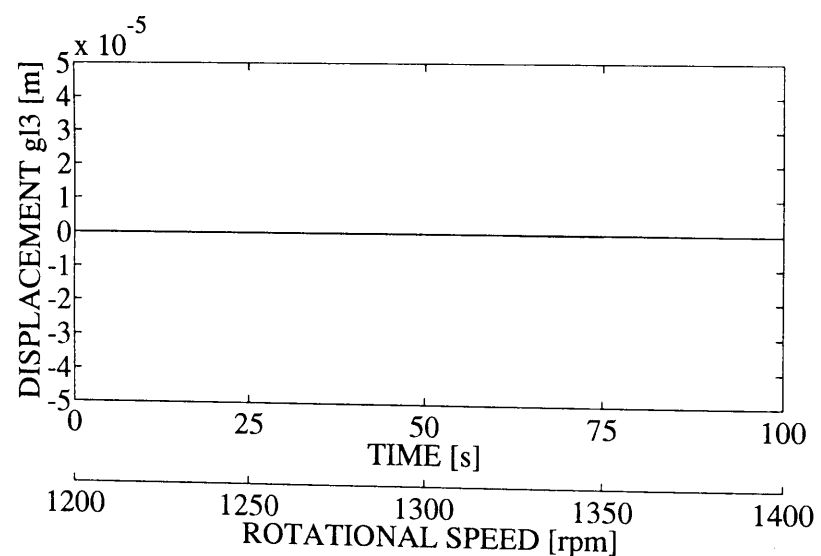
(b) **Horizontal case**

Figure 3.19: Displacement versus rotational speed with the gain scheduled H_∞ controller

3.2.6   Experimental Results

We have carried out experiments using the experimental machine shown in Fig. 3.11. In order to evaluate the practical effect of this proposed approach, the experimental tests were run within the limits of the rotational speed from 1000 to 1600 rpm (see Table 3.2.4).

The designed continuous-time controllers , K_{1300} and Gain Scheduled H_∞ controller are discretized via the well known Tustin transform at the sampling rates of $252\mu s$ and $415\mu s$, respectively.

The controller K_{1300} is linear invariant dynamical controller, hence the computing burden for real-time calculation of control input is only matrix multiplication and addition.

On the other hand, for the implementation of the gain scheduled H_∞ controller $K(\Phi)$, however, we have to renew $K(\Phi)$ every sampling period by using (3.54) . After it has obtained, the control input u is calculated. It takes longer time for the implementation of $K(\Phi)$.

All through the experiments, a small weight(20[g]) is attached at the left side of the rotor in Fig. 3.11 so as to increase the residual unbalance.

We have measured the orbits of the center of the rotor for a period of 0.5s under several conditions. Fig. 3.20(a), 3.20(b) and 3.20(c) show the results with K_{1300}, and Fig. 3.20(d), 3.20(e) and 3.20(f) show the results with Gain Scheduled H_∞ controller, at 1100, 1300 and 1500 rpm, respectively. Compared the Gain Scheduled H_∞ controller K with K_{1300}, the results with Gain Scheduled H_∞ controller K indicate better performance than the one with K_{1300} in the elimination of the unbalance vibration except at 1300 rpm.

However, it is well known that direct switching and interpolation between the controllers does not capture the dynamic effects and may lead to instability, even if the controllers can stabilize the closed-loop system for each frozen value in the parameter space. This is especially true if the scheduled parameter changes rapidly.

By the numerical simulation, we have confirmed that the closed-loop system is stable when the rotational speed changes at the rate of 2 rpm/s or less(see Fig. 3.18 and Fig. 3.19). If the rotational speed changes more than 2 rpm/s, the system became to be instable.

But magnetic bearing should be able to change the rotating speed, but it does not need high changing speed from a practical point of view. In this plant, due to the power limitation and the safety of the induction motor, the rotational speed can not be changed rapidly.

From a theoretical point of view, Gain Scheduled H_∞ controller should completely

attenuate the unbalance vibration even if the rotational speed of the rotor varies. However, this requirement for the performance have not been achieved completely. This performance deterioration may be due to measurement precision of the rotating speed. Gain Scheduled H_∞ controller relies on the accuracy of the rotational speed so much, and the bandwidth of the rotational speed that can eliminate the unbalance vibration is very narrow. Therefore if the signal of rotational speed includes some errors, effectiveness of the unbalance vibration suppression would be deteriorated.

Further investigation and experiments for the measurement precision of the rotating speed and the scheduled parameter's changing rate, will be made in the future.

3.2.7   Conclusion

In this section, we proposed the gain scheduled H_∞ robust control scheme with the free parameter for a magnetic bearing in order to eliminate the unbalance vibration. We treated the changing unbalance vibration caused by varying rotational speed as the known frequency-varying disturbance, and adjusted the controller gain according to the rotational speed of the rotor using the free parameter Φ of the H_∞ controller. The obtained controller K has high gain at the operating frequency.

First, the dynamics of the AMB system was considered and a nominal mathematical model for the system was derived. Next, the conditions for the existence of controllers were derived, and, we designed the gain scheduled H_∞ robust controllers using LSDP. It rejected the sinusoidal disturbance of the varying rotor speed.

Finally the simulations and experimental results showed the effectiveness of this proposed method.

(a) The fixed H_∞ controller K_{1300}: rotational speed: 1100 [rpm]
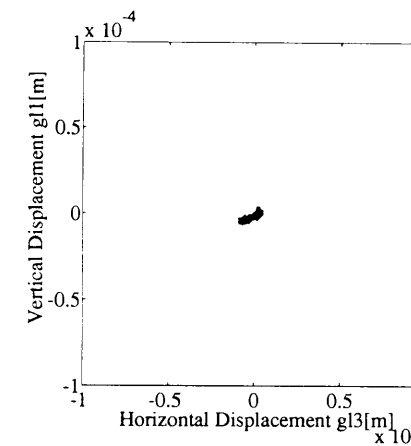
(b) The fixed H_∞ controller K_{1300}: rotational speed: 1300 [rpm]
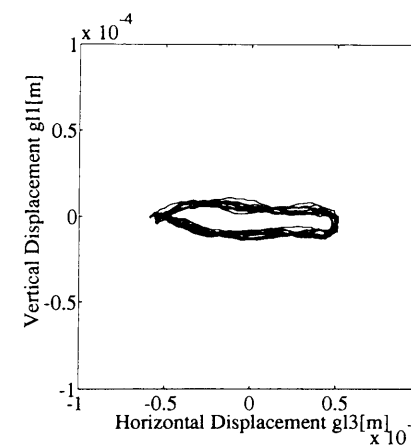
(c) The fixed H_∞ controller K_{1300}: rotational speed: 1500 [rpm]

Figure 3.20: Orbits of the center of the rotor
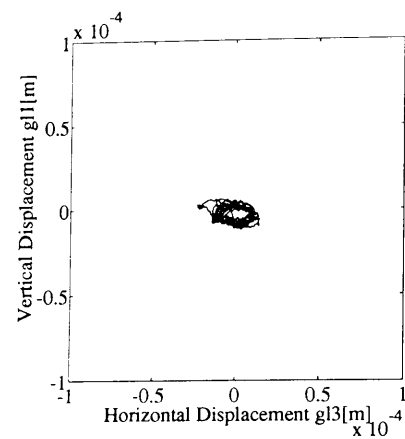
(d) The gain scheduled H_∞ controller: rotational speed: 1100 [rpm]
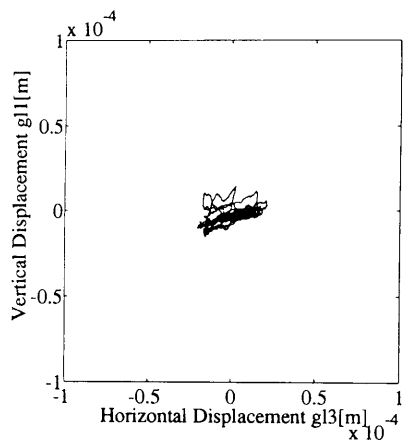
(e) The gain scheduled H_∞ controller: rotational speed: 1300 [rpm]
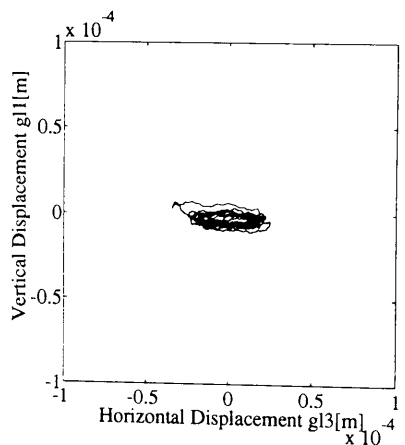
(f) The gain scheduled H_∞ controller: rotational speed: 1500 [rpm]

APPENDIX of Chapter 3

● **Definition A.** " H_∞ **problem with boundary constraints**"

Find the $K(s)$ satisfying

(s1) $K(s)$ stabilizes $F_U(P, 0)$,

(s2) $\|P_{zw}\|_\infty \le \varepsilon^{-1} := \gamma,$

(s3) $LP_{zw}(j\omega)\Pi = \Psi,$

where $P_{zw} = F_L(P,\ K)$

● **Definition B.** " **Basic constraints** "

$$L_B := P_{12}^\perp(j\omega), \quad \Psi_B := P_{12}^\perp(j\omega)P_{11}(j\omega) \tag{3.66}$$

where $P_{12}^\perp(s)P_{12}(s) = 0$

● **Definition C.** " **Extended constraints** "

$$\hat{L} := \begin{bmatrix} L_B \\ L \end{bmatrix}, \quad \hat{\Psi} := \begin{bmatrix} \Psi_B \Pi \\ \Psi \end{bmatrix} \tag{3.67}$$

where $\hat{L}$ and $\hat{\Psi}$ are row full rank.

Theorem A.

H_∞ problem with boundary constraints $\{L, \Pi, \Psi\}$ is solvable, iff the following three conditions hold:

(a) The H_∞ problem is solvable.

(b) $\text{rank} \begin{bmatrix} L_B & \Psi_B \Pi \\ L & \Psi \end{bmatrix} = \text{rank} \begin{bmatrix} L_B \\ L \end{bmatrix}.$

(c) $\hat{L}\hat{L}^* > \gamma^2 \hat{\Psi}(\Pi^*\Pi)^{-1} \hat{\Psi}^*.$

Chapter 4

Robust Control of Active Pantograph Systems

This chapter is concerned with robust force control for an experimental system of the pantograph with a Linear DC Motor. Recently higher train speeds have caused various problems such as power supply and aerodynamic noise. One of the approaches to solve these problems is to optimize the overhead wire-pantograph system. The low-noise pantograph is now being researched and developed, and needs active force control to stabilize the current. In this chapter, we use a Linear DC Motor (LDM) as an actuator of the pantograph in order to control the contact force between the overhead wiring and the pantograph. An experimental machine has been designed and developed, and has an oscillatory characteristic. We designed the robust force controller for the system in order to improve step response and the frequency-domain performance by considering model parameter perturbation and unmodeled dynamics.

At first, the experimental machine and the digital controller of the active pantograph system are introduced. Next, its linearized model is formulated in a state-space form. Then, μ controller is designed by considering parametric uncertainty and unmodeled dynamics. Finally, the several experiments are carried out so as to evaluate the control performance of the designs, where the proposed control scheme is compared with the conventional H_∞ control.

In section 3.1, uncertainties caused by a change of the operation point is written as just a unstructured uncertainty, in this chapter, however, I express the various types of uncertainties as structured in order to reduce conservativeness of the robustness evaluation.

4.1 Introduction

Recently the research for high-speed train has been done, especially for pantograph to supply electric power[26]. According to high speed, a resonance frequency of overhead wiring has become increasing, hence the present passive pantograph can not follow its vibration. Further disturbance from wind and rain, and vibration from the train body disturb a pressure between an overhead wiring and a pantograph, which cause problems, e.g., injury of power supply, and abrasion of pantograph. Hence the research for active controlled-type pantograph has been started in order to regulate a pressure between a pantograph and overhead wiring[81][38]. T-type pantograph has been developed to reduce the noise which was made by wind pressure. This pantograph has a limited surface area, hence it is considered to be effective for reducing the wind noise[42].

In this research, our objective is to control of a simply constructed T-type pantograph with a linear direction motor(LDM) as an actuator, especially in order to regulate a contact force between a pantograph and overhead wiring in spite of various disturbance.

Linear direction motor has a characteristic as follows: simple architecture, quick motion is available, fine servo characteristic, and so on[37]. On the other hand, motor does not have servomechanism by itself, we have to do feedback control by using sensor.

Up to now, researches of pantograph control has been done by using an experimental system of pantograph [48][51][57]. In these research, LQ and H_∞ Control[25] for design was used. Pantograph is suffered by the force of the natural wind and rain, and wind caused by passing each other and tunnel. Further sharp drop in rail level brings disturbance, it should be robustly controlled. And it has an oscillating characteristic, so it needs to possess robust performance on the frequency range. Until today, research for active pantograph [48][51][57][85] has been done, but the resulting robust performance is not enough at the resonance frequency. Further, at the resonance frequency, motion range of mover become wide, that varies the value of model parameters, especially electro-force constant K_a.

Hence, we measure uncertainties, model variations, and unmodeled dynamics by experiments. We setup the robust performance problem by using μ-synthesis for those uncertainties, and improve a frequency characteristic for disturbance. There are several reports which utilize μ-synthesis [34][78][79][24], and show the effectiveness of μ-synthesis. In this research, we focus on parametric uncertainties caused by mover, and unmodeled dynamics, and measure it by experiments and clarify a meaning of physical uncertainties. At last, several experimental results show the effectiveness of this design methodology.

4.2 Experimental Equipment

4.2.1 Pantograph Experimental Equipment

A rough sketch of T-type pantograph experimental machine is shown in Fig.4.1. This pantograph is in the shape of capital t from the front, as its name, it moves vertically to train and overhead wiring. It has small front area against a present diamond-shaped pantograph[26].
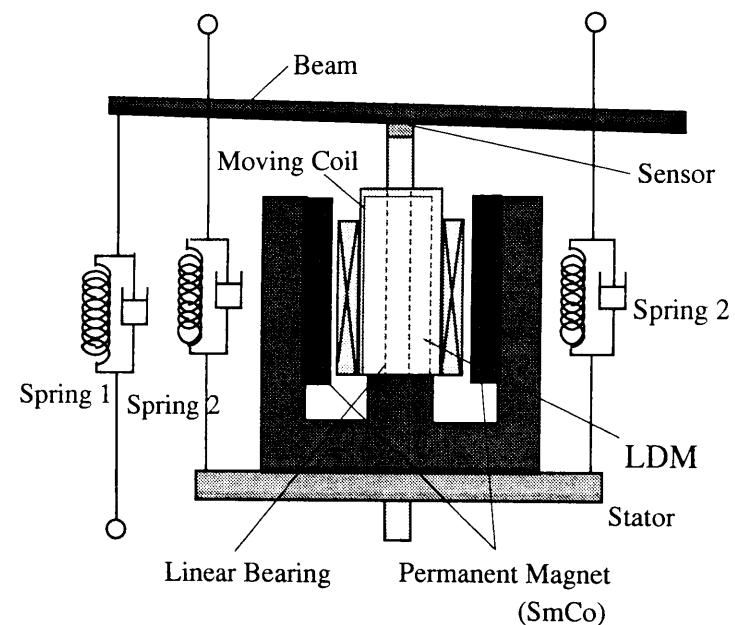
Figure 4.1: Experimental System

The system is formulated mathematically by the differential equations of overhead wiring, pantograph, train, and all their connections[85][43]. As an actuator, LDM is employed, where this LDM is included Moving Coil Type LDM, especially it is called Voice Coil Motor(VCM) in it. This type of LDM is characteristics of good servomechanism. Mover goes up and down along the rail when an electric current is sent to LDM. By controlling this current, we can regulate the pressure to be constant (20[N]) between beam and mover under no disturbance. Our objective is to control the pressure to be 20[N] against various disturbance. LDM is attached on stater, and stater is supported by four springs at the corners, and beam is supported by spring at the tip, hence beam and the stater moves oscillatory. Force sensor is attached at the tip of the mover. The beam is correspondent with overhead wiring and the mover with pantograph, and stater with train
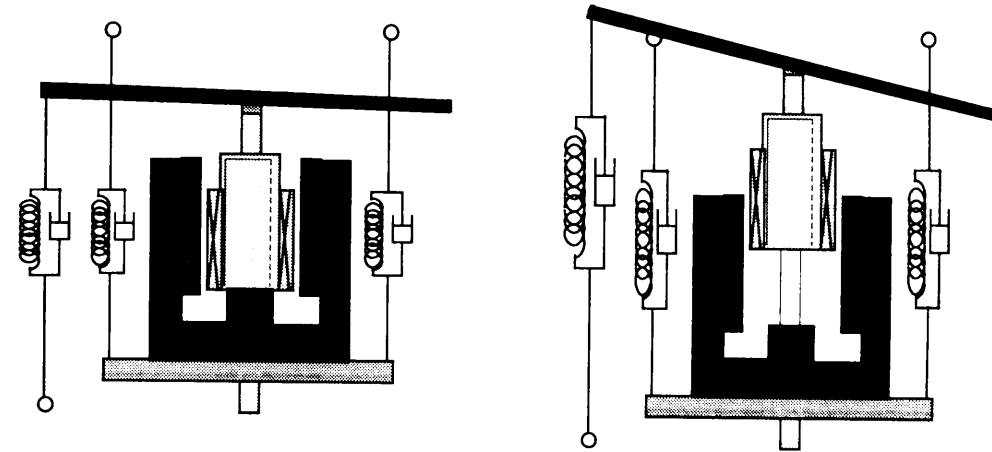
Figure 4.2: Motion of the LDM

body, respectively.

The state of movement of this system is shown in Fig. 4.2.

In the real railroad system, the mover should be a pass of a high current, it is difficult to attach the force sensor at the tip of the mover, it is unlikely to be realized. Making it fit for practical use, a force sensor should be attached at the other place which does not contact the overhead wiring, or we should not employ force sensor and utilize the state estimator (like Kalman filter).

4.2.2 Digital Control System

Configuration of Digital Control System is shown in Fig.4.3. We utilize the multi-input, multi-output digital control system AC-100/C (Integrated Systems Inc.) for the real-time control. AC-100/C is manipulated through Ethernet by the host computer; VAX station 3100 M76(DEC) CPU of AC-100/C is 80386(Intel) whose maximum clock is 20[MHz], and instruction cycle is 100[ns]. We employ Computer Aided Design(CAD); MATRIXx, System-build as an implementation tool of the controller. Further, this system has an I/O interface; 8channel 12bit-A/D, and D/A converters, respectively.
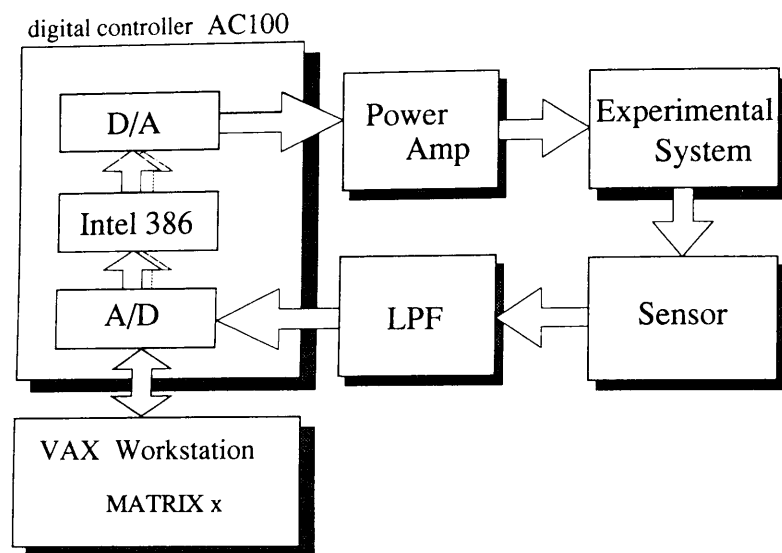
Figure 4.3: Configuration of Digital Control System

4.3 Modeling

In this section, we derive a mathematical model of the controlled plant. Fig. 4.4 is a simplified model for the modeling of the Fig. 4.1.

In this system, coil current is relatively small, hence a flux density made by permanent magnet is rather bigger than one by coil current. It is reasonable if we assume the flux density is constant at center of the permanent magnet[85][37].

When the mover is at the end of the permanent magnet, flux density should be small, as a result of it, electromagnetic force is getting down, control performance should be deteriorated. In this section, at first we derive the nominal state-space model of the plant, and further quantify the parametric uncertainties caused by the motion of mover, and neglected dynamics.

4.3.1 Differential Equation of Beam, Mover and Stater

In Fig.4.4, variable x_1, x_2 is positive it it tend to upward, and they are derivative from the steady state. If the beam is on a parallel with the baseline, $x_1 = x_2 = 0$. The differential equation of the beam is written as follows,

$$J\frac{d^2\theta}{dt_2} = -M_1 g L_1 + f_c L_1 - 4K_1 L_1{}^2\theta - 4D_1 L_1{}^2\frac{d\theta}{dt}, \qquad (4.1)$$

where J is inertia, and it is expressed by $J = 4M_1 L_1{}^2/3$. The deviate angle of the beam; θ is very small, we assume $L_1\theta = x_1$, then we obtain the following equation (4.1).

$$\frac{4}{3}M_1\frac{d^2 x_1}{dt^2} = -M_1 g + f_c - 4K_1 x_1 - 4D_1\frac{dx_1}{dt} \qquad (4.2)$$

Differential equations for mover and stater are written by using thrust of LDM: f_m, respectively.

$$M_2\frac{d^2 x_1}{dt^2} = -M_2 g - f_c + f_m \qquad (4.3)$$

$$M_3\frac{d^2 x_2}{dt^2} = -M_3 g - f_m - K_2(x_2 + X_2) - D_2\frac{dx_2}{dt} \qquad (4.4)$$

From equation (4.2) and (4.3), the output pressure f_c is represented by equations of the form

$$f_c = -\frac{M_1 M_2 g}{3M} + \frac{4M_1 f_m}{3M} + \frac{4M_2}{M}(K_1 x_1 + D_1\frac{dx_1}{dt}), \qquad (4.5)$$

where $M = 4M_1/3 + M_2$. The thrust of LDM f_m is written as

$$f_m = K_a(I + i), \qquad (4.6)$$

where I is the steady coil current, i is a deviation from I. K_a is a thrust constant of LDM, where $K_a = 2NBT$, N is turns of coil, B is flux density, T is depth of LDM. Equation of electric circuit is given as follows,

$$E + e = L\frac{di}{dt} + R(I + i) + K_a(\frac{dx_1}{dt} - \frac{dx_2}{dt}), \qquad (4.7)$$

where, E is steady state voltage of coil, e is a deviation from E, L is inductance of coil, R is resistance. The third term of the right side of equation (4.7) is velocity electromotive force.

4.3.2   state-space model

From equations (4.2), (4.3), (4.6), if we cancel f_c, then we obtain following equation.

$$M\frac{d^2x_1}{dt^2} = -(M_1 + M_2)g + K_a(I + i) - 4K_1x_1 - 4D_1\frac{dx_1}{dt} \qquad (4.8)$$

In the steady state, the following three equations hold.

$$E = RI \qquad (4.9)$$

$$(M_1 + M_2)g = K_aI \qquad (4.10)$$

$$M_3g + K_aI + K_2X_2 = 0 \qquad (4.11)$$

From equation (4.9), (4.10), (4.11), rearranging (4.4), (4.8), we have

$$M_3\frac{d^2x_2}{dt^2} = -K_ai - K_2x_2 - D_2\frac{dx_2}{dt} \qquad (4.12)$$

$$M\frac{d^2x_1}{dt^2} = K_ai - 4K_1x_1 - 4D_1\frac{dx_1}{dt}. \qquad (4.13)$$

We define $v_1 := dx_1/dt$, $v_2 := dx_2/dt$, from (4.5), (4.7), (4.12), (4.13), we derive the following linear time-invariant state space form,

$$\dot{x} = Ax + Bu, \qquad (4.14)$$

$$y = Cx, \qquad (4.15)$$

where

$$x = \begin{bmatrix} i & x_1 & v_1 & x_2 & v_2 \end{bmatrix}^T, \qquad u = e, \qquad y = f_c,$$

$$A = \begin{bmatrix} -\frac{R}{L} & 0 & -\frac{K_a}{L} & 0 & \frac{K_a}{L} \\ 0 & 0 & 0 & 0 & 1 \\ \frac{K_a}{M_{12}} & -\frac{4K_1}{M_{12}} & -\frac{4D_1}{M_{12}} & 0 & 0 \\ 0 & 0 & 0 & 0 & 1 \\ -\frac{K_a}{M_3} & 0 & 0 & -\frac{K_2}{M_3} & -\frac{D_2}{M_3} \end{bmatrix}, \qquad B = \begin{bmatrix} \frac{1}{L} & 0 & 0 & 0 & 0 \end{bmatrix}^T,$$

$$C = \begin{bmatrix} \frac{4M_1K_a}{3M_{12}} & \frac{4M_2K_1}{M_{12}} & \frac{4M_2D_1}{M_{12}} & 0 & 0 \end{bmatrix}.$$

Nominal model parameters of experimental system are probided in Table 4.1. By using these nominal parameter's values, we can easily derive the nominal A, B, C. From these

Figure 4.4: Simplified Model of the Experimental System

M_1	Mass of Beam
M_2	Mass of Moving Coil
M_3	Mass of Stater
K_1	Spring Constant of Spring1
D_1	Damping Factor of Spring1
K_2	Spring Constant of Spring2
D_2	Damping Factor of Spring2
x_1	Displacement of Moving Coil
x_2	Displacement of Stater
f_c	Contact Force
f_m	Force of LDM
θ	Displacement Angle of Beam
L_1	Half Length of Beam
X_1	Steady Position of Moving Coil
X_2	Steady Position of Stater

matrices, the transfer function $G(s)$, which is from the control input u to the output y is as follows.

$$G(s) = C(sI - A)^{-1}B \qquad (4.16)$$
$$= \frac{63.27 \cdot (s + 0.3846 \pm j95.27)(s + 4.348 \pm j22.67)}{(s + 42.50)(s + 8.289 \pm j25.21)(s + 27.30 \pm j67.00)}$$

From equation (4.16), the plant is stable and has a very oscillatory characteristics. This plant model has oscillation modes at 22.7[rad/s], 95.3[rad/s] which are caused by spring 1 and spring 2, respectively. Frequency Response of this transfer function (4.16) is shown in Fig. 4.5.

Table 4.1: Nominal Parameters of the Plant

Symbol	Parameter	Value	Unit
M_1	Mass of Beam	0.195	kg
M_2	Mass of Moving Coil	0.58	kg
M_3	Mass of Stater	4.6	kg
K_1	Spring Constant 1	590	N/m
K_2	Spring Constant 2	2450	N/m
D_1	Damping Coefficient 1	0.05	Ns/m
D_2	Damping Coefficient 2	40	Ns/m
K_a	Magnetic Coefficient	19.42	N/A
L	Inductance	0.095	H
R	Resistance	9.95	Ω
B	Magnetic Flux Density	0.38	T
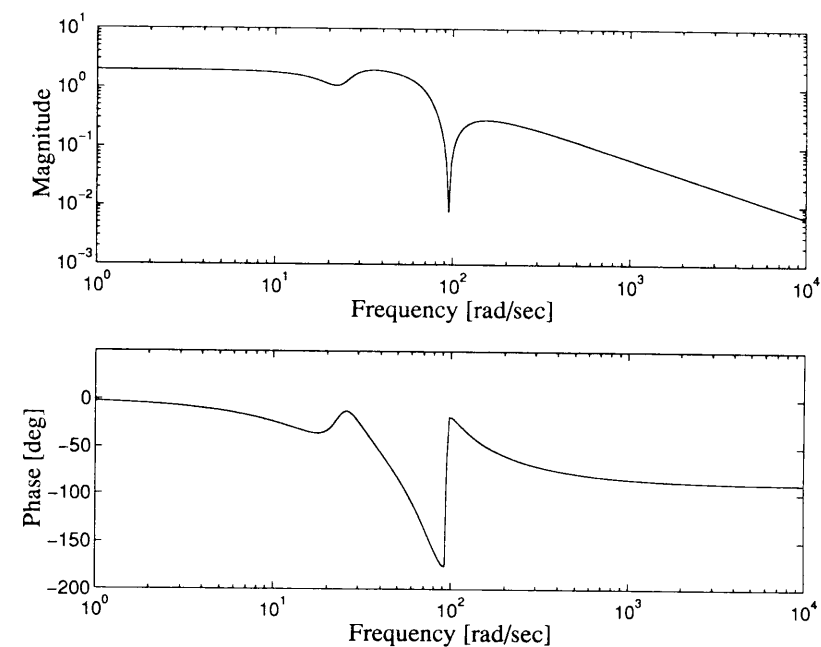
Figure 4.5: Transfer Function: G(s)

4.3.3   Parametric Uncertainty and Neglected Dynamics

When the beam moves, mover shakes against stater, and model parameter of the plant varies. Furthermore we consider the neglected linear dynamics of the plant. In this section, we measure these two types of uncertainties by experiments.

Perturbation of Model Parameters

When the distance between the stater and beam, mover sticks out of permanent magnet of stater, then the thrust goes down. Inductance of coil, resistance and spring constant vary according to the motion of mover. In this subsection, we measure and decide the limit of parameter variation. Parameter perturbations caused by the motion of mover and stater are shown in Fig. 4.6.

perturbation of parameter K_a

perturbation of parameter L

perturbation of parameter R

perturbation of parameter K_1
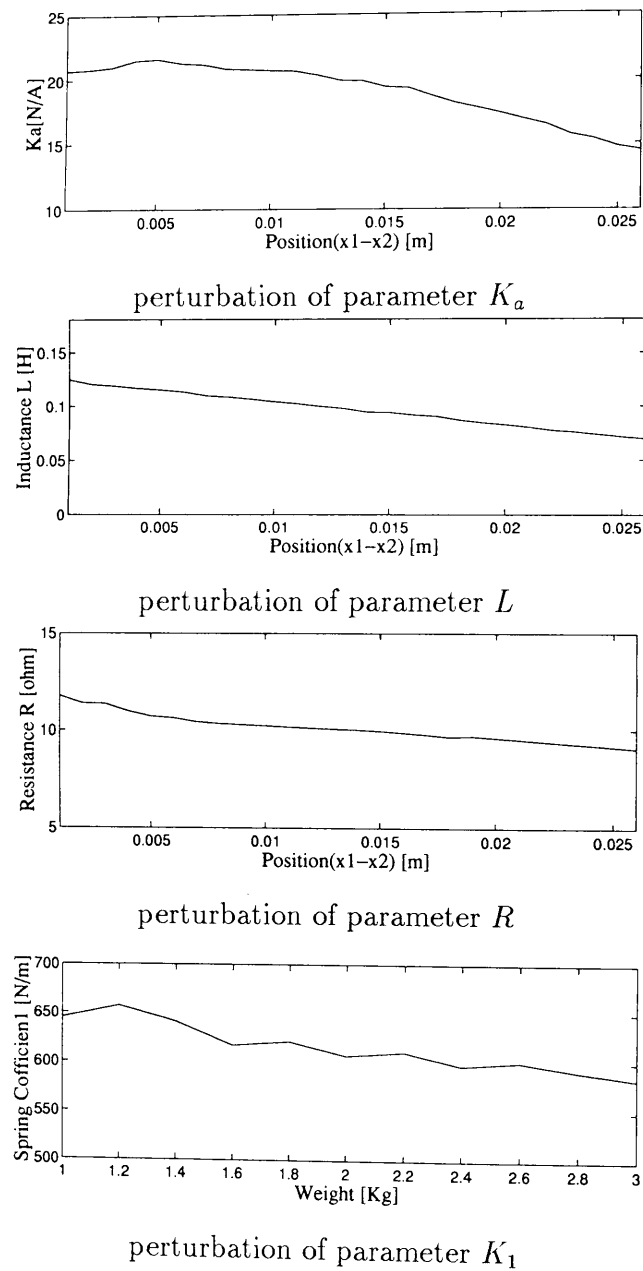
Figure 4.6: Parametric Uncertainty

From these figures, we decide the limit of the perturbation as Table 4.2. We can see that a perturbation of electromagnetic thrust constant K_a is biggest. Here we did not measure a perturbation of parameter D_1, and we assumed that a limit of perturbation of D_1 is same as one of parameter K_1.

Table 4.2: Parameter Variation

Parameter	K_a	L	R	K_1	D_1
Variation[%]	15	10	5	12	12

Uncertainties caused by neglected dynamics

In this subsection, we consider the uncertainties which was not contained in equation (4.14), (4.16). A real transfer function $G(s)_{real}$ was measured by experiments. For measurement, FFT CF-6400 (Ono Sokki) was employed.

Uncertainty caused by unmodeled dynamics: Δ_{umd} is written as output uncertainty that follows.

$$\Delta_{umd} := \frac{G_{real} - G(s)}{G(s)}, |\Delta(j\omega)| \leq |r(j\omega)| \tag{4.17}$$

Δ_{umd} is plotted with solid line, and the upper bound of Δ_{umd} $r(j\omega)$ is plotted with dashed line in Fig. 4.7, where $r(j\omega)$ is decided as

$$r(j\omega) = 6 \cdot 10^{-3}(1 + \frac{j\omega}{2\pi \cdot 0.1}). \tag{4.18}$$

This is the 1st order improper function.
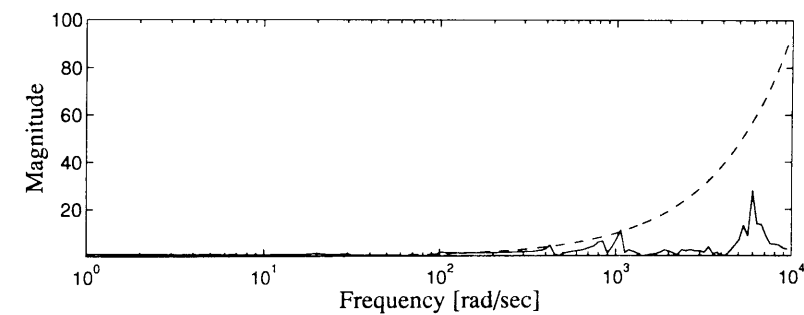
Figure 4.7: Uncertainty Δ_{umd}

4.4 Control System Design

In this section, we design a controller which satisfies the robust performance specification by using μ-synthesis[61] against uncertainties considered in the last session.

4.4.1 Review of μ-synthesis
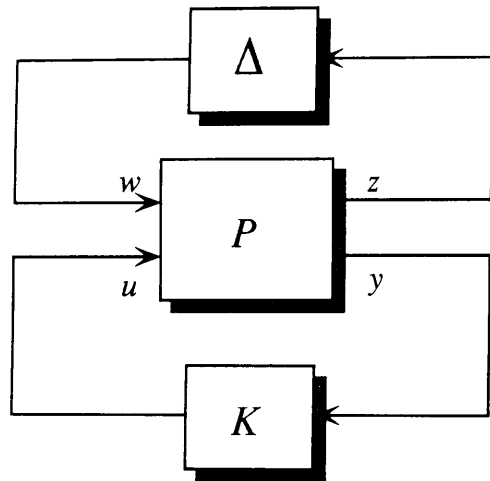
Figure 4.8: Closed-loop with Uncertainty

In Fig.4.8, for $T_{zw} := F_l(G, K) \in C^{n \times n}$, the set $\underline{\Delta} \in C^{n \times n}$ whose structure is block diagonal is generally defined as,

$$\underline{\Delta} := \{diag(\delta_1 \boldsymbol{I}_{r_1}, \cdots, \delta_s \boldsymbol{I}_{r_S}, \Delta_1, \cdots, \Delta_F) | \delta_i \in \boldsymbol{R}; \quad \Delta_j \in \boldsymbol{C}^{m_j \times m_j}\} \qquad (4.19)$$
$$\sum_{i=1}^{S} r_i + \sum_{j=1}^{F} m_j = n$$

Now, the structured singular value μ is defined as follows,

$$\mu_\Delta(\boldsymbol{T}_{zw}) := \frac{1}{min\{\sigma_{max}(\Delta) | \Delta \in \underline{\Delta}, det(I - \Delta \boldsymbol{T}_{zw}) = 0\}}, \qquad (4.20)$$

unless no $\Delta \in \boldsymbol{\Delta}$ makes $det(I - \Delta T_{zw}) = 0$, in which case, $\mu_\Delta(T_{zw}) := 0$.

If $F_l(G, K)$ is stable, then, for all Δ, the system in Fig. 4.8 is internal stable and, $\|F_u(T_{zw}, \Delta)\|_\infty < 1$ if and only if the structured singular value μ satisfies the inequality,

$$\mu_\Delta(\boldsymbol{T}_{zw}) < 1. \qquad (4.21)$$

4.4.2 Construction of the Generalized Plant

Introduction of parametric uncertainty

Based on Table 4.2, we select the uncertain physical model parameters as K_a, L, R, K_1, D_1. And we define that the 1st order parameter Pa with uncertainty is expressed by

$$Pa = (1 + \delta\xi)Pa_0, \quad \delta := \{\delta | \delta \in R, |\delta| \le 1\}, \qquad (4.22)$$

where Pa_0 is nominal value, ξ is the bound of perturbation. Further, we treat over 2nd order parameters R/L, K_a/L, $1/L$ as 1st order parameters.

Now we can calculate the generalized plant P which is considered parametric uncertainties as equations (4.23), (4.24). And its block diagram is shown in Fig. 4.9.

$$\begin{aligned}
\dot{\boldsymbol{x}} &= \boldsymbol{A}\boldsymbol{x} + \boldsymbol{M}\boldsymbol{w}_d + \boldsymbol{N}\boldsymbol{w}_u + \boldsymbol{B}u \\
y &= \boldsymbol{C}\boldsymbol{x} + \boldsymbol{O}\boldsymbol{w}_d \\
z_d &= \boldsymbol{K}_d\boldsymbol{x} \\
z_u &= K_u u
\end{aligned} \qquad (4.23)$$

$$\begin{aligned}
\Delta := \{ diag\,[\,\delta_{dj} \quad \delta_u\,]\,|\delta_{dj}, \delta_u \in \boldsymbol{R}, \\
\|\delta_{dj}\|_\infty < 1, \|\delta_u\|_\infty < 1\}(j = 1, \cdots, 6),
\end{aligned} \qquad (4.24)$$

where

$$\boldsymbol{M} = \begin{bmatrix} -1 & 0 & -1 & 1 & 0 & 0 \\ 0 & 0 & 0 & 0 & 0 & 0 \\ 0 & \frac{1}{M_{12}} & 0 & 0 & -\frac{4}{M_{12}} & -\frac{4}{M_{12}} \\ 0 & 0 & 0 & 0 & 0 & 0 \\ 0 & -\frac{1}{M_3} & 0 & 0 & 0 & 0 \end{bmatrix}, \quad \boldsymbol{O} = [\,0 \quad \frac{4}{3M_{12}} \quad 0 \quad 0 \quad \frac{4M_2}{M_{12}} \quad \frac{4M_2}{M_{12}}\,],$$

$$\boldsymbol{K}_d = \hat{\boldsymbol{K}}_d \tilde{\boldsymbol{K}}_d,$$

$$\hat{\boldsymbol{K}}_d = diag\left[\xi_{\frac{K_a}{L}} \xi_{K_a} \xi_{\frac{K_a}{L}} \xi_{\frac{K_a}{L}} \xi_{K_1} \xi_{D_1}\right], \quad \check{\boldsymbol{K}}_d = \begin{bmatrix} \frac{R}{L} & 0 & 0 & 0 & 0 \\ K_a & 0 & 0 & 0 & 0 \\ 0 & 0 & \frac{K_a}{L} & 0 & 0 \\ 0 & 0 & 0 & 0 & \frac{K_a}{L} \\ 0 & K_1 & 0 & 0 & 0 \\ 0 & 0 & D_1 & 0 & 0 \end{bmatrix}$$

$$K_u = \hat{K}_u \tilde{K}_u, \quad \hat{K}_u = \xi_{\frac{1}{L}}, \quad \tilde{K}_u = \frac{1}{L}$$

and, $\hat{K}_d$, $\hat{K}_u$ are bound of parameter perturbations[%].

Figure 4.9: Block Diagram of the Closed Loop System with Parameter Uncertainty

Introduction of Neglected Dynamics

In this section, we utilize Δ_{umd} which was derived in the previous session, and treat it as unstructured multiplicative output uncertainty, and we guarantee the stability against this uncertainty. This Δ_{umd} includes the uncertainties of K_2 which is spring constant of stater and friction of linear bearing, and so on.

Now we utilize its upper bound $r(j\omega)$, and select the weighting function $W_2(s)$ as following 1st improper function,

$$W_2 = \alpha_0 + \alpha_1 s. \tag{4.25}$$

Specification for Control Performance

To improve the control performance, we introduce the weighting W_1 for sensitivity function. The weighting function W_1 should have integral property to reject disturbance. The state space model of W_1 is defined as,

$$\begin{aligned}
\dot{x}_{w1} &= A_{w1} x_{w1} + B_{w1} u_{w1}, \\
y_{w1} &= C_{w1} x_{w1} + D_{w1} u_{w1}.
\end{aligned} \tag{4.26}$$

Generalized Plant

From equations (4.23), (4.24), (4.25) and (4.26), the final generalized plant $\hat{P}$ is as follows, and its block diagram is shown in Fig. 4.10, where we transfer the state variable to contain the pressure f_c in state variable.

$$\begin{bmatrix} \dot{x}_f \\ \dot{x}_{w1} \end{bmatrix} = \begin{bmatrix} A_f & 0_{5\times2} \\ -B_{w1}C_f & A_{w1} \end{bmatrix} \begin{bmatrix} x_f \\ x_{w1} \end{bmatrix} \\ + \begin{bmatrix} 0_{5\times1} & 0_{5\times1} & M_f & N_f \\ B_{w1} & B_{w1} & -B_{w1}O_f & 0_{2\times1} \end{bmatrix} \begin{bmatrix} w_1 \\ w_2 \\ w_d \\ w_u \end{bmatrix} + \begin{bmatrix} B_f \\ 0_{2\times1} \end{bmatrix} u \tag{4.27}$$

$$\begin{bmatrix} z_1 \\ z_2 \\ z_d \\ z_u \\ y \end{bmatrix} = \begin{bmatrix} -D_{w1}C_f & C_{w1} \\ -C_{wf} & 0_{1\times2} \\ K_{df} & 0_{1\times2} \\ 0_{1\times5} & 0_{1\times2} \\ -C_f & 0_{1\times2} \end{bmatrix} \begin{bmatrix} x_f \\ x_{w1} \end{bmatrix} \\ + \begin{bmatrix} D_{w1} & D_{w1} & -D_{w1}O_f & 0 \\ 0 & 0 & M_{wf} & N_{wf} \\ 0_{6\times1} & 0_{6\times1} & 0_{6\times6} & 0_{6\times1} \\ 0 & 0 & 0_{1\times6} & 0 \\ 1 & 1 & -O_f & 0 \end{bmatrix} \begin{bmatrix} w_1 \\ w_2 \\ w_d \\ w_u \end{bmatrix} + \begin{bmatrix} 0 \\ D_{wf} \\ 0_{1\times6} \\ K_u \\ 0 \end{bmatrix} u \tag{4.28}$$

$$\begin{aligned} \underline{\Delta} := \{ diag\,[\,\Delta_i \quad \delta_{dj} \quad \delta_u\,]\,|\Delta_i \in C, \delta_{dj}, \\ \delta_u \in R\}(i = 1,2\ j = 1,\cdots,6) \end{aligned} \tag{4.29}$$

where

$$x_f = [\,f_c \quad i \quad x_1 \quad x_2 \quad v_2\,]^T, \quad T = \begin{bmatrix} \dfrac{4M_1K_a}{3M_{12}} & \dfrac{4M_2K_1}{M_{12}} & \dfrac{4M_2D_1}{M_{12}} & 0 & 0 \\ 1 & 0 & 0 & 0 & 0 \\ 0 & 1 & 0 & 0 & 0 \\ 0 & 0 & 0 & 1 & 0 \\ 0 & 0 & 0 & 0 & 1 \end{bmatrix}$$

$$\begin{aligned}
A_f &= TAT^{-1} & K_{df} &= K_d T^{-1} \\
B_f &= TB & C_{wf} &= C_f[\alpha_1 A_f + \alpha_0 I] \\
C_f &= CT^{-1} & D_{wf} &= C_f[\alpha_1 I]B_f \\
M_f &= TM & M_{wf} &= C_f[\alpha_1 I]M_f \\
N_f &= TN & N_{wf} &= C_f[\alpha_1 I]N_f \\
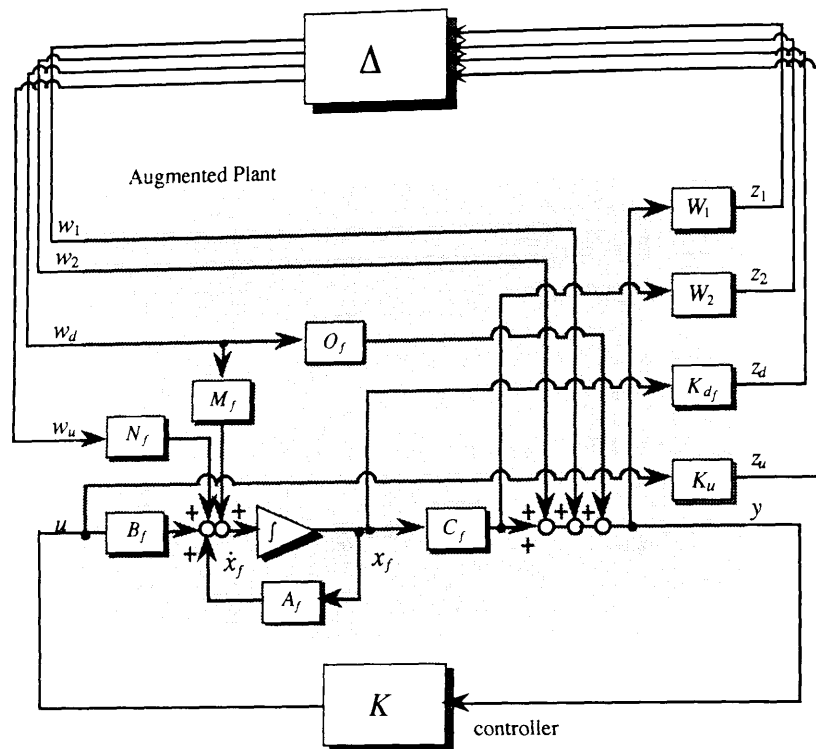O_f &= O
\end{aligned} \tag{4.30}$$

Figure 4.10: Block Diagram of Generalized Plant

4.4.3 Controller Design

After some experimental trial and error, in order to reject the disturbances at low frequency bands, the performance weighting function W_1 is chosen as

$$W_1(s) = \frac{5.0}{(1 + \dfrac{s}{2\pi \cdot 1.0})(1 + \dfrac{s}{2\pi \cdot 8.0})(1 + \dfrac{s}{2\pi \cdot 8.5})(1 + \dfrac{s}{2\pi \cdot 9.0})}. \tag{4.31}$$

From Fig.4.7 and (4.18), we choose the unstructured uncertainty weighting function W_2 for neglected uncertainty as

$$W_2(s) = r(s) = 6 \cdot 10^{-3}(1 + \frac{s}{2\pi \cdot 0.1}). \tag{4.32}$$

Then, we calculate the controller K which satisfies (4.21) and (4.29) by using $D - K$ iteration[61] approach. On each iteration, we approximated D matrix as an over 2nd order real rational function, and after five times iteration, we obtained final controller to satisfies equations (4.21) and (4.29) which achieves robust performance specification.

The order of this controller is 52 states, hence we employed balanced truncation method, and obtained 10-state final controller μ. Of course, we confirmed K_μ met the spec. The

transfer function of the final controller K_μ is written in equation(4.33) and shown in Fig. 4.11.

Here, $\|D_5 F_l(\hat{P}, K_\mu)D_5^{-1}\|_\infty = 0.885$, and $\sup_\omega \mu_\Delta(F_l(\hat{P}, K_\mu)) = 0.851$. And the frequency responses of the maximum singular value and the structured singular value μ with the controller K_1 which was obtained 1st iteration and the controller K_μ are shown in Fig.4.12.

$$\begin{aligned} K_\mu(s) &= 1.75 \cdot 10^{-5} \frac{(s + 26.5)(s + 3.64 \cdot 10^9)(s + 5.40 \pm j106)}{(s + 6.01)(s + 5.36 \cdot 10^4)(s + 5.77 \pm j23.0)} \\ &\times \frac{(s + 8.93 \pm j28.4)(s + 16.7 \pm j74.3)}{(s + 6.69 \pm j104)(s + 7.04 \pm j109)} \end{aligned} \tag{4.33}$$
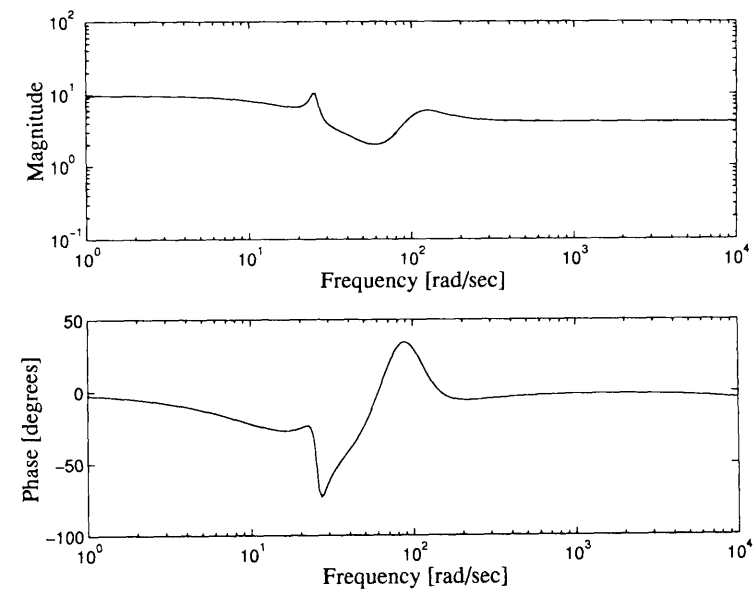
Figure 4.11: Frequency Response of Controller K_μ

4.5 Experimental Results

In this section, we evaluate the performance and stability of the obtained controller K_μ against various force disturbance, compared with conventional H_∞ controller[57].

4.5.1 H_∞ controller based on differential game theory

For a comparison, we introduce H_∞ controller based on differential game theory[82][57]. This controller was designed to improve a step response in the time domain[57]. We define

1st Iteration

5th Iteration
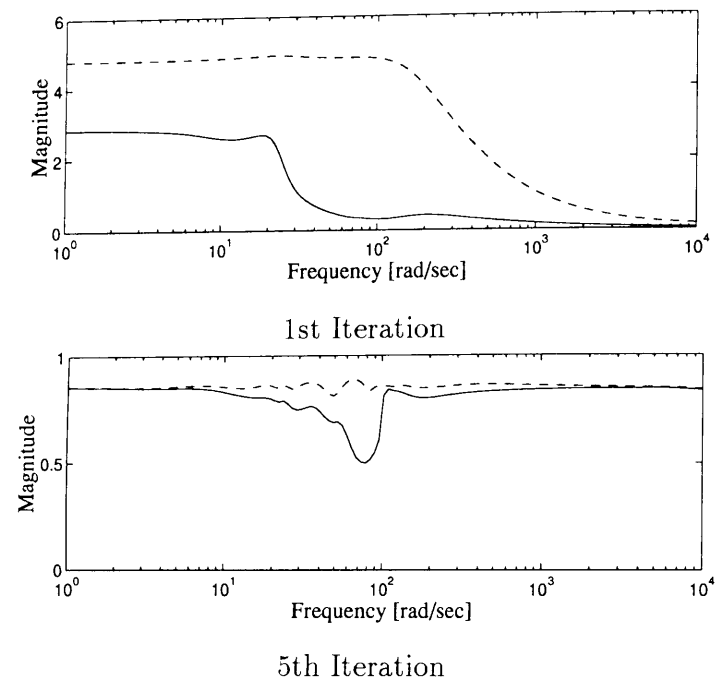
Figure 4.12: $\bar{\sigma}(T_{zw})$ (dashed) and μ (solid)

it K_{game}. The transfer function of the controller K_{game} is written in (4.34), and frequency response of K_μ and K_{game} are plotted in Fig.4.13, by solid and dashed line, respectively.

$$K_{game}(s) = \frac{529.0 \cdot (s + 3.14)(s + 4.71)(s + 5.54 \pm j22.7)}{(s + 0.625)(s + 2.05 \pm j22.5)(s + 2.79)(s + 6.42)}$$
$$\times \frac{(s + 38.2 \pm j67.9)(s + 54.7 \pm j16.3)}{(s + 85.7)(s + 496)(s + 10.4 \pm j95.4)} \qquad (4.34)$$

K_{game} has a higher gain at the low and middle frequency range, and lower gain at the high frequency range, than K_μ. On the other hand, a phase of K_μ leads at the middle and high frequency in comparison with K_{game} which shows robust stability.

4.5.2 Experiments

Controller design was done in continuous time domain, then we have to discretize obtained controllers, because we utilize digital controller. Obtained controllers was discretized by the well-known Tustin transform as

$$s = \frac{2}{T} \cdot \frac{z - 1}{z + 1}, \qquad (4.35)$$

where sampling rate is 1[ms].

We gave 2.5[N] force disturbance at the output of the plant all through the experiments, where reference force is 20[N]. It is said that system should be controlled up to about 20 [Hz]
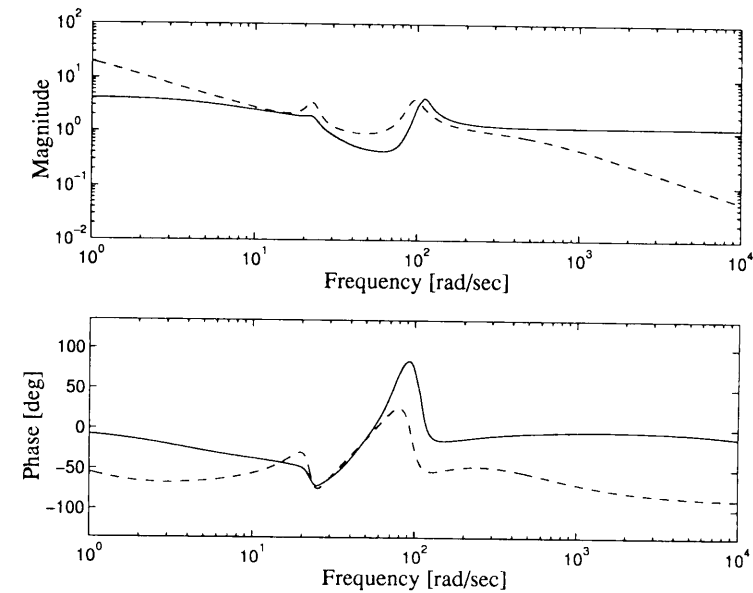
Figure 4.13: Frequency Response of K_μ and K_{game}

to control the real active pantograph. We consider this specification, we applied following four types of disturbance to the plant in order to evaluate control performance.

(i) Step disturbance

(ii) Sinusoidal disturbance (25.1[rad/sec])

(iii) Sinusoidal disturbance (75.4[rad/sec])

(iv) Sinusoidal disturbance (100.5[rad/sec])

Frequency of the disturbance (ii) and (iv) are both resonant frequency of springs, and at this point, mover and stater would vibrate extremely. Each experimental results is shown in Fig. 4.14, 4.15, 4.16, 4.17.

4.5.3 Consideration

The results of experiments (i) are almost same with both controllers, however, the response of K_μ shows that a little steady state error is left.

This result with K_μ was caused by the low gain of K_μ at the low frequency. Improvement of the robust stability of K_μ made its gain lower at the low frequency.

The results of experiments (ii) show good disturbance attenuation property of both controllers K_{game} and K_μ.

In experiments (iii) and (iv), both mover and stater vibrate extremely, distance between mover and stater is getting long. According to this motion, parameter perturbations get largest of all situations.

Especially on experiment (iii), compared with both controllers, μ controller K_μ attenuates disturbance, however, H_∞ controller K_{game} can not follow the speed, and amplifies vibration. Further, Frequency response of disturbance attenuation property is shown in Fig.4.18. This figure indicates K_μ presses the vibration peak at the 75[rad/s].

And we can see that controllable frequency range of K_{game} is only 100[rad/s], but one of K_μ is wider, and the limit is about 180[rad/s]. As a result, μ controller sacrifices the performance at the low frequency, and improves performance and stability at the middle and high frequency, then we conclude this μ controller is a well-balanced in the frequency range.

A) Controller K_μ

B) Controller K_{game}
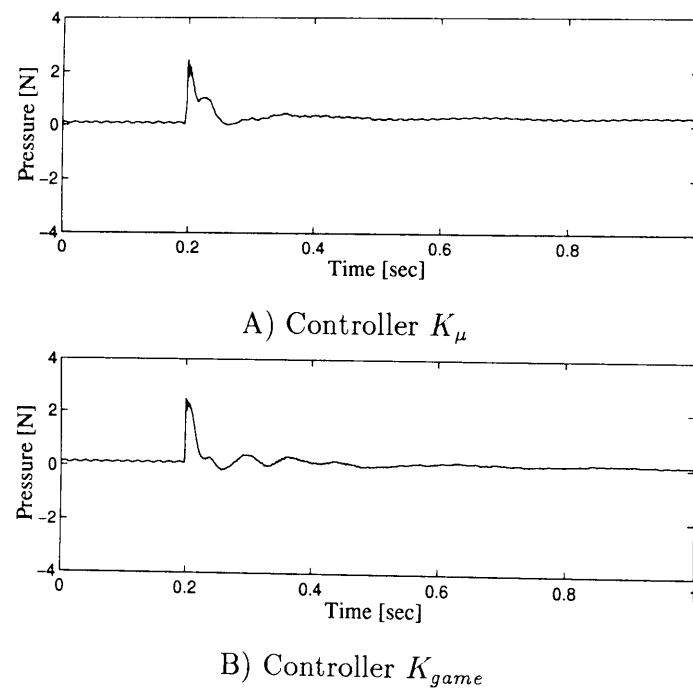
Figure 4.14:   Time Response for Step Disturbance (2.5[N])

A) Controller K_μ

B) Controller K_{game}
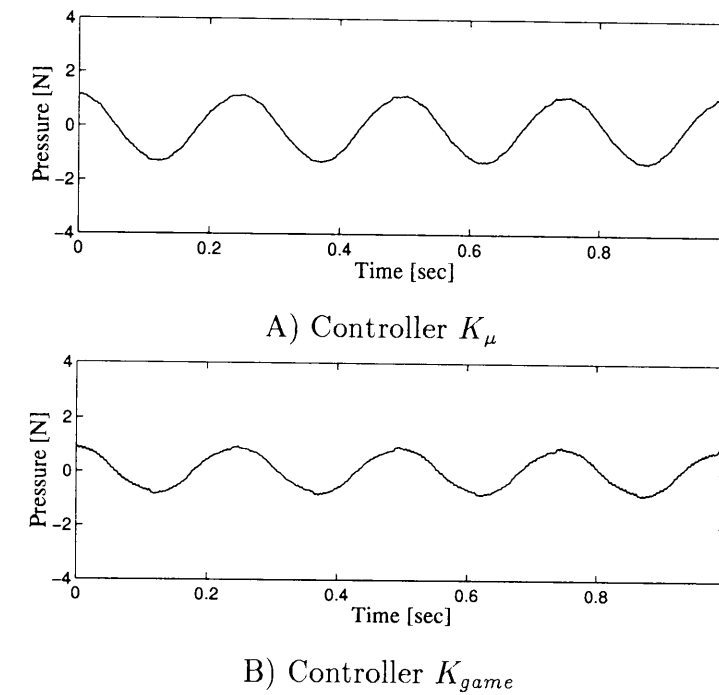
Figure 4.15:   Time Response for Periodic Disturbance (4[Hz], 2.5[N])

A) Controller K_μ

B) Controller K_{game}
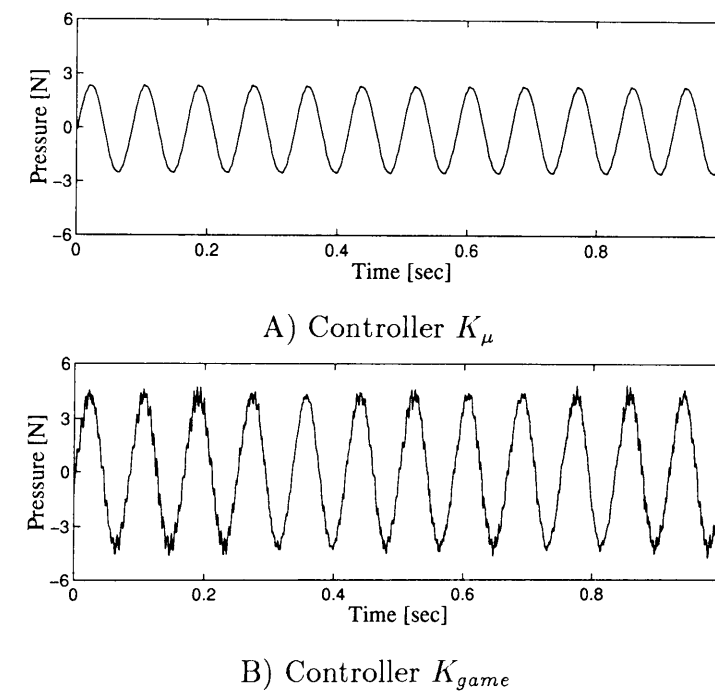
Figure 4.16:   Time Response for Periodic Disturbance (12[Hz], 2.5[N])

A) Controller K_μ

B) Controller K_{game}
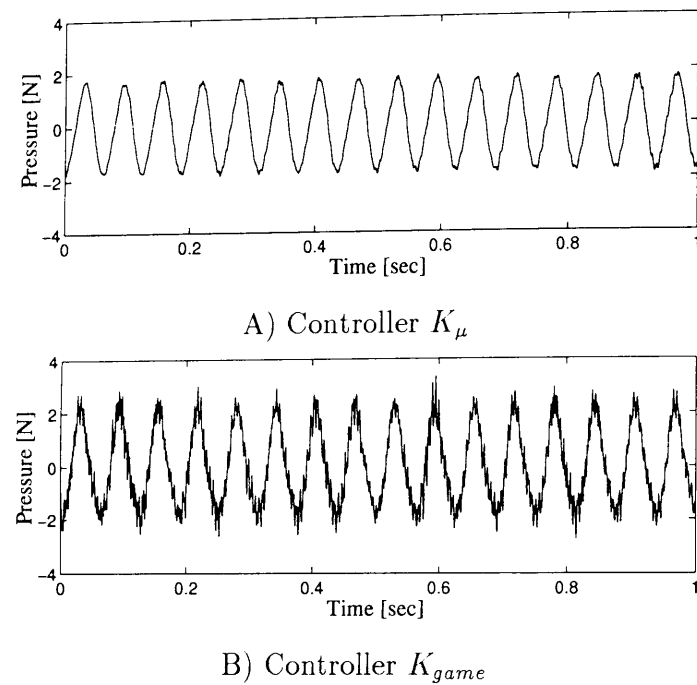
Figure 4.17:   Time Response for Periodic Disturbance (16[Hz], 2.5[N])
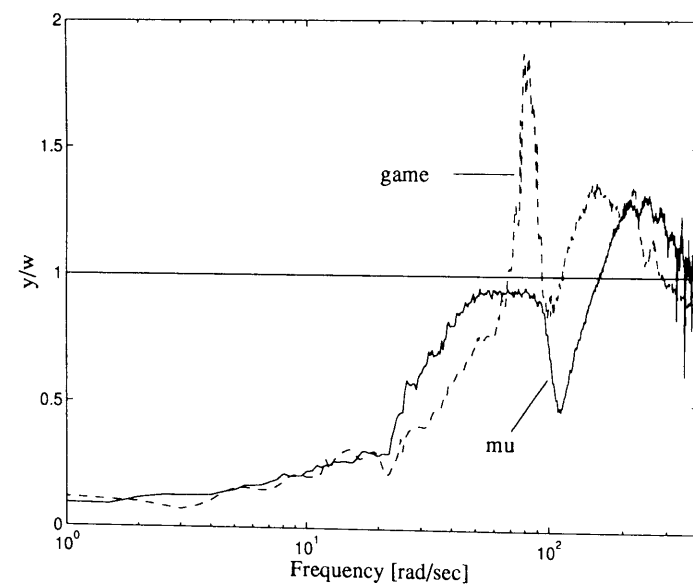
Figure 4.18:   Frequency Response for Periodic Disturbance

K_μ: solid line, K_{game}: dashed line

4.6   Conclusion

In this chapter, we improved the control performance of active pantograph system which has very oscillating property, at the resonance frequency by applying μ-synthesis approach.

We considered parametric uncertainty and uncertainty caused by unmodeled dynamics, and measure their quantities, and we expressed them as structured uncertainties via LFT, setup the robust performance problem. And then, we solved the above problem, designed a robust controller.

Finally, we showed several experimental results, and indicated the effectiveness of proposed control system design methodology by comparing conventional H_∞ controller with time and frequency response.

Chapter 5

Robust Control of Robot Manipulators

Robot dynamics is highly interfered, nonlinear, and complicated. Experimental evaluations of H_∞/μ control to nonlinear plants are now expected. Hashimoto and Asai treated H_∞ control or μ synthesis of a robot manipulator, but dynamic couplings between joints were not considered, and the uncertainties caused by modeling errors was treated the external disturbance[27][4].

In this chapter, I apply robust H_∞/μ control to robot manipulators and evaluate its effectiveness. We guarantee the robust stability of the robot manipulator control system against model perturbations and dynamic couplings.

Our approaches taken here are as follows.

- μ-synthesis with exact linearization (**Section 5.1**)

- constant scaled H_∞ control considering structured uncertainties (**Section 5.2**)

- linear parameter varying representation approach (**Section 5.3**)

5.1 μ-Synthesis of the Robot Manipulator Using Exact Linearization

In this section, I evaluate the controller performance depends on the sampling period, and indicate high-speed processing system are indispensable for a sufficient achievement of H_∞/μ control. μ-synthesis and high-speed DSP are utilized in order to achieve robust performance of the trajectory tracking control for a robot manipulator.

First, we consider the dynamics of the robot manipulator, and derived a linear model as well as the uncertainties for the plant. Then we construct a generalized plant considered the time delay, and setup robust performance objectives. After that, we apply μ-synthesis to robust control for a real robot manipulator. We design control systems by $D-K$ iteration approach, and three controllers designed in consideration of time delay are obtained. Finally, the experimental results show that high-speed processors can bring out the high performance of the designed controllers.

5.1.1 Introduction

The latest digital signal processors have high-speed and high-precision performance, and they cut time delay and quantization errors of real-time control. This contributes the development for practical use of H_∞/μ control theory[61][74]. If you do H_∞/μ design, the order of an obtained controller would be far higher than the order of a model for the plant. And when you control robot manipulators, you have to deal with nonlinearities of dynamics. In order to implement high order controllers or to compensate nonlinearities of the plant dynamics, we let processors do a tremendous number of multiplication for computing of control inputs. Implementation of high-order controllers and/or nonlinear compensations would be so complex that usual digital controllers could not realize designed controllers very well. The latest digital signal processors have high-speed and high-precision performance, and they cut time delay and quantization errors of real-time control.

Here we particularly consider a time delay. The sampling period of controllers mainly depends on the time delay which includes a hardware specification, controller computation, and so on. High-speed processors can bring out the high performance in the designed controllers. Even if you design a complex controller which may have a good performance, an usual slow processor could not realize its performance [28]. In this section, we utilize μ-synthesis and high-speed DSP in order to achieve robust performance of the trajectory tracking control for robot manipulators. Further, we evaluate the performance of the controller depends on the sampling period experimentally.

The remainder of this section is organized as follows. At First, we consider a dynamics of the robot manipulator, and derived a linear model as well as the uncertainties for the model. Next, we construct the generalized plant which is considered the above uncertainties. Then, we design control systems by $D-K$ iteration approach, and three controllers designed in consideration of time delay are obtained. Finally, we carry out experiments using a

DSP. The experimental results show that high-speed processors can bring out the high performance in the designed controllers. Robust performance can be realized owing to the latest high-speed digital signal processors.

5.1.2   Robot Manipulator Dynamics and Uncertainty Modeling

We know that the ideal dynamics for an n-link manipulator derived from the Euler-Lagrange equations is shown as follows [10].

$$M(q)\ddot{q} + h(q,\dot{q}) = u \qquad (5.1)$$

where $q(t) \in R^n$ denotes the generalized coordinates which represents joint positions, $M(q)$ is a positive definite $n \times n$ generalized inertia matrix, and $h(q,\dot{q})$ represents coliolis, centripetal, gravity forces, moments and frictional forces. The control input $u \in R^n$ denotes the vector of generalized input forces. Let

$$q^d(t) = \left(q_1^d(t), ..., q_n^d(t)\right)^T \qquad (5.2)$$

represent a desired path in joint space that we would like to the manipulator to track. We assume that $q^d(t)$ is continuously differentiable with q^d, $\dot{q}^d$, $\ddot{q}^d$. For the problem of tracking the desired trajectory (5.2) and its velocity, we define the error vectors

$$e = [e_1,\ e_2]^T = [q - q^d,\ \dot{q} - \dot{q}^d]^T. \qquad (5.3)$$

Now (5.1) and (5.3) give the error dynamics shown as follows.

$$\dot{e}_1 = e_2 \qquad (5.4)$$

$$\dot{e}_2 = -M^{-1}h + M^{-1}u - \ddot{q}^d \qquad (5.5)$$

We replaced the problem of path tracking by one of stabilizing the system (5.4) and (5.5) in error space. Next, we define an implementing model of the ideal dynamical model (5.1) as

$$\hat{M}(q)\ddot{q} + \hat{h}(q,\dot{q}) = u \qquad (5.6)$$

where $\hat{M}$ and $\hat{h}$ are the available models of M and h, respectively.

Given the plant (5.1) and the available model (5.6) we shall implement a feedback control law of the following form.

$$u(t) = \hat{M}(\hat{q})(\ddot{q}^d + v) + \hat{h}(\hat{q}, \dot{\hat{q}}) \qquad (5.7)$$

Equation (5.7) represents the familiar inverse dynamics algorithm, but applied to the available model rather than to the real physical model, and moreover, it uses the measured and hence noisy values of the state. Substituting the control law (5.7) into (5.5) and (5.6), we have

$$\dot{e}_1 = e_2, \qquad (5.8)$$

$$\dot{e}_2 = -M^{-1}h + M^{-1}\left(\hat{M}(\hat{q})(\ddot{q}^d + v) + \hat{h}(\hat{q},\dot{\hat{q}}) + u^d\right) - \ddot{q}^d. \qquad (5.9)$$

The equation (5.9) is rewritten as follows.

$$\dot{e}_2 = v + \eta \qquad (5.10)$$

$$\eta = E(\ddot{q}^d + v) + M^{-1}(\Delta h + u^d) \qquad (5.11)$$

where

$$E := M^{-1}\hat{M} - I, \quad \Delta h = \hat{h}(q,\dot{q}) - h(q,\dot{q}) \qquad (5.12)$$

Finally, the error equations (5.8) and (5.11) may be written in the following state-space form:

$$\dot{e} = Ae + B(v + \eta) \qquad (5.13)$$

$$y := Ce \qquad (5.14)$$

where

$$e = \begin{bmatrix} e_1 \\ e_2 \end{bmatrix}, \quad A = \begin{bmatrix} 0 & I \\ 0 & 0 \end{bmatrix}, \quad B = \begin{bmatrix} 0 \\ I \end{bmatrix}, \quad C = \begin{bmatrix} I & 0 \end{bmatrix}.$$

Next, we consider the system (5.13), (5.14) when the control signal v is the output of a linear controller applied to the measured tracking error e. Let the transfer function of the plant $G(s) = C(sI - A)^{-1}B$. Note that $G(s)$ represents a set of uncoupled double integration. The system (5.13), (5.14) may now be represented by the block diagram of Fig. 5.1, where the lower loop has been closed by a controller $K(s)$ which is to be designed. From equation (5.12), we define the function $H(\cdot) : R^n \times R^n \times R^n \to R^n$ as follows.

$$H(q^d(t), q(t), \dot{q}(t)) = \eta - Ev \qquad (5.15)$$

$$= E\ddot{q}^d + M^{-1}(\Delta h + u^d).$$

Figure 5.1: Feedback structure.

5.1.3 Control System Synthesis

For the control system design, we employ the μ-synthesis in order to achieve robust performance of the trajectory tracking control. A computing environment μ-analysis and synthesis toolbox [6] with MATLAB is then employed to calculate controllers.

Construction of the Generalized Plant

Consider the block diagram in Figure 5.1. We must design a robust controller to stabilize the closed loop system for the function E and H which have uncertainties. Furthermore, we would like to design a controller to maintain performance against disturbances and noises. These control objectives should be fitted in μ-synthesis formulation[6][74]. First, we employ the following assumptions for the uncertainty function E and H.

Assumption

- We treat the functions H and E as a linear time invariable uncertainty depend on $y(t)$ and $v(t)$, respectively. And they can be written using $\rho_H \in C^{n \times n}$, $\rho_E \in C^{n \times n}$, $W_E \in C^{n \times n}$, $W_H \in C^{n \times n}$, $\Delta_H \in C^{n \times n}$, $\Delta_E \in C^{n \times n}$, as follows.

$$H = \rho_H \Delta_H W_H, \quad \|\Delta_H\|_\infty \leq 1. \tag{5.16}$$

$$E = \rho_E \Delta_E W_E, \quad \|\Delta_E\|_\infty \leq 1. \tag{5.17}$$

ρ_H, ρ_E, W_E and W_H are the weighting functions for Δ_H and Δ_E. Rearranging the block diagram in Fig. 5.1 with these weighting functions, we can construct the generalized plant shown in Fig. 5.2. The fictitious uncertainty block Δ_P ($\|\Delta_P\|_\infty \leq 1$) is introduced in order to fit the above control objectives exactly in the μ-synthesis framework. The appended

uncertainty block Δ_P is used to incorporate the robust performance calculation. $\rho_P \in C^{n \times n}$ and $\Delta_P \in C^{n \times n}$ are the weighting function for Δ_P. ρ_H, W_H, ρ_E, W_E, ρ_P, W_P are all design specifications as well as design parameters.

Then the block diagram T_D represents time delay which is given by,

Time delay

$$T_D(s) = I e^{-sT}, \tag{5.18}$$

where T is a sampling period. The open-loop interconnection P which includes T_D in Fig. 5.2 is often referred to as the generalized plant. The problem to be evaluated in this section is as follows.

Problem

The controller performance depends on the sampling period.

Figure 5.2: Generalized plant.

μ-Synthesis

Considering the generalized plant in Fig. 5.2. We first define a block structure $\boldsymbol{\Delta}$ as

$$\boldsymbol{\Delta} := \left\{ \begin{bmatrix} \Delta_P & 0 & 0 \\ 0 & \Delta_E & 0 \\ 0 & 0 & \Delta_H \end{bmatrix} : \Delta_P \in C^{n \times n}, \Delta_E \in C^{n \times n}, \Delta_H \in C^{n \times n} \right\}. \tag{5.19}$$

Next, we treat the consider a generalized plant P partitioned as

$$P = \begin{bmatrix} P_{11} & P_{12} \\ P_{21} & P_{22} \end{bmatrix}.$$

(5.20)

Obviously, we can get a lower linear fractional transformation $\mathcal{F}_l(P,K)$ on P by K

$$\mathcal{F}_l(P,K) := P_{11} + P_{12}K\left(I - P_{22}K\right)^{-1}P_{21}.$$

(5.21)

Then, robust performance condition is equivalent to the following structured singular value test

$$\sup_{\omega \in \mathbf{R}} \mu_{\underline{\Delta}}\left(\mathcal{F}_l(P,K)(j\omega)\right) < 1.$$

(5.22)

For $M \in \mathbf{C}^{n \times n}$, $\mu_{\underline{\Delta}}(M)$ is defined as

$$\mu_{\underline{\Delta}}(M) := \frac{1}{\min\{\bar{\sigma}(\Delta) : \Delta \in \underline{\Delta},\ \det\left(I - M\Delta\right) = 0\}},$$

(5.23)

unless no $\Delta \in \underline{\Delta}$ makes $I - M\Delta$ singular, in which case $\mu_{\underline{\Delta}}(M) := 0$.

5.1.4   Application of μ-synthesis for a Robot Using DSP

In this section we apply the previously described μ-synthesis methodology to design a control system for a parallel link robot manipulator.

Parallel Link Robot Manipulator

A simple parallel link robot manipulator with two degrees of freedom is utilized for experiments. It is shown schematically in Fig. 5.3. Each joint is actuated by an 11 watt DC motor through reduction gear. The reduction ratio is 1:8. Two incremental encoders are used to obtain the rotating angles of each joint. A mass of the robot manipulator system is about 2 kg.

Linearized Model

Consider the parallel link robot manipulator shown in Fig. 5.3. Here q_1 and q_2 denote the angles of the link 1 and link 2, respectively. Let

$$q = [q_1 \quad q_2]^T$$

(5.24)

denote a generalized coordinate representing the joint position. The dynamics of this 2-link manipulator can be expressed as

$$M(q)\ddot{q} + h(q, \dot{q}) = u,$$

(5.25)

$\bigoplus$ --- **center of mass**

m_i : **mass of link i**

l_i : **length of link i**

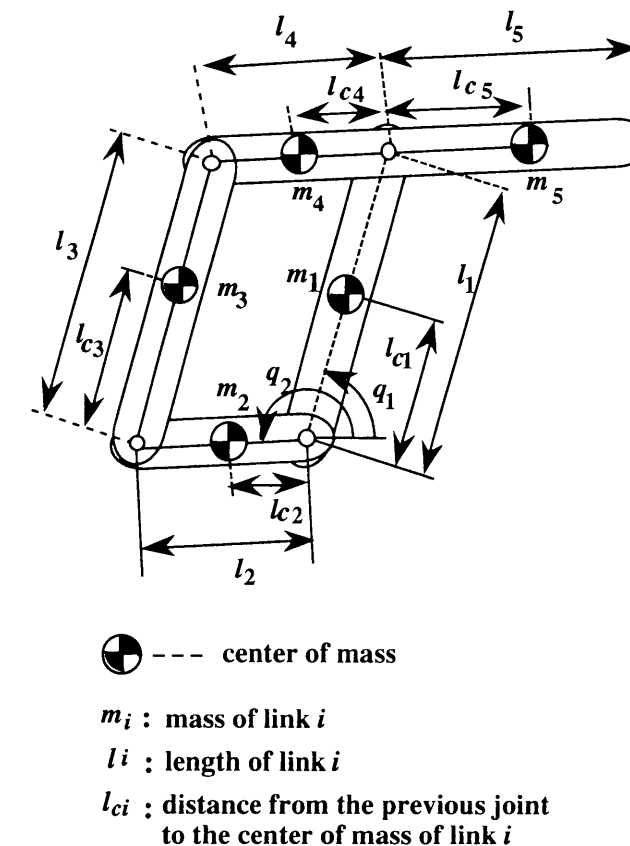l_{ci} : **distance from the previous joint to the center of mass of link i**

Figure 5.3: Parallel link robot manipulator

where

$$M(q) = \begin{bmatrix} c_1 & c_2 \cos(q_2 - q_1) \\ c_2 \cos(q_2 - q_1) & c_3 \end{bmatrix}, \quad h(q, \dot{q}) = \begin{bmatrix} -c_2 \sin(q_2 - q_1)\dot{q}_2^2 + c_4 \cos q_1 \\ -c_2 \sin(q_2 - q_1)\dot{q}_1^2 + c_5 \cos q_2 \end{bmatrix},$$

$$u = [\tau_1, \ \tau_2]^T.$$

The values of constants in (5.25) are as follows.

$$[\, c_1 \ c_2 \ c_3 \ c_4 \ c_5 \,] = [\, 6.78 \times 10^{-3} \ -4.23 \times 10^{-4} \ 1.61 \times 10^{-3} \ 7.43 \times 10^{-2} \ 7.12 \times 10^{-3} \,]$$

According to (5.13) and (5.14), the state space representation of the experimental manipulator is easily derived. This robot manipulator has 2-links, when we do real-time control with this manipulator, however, we treat them independently. Hence the state-space representation for each link is expressed in the following form.

$$\dot{x} = \hat{A}x + \hat{B}v, \quad y =: \hat{C}x \tag{5.26}$$

where

$$x = \begin{bmatrix} q_i \\ \dot{q}_i \end{bmatrix}, \quad v = v_i, \quad y = q_i \ (i = 1, \ 2), \quad \hat{A} = \begin{bmatrix} 0 & 1 \\ 0 & 0 \end{bmatrix}, \quad \hat{B} = \begin{bmatrix} 0 \\ 1 \end{bmatrix}, \quad \hat{C} = \begin{bmatrix} 1 & 0 \end{bmatrix}.$$

DSP-based Digital Control System

The experimental machine is controlled by a digital controller DSP-CITpro (dSPACE GmbH) [15]. The configuration of the DSP system is shown in Fig. 5.4. This system is mainly constructed with DS1002 which is a processor board, DS2101 which is a 12-bit D/A converter board and DS3001 which is an incremental encoder board. Processor board DS1002 uses a DSP TMS320C30 which can execute one instruction in 60 ns with 32-bit floating point arithmetic, and D/A converters have the maximum conversion speed of 3 μs. All programs are written in C language under the DOS/V environment. We utilizes the C code generator which convert MATLAB data into C language. The motor driver amplifies control signals twice to actuate DC motors. This DSP system has enough processing s peed for the real-time control of this robot manipulator.

D-K iteration

The $D - K$ iteration involves a sequence of minimizations over either K or D while holding the other fixed, until a satisfactory controller is constructed. First, for $D = I$ fixed, the controller K_1 is synthesized using the well-known H_∞ optimization method. Let $G = \hat{G}$,
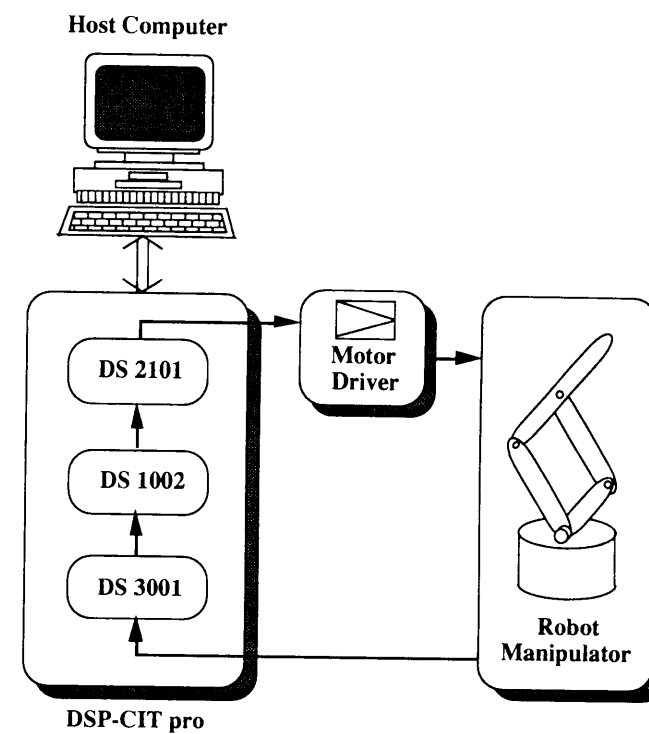
Figure 5.4: Digital control system

and $P = P_1$. P_1 involves the linear model $\hat{G}$ and all frequency weighting functions W_P, W_E, W_H, ρ_P, ρ_E, ρ_H and time delay T_D. First of all, we ignore the time delay T_D, that is

$$T_D := I. \tag{5.27}$$

After some preliminary design experience, the weighting functions are chosen as follows.

$$W_P = \frac{1.1 \times 10^8}{1 + s/1 \times 10^{-4}}, \qquad \rho_P = 1.0 \times 10^{-2} \tag{5.28}$$

$$W_E = 3.6 \times 10^{-9} \frac{1 + s/1.0 \times 10^{-3}}{1 + s/34.5}, \qquad \rho_E = 2.5 \times 10^3 \tag{5.29}$$

$$W_H = 1.0 \times 10^{-9} \frac{1 + s/1.0 \times 10^{-3}}{1 + s/30}, \qquad \rho_H = 1.0 \times 10^3 \tag{5.30}$$

First, the following H_∞ control problem yields the central controller K_1.

$$\|\mathcal{F}_l(P_1, K_1)\|_\infty < \gamma_1, \qquad \gamma_1 = 1.3. \tag{5.31}$$

There are several algorithms for the calculation of the Riccati equations and we employed the standard Schur method. After second iterations, this value γ was reduced to 1.0. The following H_∞ control problem

$$\|\mathcal{F}_l(P_2, K_2)\|_\infty < \gamma_2, \qquad \gamma_2 = 1.0, \tag{5.32}$$

yields the controller K_2, where P_2 denote the second open-loop interconnection structure. Robust performance condition is now achieved with the μ controller K_2.

Time Delay and Performance

The sampling rates of controllers mainly depends on the time delay which includes a hardware specification, controller computation, and so on. In this section, we evaluate the relation between performance and sampling period. We calculate the maximum sampling period T which achieves the robust performance specification (5.22) by iteration with above design parameters (5.28), (5.29), (5.30). The current controller K_2 has 9 orders, and time delay function T_D is approximated to the 1st order transfer function by Pade approximation[35]. A prospective controller K_2 will be 10-order one for each joint. Consequently, we obtain the maximum sampling period $T_{\max}$, where

$$T_{\max} = 250\ \mu s. \tag{5.33}$$

If T is greater than $250\mu s$, we could not find any controllers to achieve the robust performance condition. With the digital control system depicted in Fig. 5.4, the fastest sampling rate $T_{\min}$ which was realized is

$$T_{\min} = 140\ \mu s. \tag{5.34}$$

Hence as the sampling period T, the following three constants T_a, T_b and T_c are chosen.

$$\circ \quad T_a \;=\; 150\mu s < 250\mu s, \quad \gamma_2 = 1.00 \tag{5.35}$$

$$\circ \quad T_b \;=\; 210\mu s < 250\mu s, \quad \gamma_2 = 1.00 \tag{5.36}$$

$$\bullet \quad T_c \;=\; 350\mu s > 250\mu s, \quad \boldsymbol{\gamma_2 = 1.03} \tag{5.37}$$

The resulting 10-order controllers

$$\circ\ K_a, \quad \circ\ K_b, \quad \bullet\ K_c$$

are obtained respectively. The controllers K_a and K_b are satisfied robust performance condition, on the other hand, The controllers K_c does not achieve robust performance. These controllers K_a, K_b and K_c are obtained as results of the second $D-K$ iteration.

5.1.5   Experimental Results

The designed controllers K_a, K_b and K_c are continuous-time systems. In order to implement these three controllers with the digital control system shown in Figure 5.4, we discretized them via the well known Tustin transform.

The obtained H_∞ controller K_c achieves robust stability condition, and μ controller K_a and K_b achieves not only robust stability but also robust performance specification. Hence, we will evaluate robust performance as well as robust stability of the closed-loop system.

The manipulator succeeded in tracking of the specified path using the controllers K_a, K_b and K_c. Further in order to evaluate robustness, we changed the dynamics by adding a load of 30[g] to the edge of the link 5 in Fig. 5.3. This weight is enough heavy for this simple manipulator to evaluate robust performance. In this circumstance, manipulator also succeeded in tracking.

The desired trajectory in the joint space given by

Desired trajectory

$$q_1^d(t) = \frac{\sin 4\pi f t - 1}{4}\ [\text{rad}], \quad q_2^d(t) = \frac{\cos 2\pi f t - 1}{4}\ [\text{rad}]. \tag{5.38}$$

The experimental results are shown in Fig. 5.5 through Fig. 5.7, where the dashed lines indicate desired trajectories, and the solid lines indicate sensor outputs in the joint space. All of experiments are carried out with a load of 30[g].

- If frequency f is equal to 1[Hz], all of three controllers show good performance. The results shown in Fig. 5.5 indicate these three controllers achieves robust stability. But we can not distinguish the performance of these three controllers from these data.

- If frequency f is equal to 2[Hz] which mean that the manipulator's moving speed is twice as fast as the former, tracking responses with all of the controllers deteriorate. Comparing Fig. 5.6 (c) with Fig. 5.6 (a) and Fig. 5.6 (b), we can see that the response with K_c deteriorate extremely, but the responses with the controller K_a and K_b maintain better tracking characteristics against a relatively hard requirement.

- Next, 9-order controller K_2 designed without considering time delay is realized with the sampling periods of T_a, T_b, T_c. The obtained discrete-time controllers by Tustin transform are defined as

$$\circ\ Kd_a, \quad \circ\ Kd_b, \quad \bullet\ Kd_c.$$

Controllers K_a, K_b and K_c are different since they are designed. On the other hand, controllers Kd_a, Kd_b and Kd_c are same one when designed, but they are implemented

with different sampling periods. Using these controllers Kd_a, Kd_b and Kd_c, some experiments were carried out under the condition that $f = 2[\text{Hz}]$. Corresponding experimental results are shown in Fig. 5.7. These results are really similar to Fig. 5.6. We can notice that performance of Kd_c is remarkably bad. Controllers Kd_a and Kd_b maintain their performance.
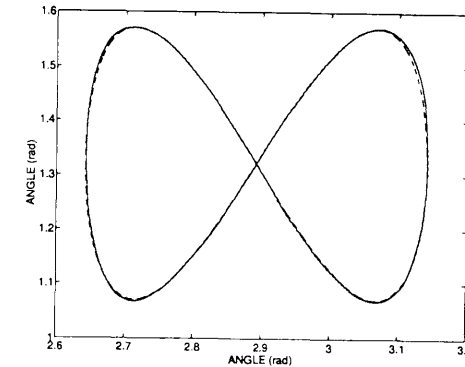
From all these results, we can see that the controller performance depends on the sampling period. Further we showed that the H_∞/μ control application needs a high-speed processor like DSP in order to bring out the full performance which a controller has by nature. In other words, high-speed processors like DSP can realize the complex control law as H_∞/μ.

5.1.6 Conclusion

This section has presented that performance of controllers depend on their sampling rates experimentally. We have indicated that if time delay for implementation get over a threshold value $T_{\max}$, the design specification of the controller is not satisfied. This represents that high-speed processors are indispensable, and control system design should be considered time delay for the achievement of performance specification.

For the control system design, we utilized μ-synthesis methodology and carried out experiments with a robot manipulator using DSP. First, we considered a dynamics of the robot manipulator, and derived a linear model as well as the uncertainties for the model. We employed the computed-torque method to obtain a simple linear model for manipulators.Secondly, we constructed the generalized plant which is considered the above uncertainties, and set robust performance objectives as a structured singular value test. We designed control systems by $D - K$ iteration approach. Three controllers: T_a, T_b, and T_c are obtained, which are designed in consideration of time delay. Next, continuous controller K_2 designed without considering time delay was discretized to Kd_a, Kd_b, and Kd_c with the sampling rate of T_a, T_b, and T_c, respectively.

After that, we carried out a lot of experiments using a DSP. Experimental results show that controller K_c and Kd_c which have long sampling period are not satisfied robust performance. This showed that high-speed processors can bring out the high performance in the designed controllers. In other words, robust performance can be realized owing to the latest high-speed digital signal processors.

(a) Tracking response with K_a (+30g, f =1Hz)
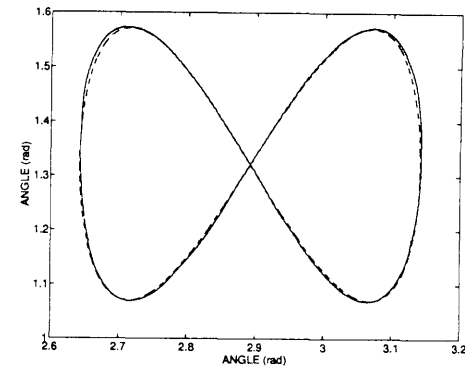
(b) Tracking response with K_b (+30g, f =1Hz)
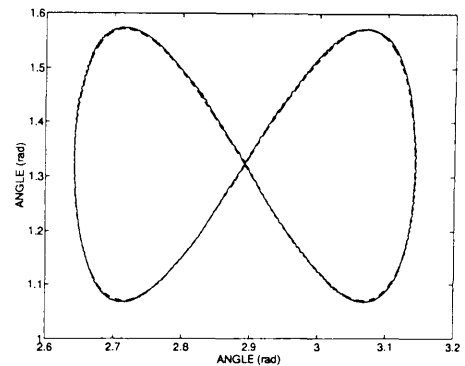
(c) Tracking response with K_c (+30g, f =1Hz)

Figure 5.5: Tracking response with 30g weight at 1Hz

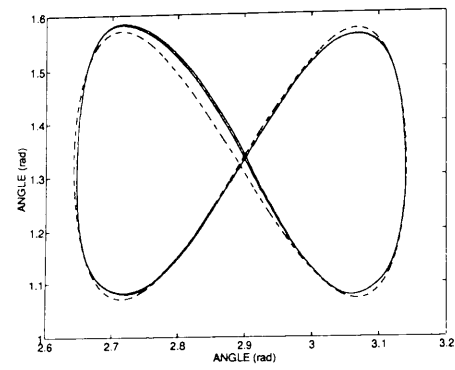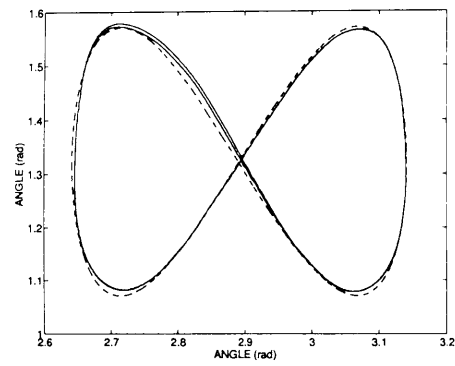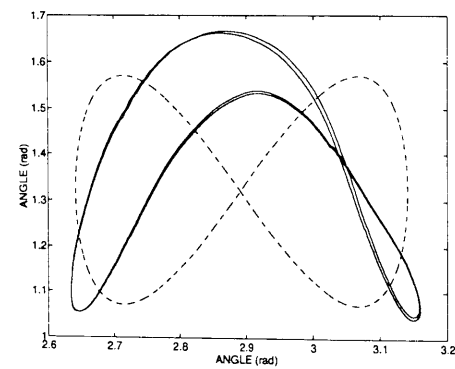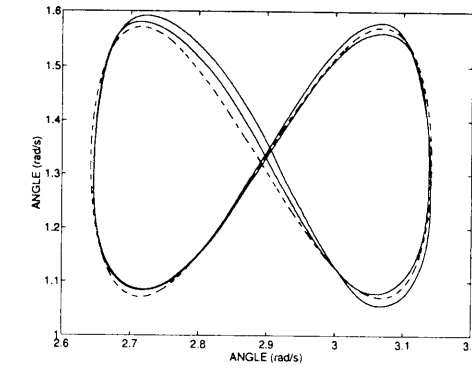(a) Tracking response with K_a (+30g, f =2Hz)

(b) Tracking response with K_b (+30g, f =2Hz)

(c) Tracking response with K_c (+30g, f =2Hz)

Figure 5.6: Tracking response with 30g weight at 2Hz

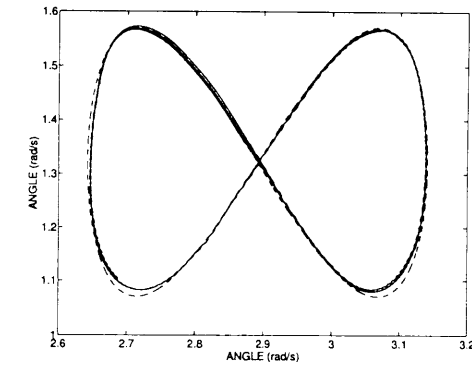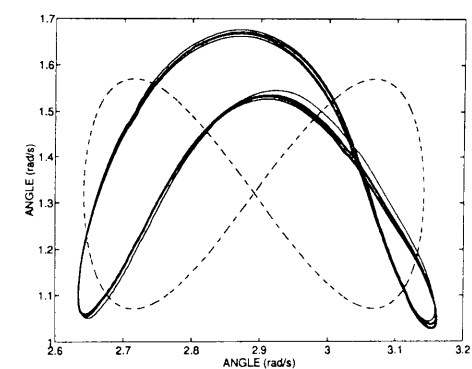(a) Tracking response with Kd_a (+30g, f =2Hz)

(b) Tracking response with Kd_b (+30g, f =2Hz)

(c) Tracking response with Kd_c (+30g, f =2Hz)

Figure 5.7: Tracking response with 30g weight at 2Hz

5.2   Robust H_∞ Control of Robot Manipulators considering structured uncertainties

This section proposes a linear robust control scheme for robotic trajectory tracking based on the H_∞ control theory. After the introduction of our experimental manipulator, the dynamics and model uncertainties of the whole robot system including actuator are discussed. Then, setting up the control objectives in H_∞ synthesis framework, an H_∞ controller is designed with the static constant scaling matrix D. Finally, with experimental results, we show the effectiveness of the proposed linear robust H_∞ control scheme for a robot manipulator.

5.2.1   Introduction

Almost all the industrial robots are controlled by independent joint PD (proportional and derivative) controllers, and they have good control performance to a certain extent. The reason this approach is useful for the nonlinear coupled robots control is most of them(except direct drive robot) have reduction systems which possess large gear ratio, hence they could be treated as linear independent plants approximately. However, PD controllers can not achieve sufficient performance on tasks which require both quick and accurate trajectory tracking, because they are designed without consideration of the dynamic coupling between joints.

The model-based control, including the PD control, is an advanced control scheme which uses the dynamic model of the manipulator. When a precise model is available, this control scheme completely linearizes and decouples the manipulator dynamics. However, use of an inaccurate model easily degrade the performance and the obtained tracking accuracy may be inferior to the independent joint PD control. Since the modeling error is inevitable in the modeling procedure, robust control is necessary to accomplish high performance[72][73].

This section proposes a robust compensation scheme based on the H_∞ control theory [61] [74]. The controller consists of a model-based linear robust controller, and it is not employed inverse dynamic computation, hence once the controller is obtained, computational burden for H_∞ controller is small add on, because the H_∞ controller is linear and time-invariant and the computational burden is only matrix vector multiplications. The sampling period of this approach is shorter than the other nonlinear control schemes.

Moreover, the control input is continuous. Therefore, the H_∞ controller is suitable for realization of real-time model-based robust control.

We demonstrate the robustness of the proposed scheme by experiments on a parallel link miniature robot manipulator. Taking the actuator dynamics into account, the nominal linear dynamic model of the manipulator is derived. Dynamic couplings between joints and the gravity forces are treated as the structured uncertainties. These uncertainties are nonlinear, but bounded by known constants, hence we employ the H_∞ control approach with small gain theory to achieve robust stability. The controller is designed with consideration of the perturbations of link parameters caused by loads putted on the end of the hand. The experimental results exhibit remarkable robustness of the proposed controller compared with the conventional computed torque method with PD controller.

5.2.2   Robot Control System

Experimental Robot Manipulator

A simple parallel link(four-bar linkage) robot manipulator with two degrees of freedom is utilized for experiments. It is shown schematically in Fig. 5.8. Each joint is actuated by an 11 watt DC motor through a reduction gear whose ratio is 1:8. This manipulator has two incremental encoders and potentiometers, but we use only encoders to obtain the rotating angles of joints. The total mass of this robot manipulator system is about only 2 [kg]. The link construction of this manipulator is as in Fig. 5.9.

5.2.3   Robot Dynamics

Generally, the ideal n-link robot dynamics is shown as follows [10].

$$M(q)\ddot{q} + h(q,\dot{q}) + V\dot{q} + g(q) = \tau. \tag{5.39}$$

where

$$\begin{aligned}
M(q) &\in R^{n \times n} &&: \text{inertia matrix} \\
h(q,\dot{q}) &\in R^n &&: \text{Coliolis and centrifugal force} \\
V &\in R^{n \times n} &&: \text{viscous frictional matrix} \\
g(q) &\in R^n &&: \text{gravity force} \\
q(t) &\in R^n &&: \text{joint angle} \\
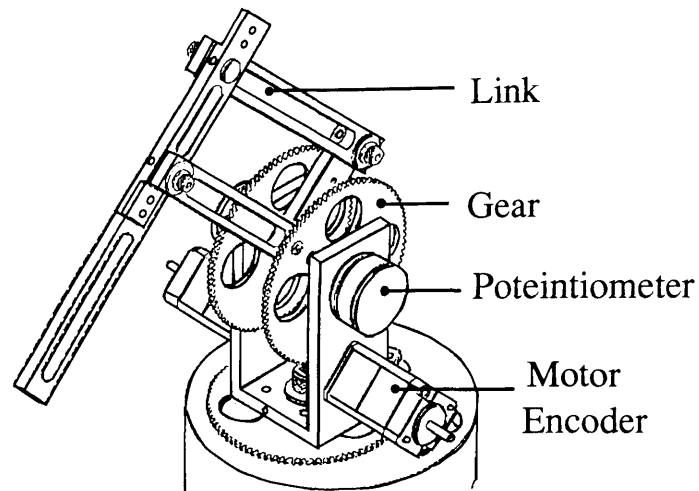\tau &\in R^n &&: \text{control input}
\end{aligned}$$
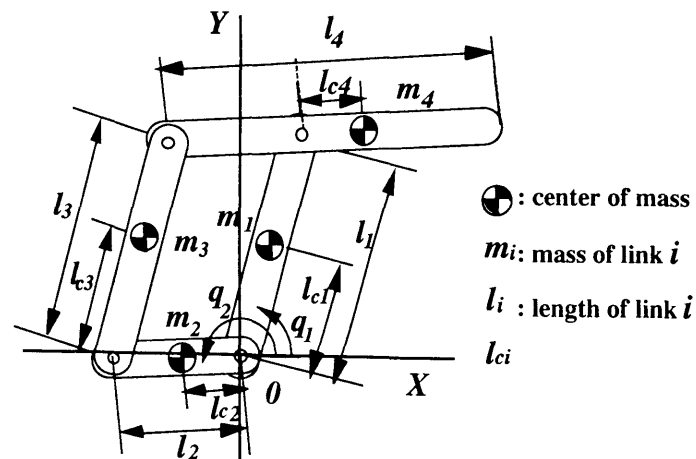
Figure 5.8: Robot Manipulator

Figure 5.9: Link Construction of the Manipulator

Correspondent dynamics of this four-bar linkage manipulator is as follows.

$$
\begin{bmatrix} M_{11} & M_{12}\cos(q_2-q_1) \\ M_{12}\cos(q_2-q_1) & M_{22} \end{bmatrix} \begin{bmatrix} \ddot{q}_1 \\ \ddot{q}_2 \end{bmatrix}
$$
$$
+ \begin{bmatrix} 0 & -M_{12}\dot{q}_2\sin(q_2-q_1) \\ M_{12}\dot{q}_1\sin(q_2-q_1) & 0 \end{bmatrix} \begin{bmatrix} \dot{q}_1 \\ \dot{q}_2 \end{bmatrix}
$$
$$
+ \begin{bmatrix} F_1 & 0 \\ 0 & F_2 \end{bmatrix} \begin{bmatrix} \dot{q}_1 \\ \dot{q}_2 \end{bmatrix} + \begin{bmatrix} V_1\cos q_1 \\ V_2\cos q_2 \end{bmatrix} = \begin{bmatrix} \tau_1 \\ \tau_2 \end{bmatrix}. \tag{5.40}
$$

$$
\begin{aligned}
M_{11} &= m_1 l_{c1}^2 + m_3 l_{c3}^2 + m_4 l_1^2 + I_1 + I_3 &&= 3.7672 \times 10^{-3} \\
M_{12} &= m_3 l_2 l_{c3} - m_4 l_1 l_{c4} &&= -1.6806 \times 10^{-5} \\
M_{22} &= m_2 l_{c2}^2 + m_3 l_2^2 + m_4 l_{c4}^2 + I_2 + I_4 &&= 2.8659 \times 10^{-3} \\
F_1 &= F_2 = 0 \quad (\text{ ignored }) \\
V_1 &= (m_1 l_{c1} + m_3 l_{c3} + m_4 l_1)g &&= 9.0108 \times 10^{-2} \\
V_2 &= (m_2 l_{c2} + m_3 l_2 - m_4 l_{c4})g &&= 1.9183 \times 10^{-2}
\end{aligned}
$$

5.2.4   Actuator Dynamics

The gear ratio η (>1) gives the following equation.

$$
q_{mi} = \eta q_i, \qquad (i = 1, 2.) \tag{5.41}
$$

where $q_m = [q_{m1},\ q_{m2}]^T$ is the motor angle. Writing a torque balance for this system in terms of torque at the rotor yields

$$
\tau_{mi} = J_{m1}\ddot{q}_{mi} + D_{mi}\dot{q}_{mi} + \tau_{ai}, \qquad (i = 1, 2.) \tag{5.42}
$$

where J_{m1} and J_{m2} are the inertia of the motor rotor and D_{m1}, D_{m2} are viscous friction coefficients for the rotor, and $\tau_a = [\tau_{a1},\ \tau_{a2}]^T$ is driving power translated to links. The torque is stated by means of a single motor torque constant which relates armature current to the output torque as

$$
\tau_{mi} = K_t i_i, \qquad (i = 1, 2.) \tag{5.43}
$$

where $i = [i_1,\ i_2]^T$ is the armature current, and K_t is the motor torque constant. The back electromotive force (emf) constant describes the voltage generated for a given rotational velocity as

$$
v_{bi} = K_b \dot{q}_{mi}, \qquad (i = 1, 2.) \tag{5.44}
$$

where K_b is the back emf constant and $v_b = [v_{b1}, v_{b2}]^T$ is the back emf.

The output voltage of the D/A converter, i.e., the control signal is usually amplified and put into servo motor. Here its amplifier gain: K_a is defined as constant($:=2$).

The armature circuit of a DC torque motor is described by a first-order differential equation given by

$$L\frac{d}{dt}i_i + Ri_i + v_{bi} = K_a v_i, \qquad (i = 1, 2.) \qquad (5.45)$$

where L is the inductance of the armature winding, R is the resistance, and $v = [v_1, \ v_2]^T$ is the armature voltage. From the principle of virtual work, the following equation is derived.

$$\tau_i = \eta \tau_{ai}, \qquad (i = 1, 2.) \qquad (5.46)$$

where $\tau = [\tau_1, \ \tau_2]^T$ is torque at the load.

If $L << R$ (in this motor, $L = 9.0 \times 10^{-4}$[H] and $R = 7.9$[Ω], hence its condition is sufficiently satisfied), then from these above equations, the dynamic model of this robot manipulator containing actuator is shown as follows.

Robot Dynamics with actuator

$$\begin{bmatrix} \hat{m}_{11} & \hat{m}_{12} \\ \hat{m}_{21} & \hat{m}_{22} \end{bmatrix} \begin{bmatrix} \ddot{q}_1 \\ \ddot{q}_2 \end{bmatrix} + \begin{bmatrix} \hat{d}_{11} & \hat{d}_{12} \\ \hat{d}_{21} & \hat{d}_{22} \end{bmatrix} \begin{bmatrix} \dot{q}_1 \\ \dot{q}_2 \end{bmatrix} + \begin{bmatrix} \hat{g}_1 \\ \hat{g}_2 \end{bmatrix} = \alpha \begin{bmatrix} v_1 \\ v_2 \end{bmatrix}. \qquad (5.47)$$

where

$$\hat{m}_{11} = \eta^2 J_{m1} + M_{11}, \qquad \hat{m}_{12} = M_{12} \cos(q_2 - q_1),$$
$$\hat{m}_{21} = M_{12} \cos(q_2 - q_1), \qquad \hat{m}_{22} = \eta^2 J_{m2} + M_{22},$$
$$\hat{d}_{11} = \eta^2 (D_{m1} + \frac{K_t K_b}{R}), \qquad \hat{d}_{12} = -M_{12} \dot{q}_2 \sin(q_2 - q_1),$$
$$\hat{d}_{21} = M_{12} \dot{q}_1 \sin(q_2 - q_1), \qquad \hat{d}_{22} = \eta^2 (D_{m2} + \frac{K_t K_b}{R}),$$
$$\hat{g}_1 = V_1 \cos q_1, \qquad \hat{g}_2 = V_2 \cos q_2,$$
$$\alpha = \frac{\eta K_a K_t}{R}.$$

Numerical values of the parameters of the arm and the actuator are shown in Table 5.1 and Table 5.2, respectively. Those tables give following numerical values of the model parameters.

Model Parameters

$$\hat{m}_{11} = 3.91 \times 10^{-3}, \qquad \hat{m}_{22} = 2.39 \times 10^{-3}$$
$$\hat{m}_{12} = 1.68 \times 10^{-5} \cdot \cos(q_2 - q_1)$$
$$\hat{m}_{21} = -1.68 \times 10^{-5} \cdot \cos(q_2 - q_1)$$
$$\hat{d}_{11} = 9.37 \times 10^{-3} \qquad \hat{d}_{22} = 9.37 \times 10^{-3}$$
$$\hat{d}_{12} = -1.68 \times 10^{-5} \cdot \dot{q}_2 \cdot \sin(q_2 - q_1)$$
$$\hat{d}_{21} = 1.68 \times 10^{-5} \cdot \dot{q}_1 \cdot \sin(q_2 - q_1)$$
$$\hat{g}_1 = 9.01 \times 10^{-2} \cdot \cos q_1, \quad \hat{g}_2 = 1.92 \times 10^{-2} \cdot \cos q_2$$
$$\alpha = 6.89 \times 10^{-2}$$

$$(5.48)$$

Table 5.1: Parameters of Arm

i	m_i [g]	l_i [mm]	l_{ci} [mm]	I_i [kgm^2]
1	86.7	128.0	0.0	2.87×10^{-3}
2	74.4	50.0	0.0	2.70×10^{-3}
3	18.0	128.0	64.0	1.33×10^{-4}
4	28.0	178.0	39.0	6.00×10^{-5}

Table 5.2: Parameters of Actuators

Symbol	Value
$J_{m1}, \ J_{m2}$	2.25×10^{-6} [kgm^2]
η	8
$D_{m1}, \ D_{m2}$	0 (ignored)
R	7.9 [Ω]
$K_t, \ K_b$	3.4×10^{-2}
K_a	2

Linear Robot Dynamics

In equation (5.48), $\hat{m}_{11}$, $\hat{m}_{22}$, $\hat{d}_{11}$, $\hat{d}_{22}$ and α are constant model parameters. It is obvious that $|\hat{m}_{11}|$ and $|\hat{m}_{22}|$ are far larger than max $|\hat{m}_{12}(q)|$ and max $|\hat{m}_{21}(q)|$, and $|\hat{d}_{11}|$, $|\hat{d}_{22}|$ are

larger than $\max |\hat{d}_{12}(q,\dot{q})|$ and $\max |\hat{d}_{21}(q,\dot{q})|$, if $\dot{q} \simeq 1$. Hence we treat the nonlinear term in (5.48), i.e.,

$\hat{m}_{12}, \hat{m}_{21}, \hat{d}_{12}, \hat{d}_{21}$ $\hat{g}_1$, and $\hat{g}_2$ as structured uncertain terms. The constant terms, i.e.,

$\hat{m}_{11}, \hat{m}_{22}, \hat{d}_{11}, \hat{d}_{22}$, and α construct the nominal linear robot dynamics, which is defined as follows.

$$\begin{bmatrix} \hat{m}_{11} & 0 \\ 0 & \hat{m}_{22} \end{bmatrix} \begin{bmatrix} \ddot{q}_1 \\ \ddot{q}_2 \end{bmatrix} + \begin{bmatrix} \hat{d}_{11} & 0 \\ 0 & \hat{d}_{22} \end{bmatrix} \begin{bmatrix} \dot{q}_1 \\ \dot{q}_2 \end{bmatrix} = \alpha \begin{bmatrix} v_1 \\ v_2 \end{bmatrix}. \tag{5.49}$$

Linear Robot Dynamics with Uncertainties

Next, consider the ignored nonlinear terms, $\hat{m}_{12}, \hat{m}_{21}, \hat{d}_{12}, \hat{d}_{21}, \hat{g}_1$, and $\hat{g}_2$. It is obvious

$$\sin(q_2(t) - q_1(t)) \le 1, \quad \cos(q_2(t) - q_1(t)) \le 1 \quad \forall \, q_1, \, q_2. \tag{5.50}$$

And there are same upper bound of the rotating speed.

$$\dot{q}_1(t), \quad \dot{q}_2(t) \le \dot{q}_{\max} \quad \forall \, t. \tag{5.51}$$

The positive constant number $\dot{q}_{\max}$ [rad/s] is the maximum rotating angle speed $\dot{q}$ to be stabilizable the system. In this system, $\dot{q}_{\max}$ is defined as 30[rad/s]. Therefore, the magnitudes of the ignored nonlinear terms are bounded by known constants such that

$$|\hat{m}_{12}| \le 1.68 \times 10^{-5} := \Delta\hat{m}_{12},$$
$$|\hat{m}_{21}| \le 1.68 \times 10^{-5} := \Delta\hat{m}_{21},$$
$$|\hat{d}_{12}| \le 5.04 \times 10^{-4} := \Delta\hat{d}_{12},$$
$$|\hat{d}_{21}| \le 5.04 \times 10^{-4} := \Delta\hat{d}_{21},$$
$$|\hat{g}_1| \le 9.01 \times 10^{-2} := \Delta\hat{g}_1,$$
$$|\hat{g}_2| \le 1.92 \times 10^{-2} := \Delta\hat{g}_2. \tag{5.52}$$

Furthermore, we would like to design robust controller against change of the load at the end of link 4. If a certain load m_L would be attached in that place, arm parameter, m_4, l_{c4}, I_4 (Table 5.1) would change. According to them, $\hat{m}_{11}, \hat{m}_{12}, \hat{m}_{21}, \hat{m}_{22}$ $\hat{d}_{12}, \hat{d}_{21}, \hat{g}_1$, and $\hat{g}_2$ would vary.

Hence its perturbations caused by the pay-load of them are defined as,

$$\delta\hat{m}_{11}, \delta\hat{m}_{12}, \delta\hat{m}_{21}, \delta\hat{m}_{22}, \delta\hat{d}_{12}, \delta\hat{d}_{21}, \delta\hat{g}_1, \delta\hat{g}_2. \tag{5.53}$$

From (5.52) and (5.53), we define the following terms.

$$\begin{aligned} \tilde{m}_{11} &:= \delta\hat{m}_{11}, & \tilde{m}_{12} &:= \Delta\hat{m}_{12} + \delta\hat{m}_{12}, \\ \tilde{m}_{21} &:= \Delta\hat{m}_{21} + \delta\hat{m}_{21} & \tilde{m}_{22} &:= \delta\hat{m}_{22}, \\ \tilde{d}_{12} &:= \Delta\hat{d}_{12} + \delta\hat{d}_{12}, & \tilde{d}_{21} &:= \Delta\hat{d}_{21} + \delta\hat{d}_{21}, \\ \tilde{g}_1 &:= \Delta\hat{g}_1 + \delta\hat{g}_1, & \tilde{g}_2 &:= \Delta\hat{g}_2 + \Delta\hat{g}_2. \end{aligned} \tag{5.54}$$

Hence the robot dynamics with the uncertainties is defined as

$$\begin{aligned} &\begin{bmatrix} \hat{m}_{11} + \tilde{m}_{11}\delta_1 & \tilde{m}_{12}\delta_3 \\ \tilde{m}_{21}\delta_4 & \hat{m}_{22} + \tilde{m}_{22}\delta_2 \end{bmatrix} \begin{bmatrix} \ddot{q}_1 \\ \ddot{q}_2 \end{bmatrix} \\ &+ \begin{bmatrix} \hat{d}_{11} & \tilde{d}_{12}\delta_5 \\ \tilde{d}_{21}\delta_6 & \hat{d}_{22} \end{bmatrix} \begin{bmatrix} \dot{q}_1 \\ \dot{q}_2 \end{bmatrix} + \begin{bmatrix} \hat{g}_1 \\ \hat{g}_2 \end{bmatrix} \Delta = \alpha \begin{bmatrix} v_1 \\ v_2 \end{bmatrix} \end{aligned} \tag{5.55}$$

where

$$|\delta_j(t)| \le 1 \quad (1 \le j \le 6), \qquad ||\Delta|| \le 1.$$

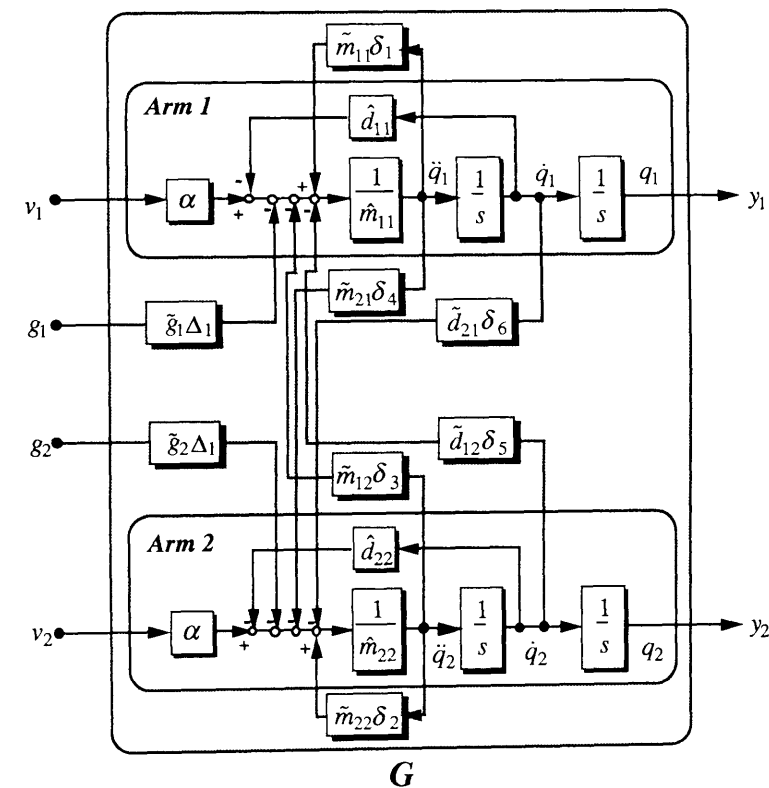The block diagram of the robot dynamics is shown in Fig. 5.10.

Figure 5.10: Block Diagram of the Robot Dynamics

5.2.5 Design

General Design Objective

We defined the design specification of the performance and the stability of the system as follows. Our objective is to achieve the robust stability for structured/unstructured uncertainties caused by nonlinear dynamical coupling of the links and pay-load m_L, and to achieve the asymptotic tracking for the reference signal. To put it concretely, the objective is expressed as following 3 points. (See Fig. 5.11).
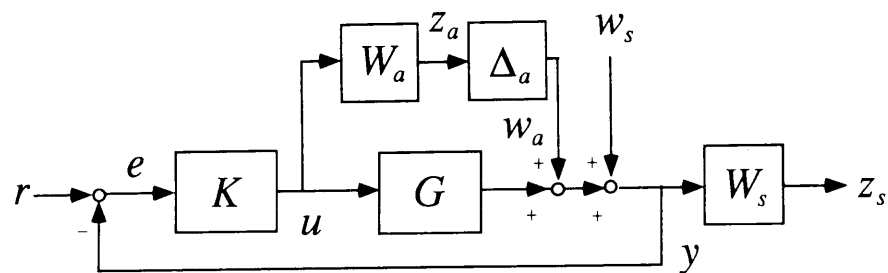

Figure 5.11: Closed-loop Interconnection Structure

1. The controller K stabilizes the closed-loop system against δ_1, δ_2, $\sim$, Δ_2, which are included in G (see Fig. 5.10 and Fig. 5.11).

2. We define the another unstructured uncertainties $W_a(s)\Delta_a(\|\Delta_a\| \leq 1)$ which indicates the neglected dynamics in the modeling process. W_a is a stable, rational transfer matrix. The system should maintain stability against this uncertainty.

3. The closed-loop system should have low sensitive characteristic. The weighting function for the performance condition is given by W_s. W_s is also a stable, rational transfer matrix.

Then the obtained open-loop interconnection structure is shown in Fig. 5.12, where

$$W_a = \begin{bmatrix} W_{a1} & 0 \\ 0 & W_{a2} \end{bmatrix}, \qquad W_s = \begin{bmatrix} W_{s1} & 0 \\ 0 & W_{s2} \end{bmatrix}. \tag{5.56}$$

In Fig. 5.12, $[v_1, v_2]^T$ are control inputs, which are motor voltages, and $[q_1, q_2]$ are the outputs, which are rotating angles. The velocity of the angle is not used for feedback control.

Robust H_∞ Control

First, let define the uncertainty block structure $\boldsymbol{\Delta}$ as

$$\boldsymbol{\Delta} := \{diag\,[\delta_1,\ \delta_2,\ \delta_3,\ \delta_4,\ \delta_5,\ \delta_6,\ \Delta_g,\ \Delta_a,\ \Delta_s],$$
$$: \quad \Delta_k(1 \leq k \leq 3)\ \in \mathbf{C^{2\times2}},\ \delta_j(1 \leq j \leq 6) \in \mathbf{R}\}, \tag{5.57}$$

where, $\Delta_g = diag[\Delta_1,\ \Delta_2]$, and Δ_s is a fictitious uncertainty for performance. Suppose that P denote the generalized plant, and LFT on P by K is defined as $\mathcal{F}_l(P, K)$.
$\boldsymbol{\Delta}$ is an nonlinear uncertainty, but its L_2 gain is bounded as $\|\boldsymbol{\Delta}\| \leq 1$. $\boldsymbol{\Delta}$ satisfies input-output stability. By using small gain theorem, the control problem is to find a controller K which satisfies

$$\|\,(\mathcal{F}_l(P, K)\,(j\omega))\,\|_\infty < 1, \tag{5.58}$$

This is the sufficient condition of the stability. To reduce the conservatism of the stability, the static constant scaling matrix D is employed [62]. Hence the condition should is transformed as follows.

$$\|D\,(\mathcal{F}_l(P, K)\,(j\omega))\,D^{-1}\|_\infty < 1, \tag{5.59}$$

where

$$D := diag[d_1, d_2, ..., d_6, d_7 \times I_{2\times2}, d_8 \times I_{2\times2}, d_9 \times I_{2\times2}, I_{2\times2}]$$

Controller Design

Specification and Design Parameters

The specification of the controller K is as follows.

- The close-loop system is internally stable and maintains the performance toward the plant perturbation by the added load m_L (=30[g]) at the hand.

The driving DC motor does not have much power (11[W]), and gear ratio η is relatively small ($\eta = 8$), hence the physical maximum load capacity is 100[g]. This 30[g] load bring 107 % increase of m_4, 230 % increase of l_{c4} and 820 % increase of I_4.

The arm parameters in Table 5.1 is changed by an added load m_L. Changed parameters are shown in Table 5.3. This table gives the magnitude of structured uncertainties as below. These parameters are employed for the controller design.
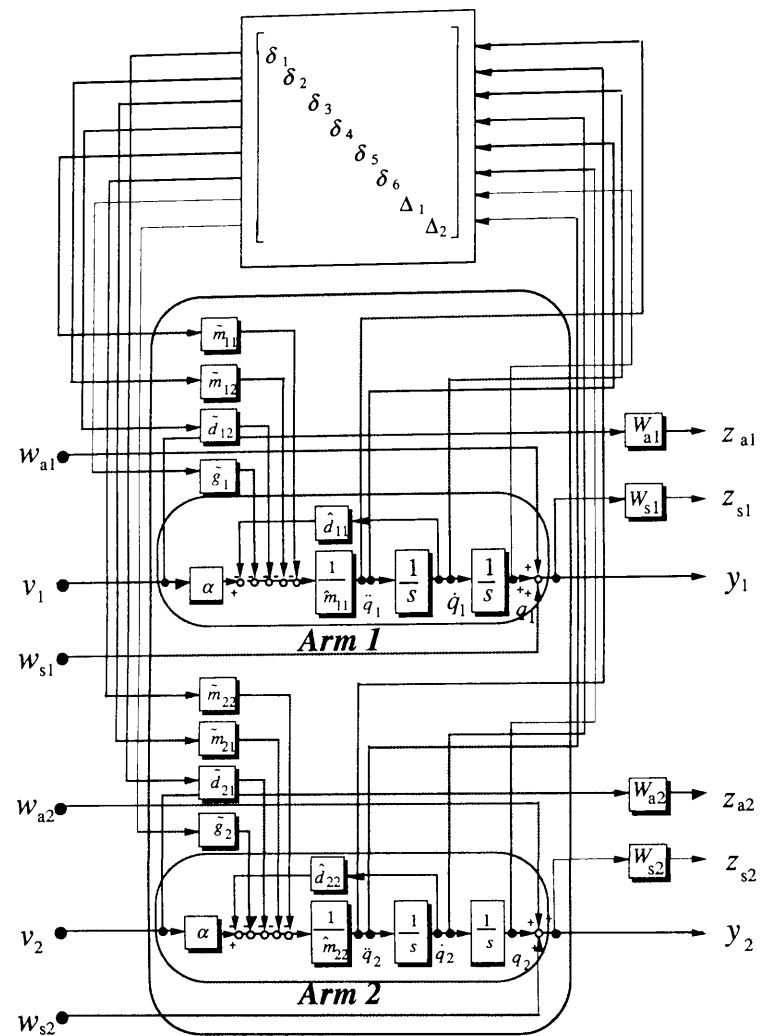
Figure 5.12: Open-Loop Interconnection Structure

$$\delta\hat{m}_{11} = 4.92 \times 10^{-4} \qquad \delta\hat{m}_{12} = 8.93 \times 10^{-4}$$

$$\delta\hat{m}_{21} = 8.93 \times 10^{-4} \qquad \delta\hat{m}_{22} = 1.40 \times 10^{-3}$$

$$\delta\hat{d}_{12} = 1.78 \times 10^{-3} \qquad \delta\hat{d}_{21} = 1.78 \times 10^{-3}$$

$$\delta\hat{g}_1 = 8.40 \times 10^{-2} \qquad \delta\hat{g}_2 = 6.39 \times 10^{-2}$$

After some primitive trial and error experiments, we decided the design parameters as follows.

$$W_{a1} = W_{a2} = 5 \times 10^{-5},$$

$$W_{s1} = W_{s2} = 5 \times 10^{-3}. \tag{5.60}$$

Table 5.3: Changed link parameters

$i = 4$	m_i[g]	l_i[mm]	l_{ci}[mm]	I_i[kgm^2]
Original	28.0	178.0	39.0	6.00×10^{-5}
Changed	**58.0**	**178.0**	**128.0**	$\mathbf{5.52 \times 10^{-4}}$

The final controller $K(s)$ is obtained, which satisfies the H_∞ norm specification (5.59). We employed a static constant scaling matrix D as follows [62].

$$D = diag[3.74 \times 10^{-7}, 6.10 \times 10^{-7}, 3.37 \times 10^{-7},$$
$$6.72 \times 10^{-7}, 2.07 \times 10^{-5}, 2.79 \times 10^{-5},$$
$$1.13 \times 10^{0} \cdot I_{2\times2}, 6.26 \times 10^{-3} \cdot I_{2\times2},$$
$$1.00 \cdot I_{2\times2}, I_{2\times2}] \tag{5.61}$$

The controller K is as below.

$$K(s) = \begin{bmatrix} K_{11}(s) & K_{12}(s) \\ K_{21}(s) & K_{22}(s) \end{bmatrix}, \tag{5.62}$$

Frequency response of the controller is shown in Fig. 5.13, and the singular value of the closed-loop transfer function $F_l(P, K)$ is plotted in Fig. 5.14. In Fig. 5.13, $K_{12}(s)$ and $K_{21}(s)$ are nearly 0, hence they does not appear. It can be seen that the design objective has been satisfied from Fig. 5.14.

5.2.6　Experiments

PD Computed-Torque Control

We prepared the computed-torque controller with PD compensator so as to compare with a H_∞ controller. The employed PD computed-torque controller is shown below.

$$v = M(q)u + h(q, q) + V\dot{q} + g(q),$$
$$u = \ddot{q}_d + K_v(\dot{q}_d - \dot{q}) + K_p(q_d - q), \tag{5.63}$$

where, $K_p = 10000$, $K_v = 200$, and $M(q)$, $h(q, \dot{q})$, V, $g(q)$ are defined in (5.39) and (5.40). The gains: K_p and K_v are selected to be satisfied a critical damping condition [10].
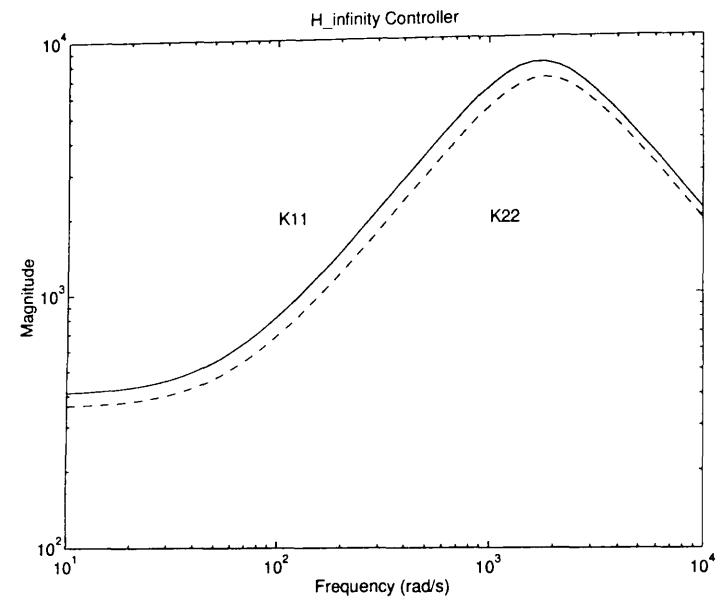
Figure 5.13: Frequency Response of the Controller

Experimental Results

The designed H_∞ controller is a continuous-time system. In order to implement this controller with the DSP system, it is discretized via the well known Tustin transform, where sampling period is $50\mu s$. But the computed torque controller is implemented with the $100\mu s$ sampling period, because of its calculation of nonlinear compensater. Digital Control System possesses DSP TMS320C30(TI). The manipulator succeeded in tracking of the smooth desired trajectories using the H_∞ controller. Then, the results of the step responses are shown in Fig. 5.15 and 5.16, where dashed and solid lines indicate desired trajectories and sensor outputs in the joint space, respectively. Step width is 0.5[rad](28.65[deg]) in the all figures.

1. **Result 1:** In Fig. 5.15, the hand does not have any load. Both results show good responses.

2. **Result 2:** When the hand has 30[g] load, both controllers indicated good response as **Result 1**. Specification had been satisfied.

3. **Result 3:** In Fig. 5.16, the hand has 60[g] load. The H_∞ controller shows better response in these figures.
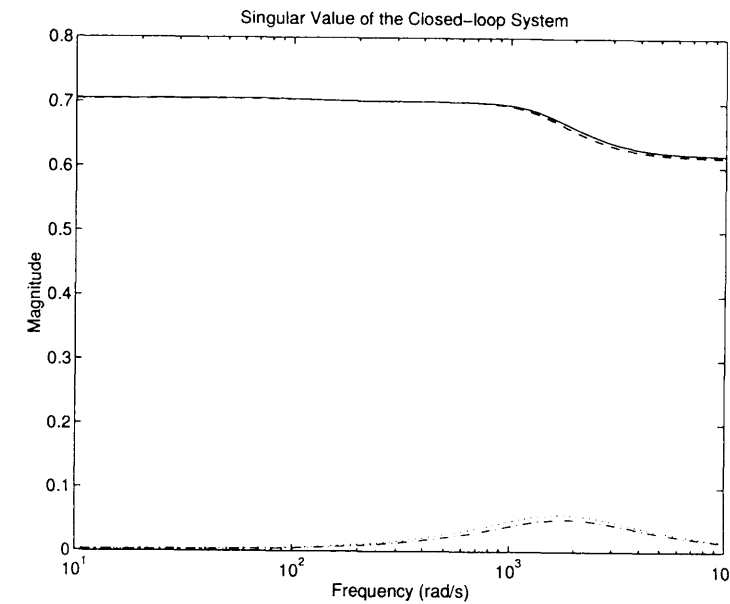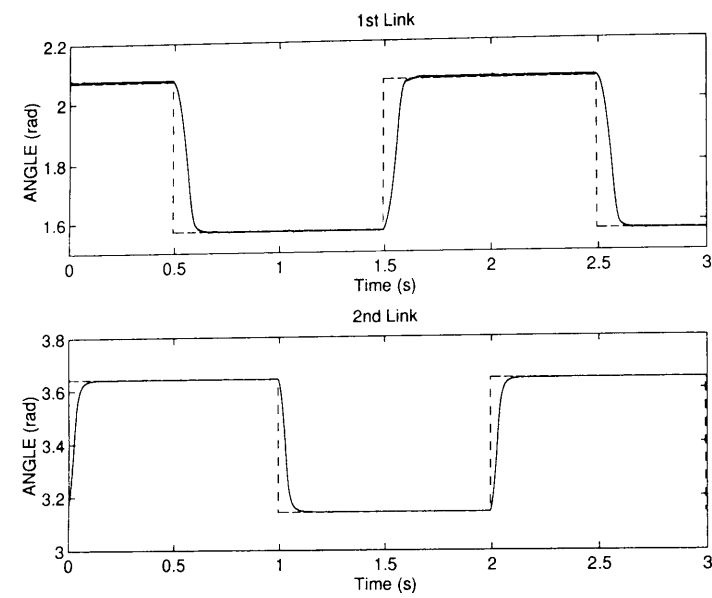
Figure 5.14: Singular Value plot of $F_l(P, K)$

From the above experimental results, it has been indicated that the proposed H_∞ controller holds good robust performance experimentally.

5.2.7   Conclusions

This section proposed a linear robust control scheme for the robotic trajectory tracking based on the H_∞ control theory. We demonstrated the robustness of the proposed scheme by experiments on a parallel link robot manipulator.

Taking the actuator dynamics into account, the nominal linear dynamic model of the manipulator was derived. The coupling between joints and the gravity forces were treated as the real structured uncertainties. These uncertainties are nonlinear, but bounded by known constants, hence the constant scaled H_∞ control scheme was employed to achieve robust performance specifications. The controller was designed with consideration of the perturbation of link parameters, which was caused by loads putted on the end of the hand. The experimental results showed remarkable robustness of the proposed controller.

(a) H_∞ Control (no load)
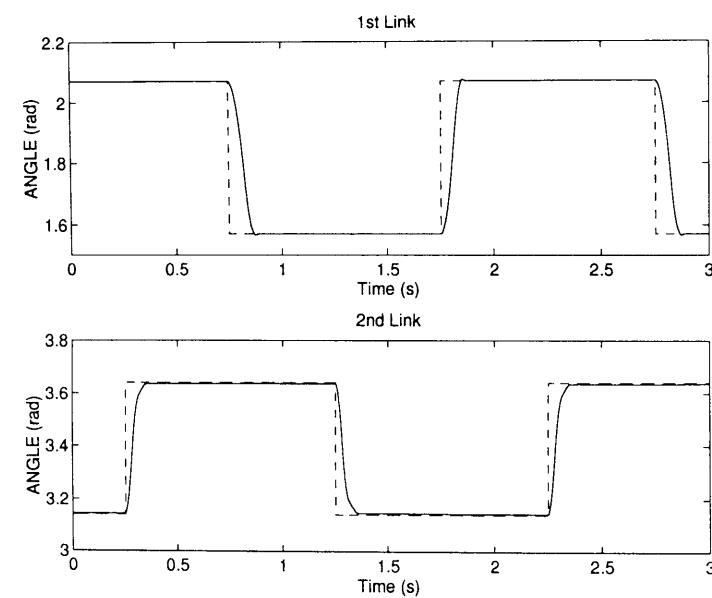
(b) PD Computed-Torque Control (no load)

Figure 5.15: Step Response: H_∞ Control and PD Computed-Torque Control (no load)
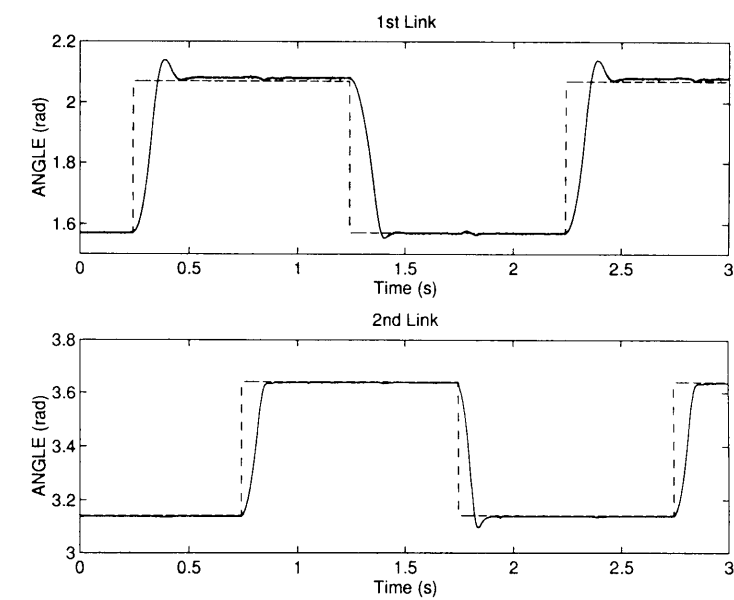
(a) H_∞ Control (60[g] load)
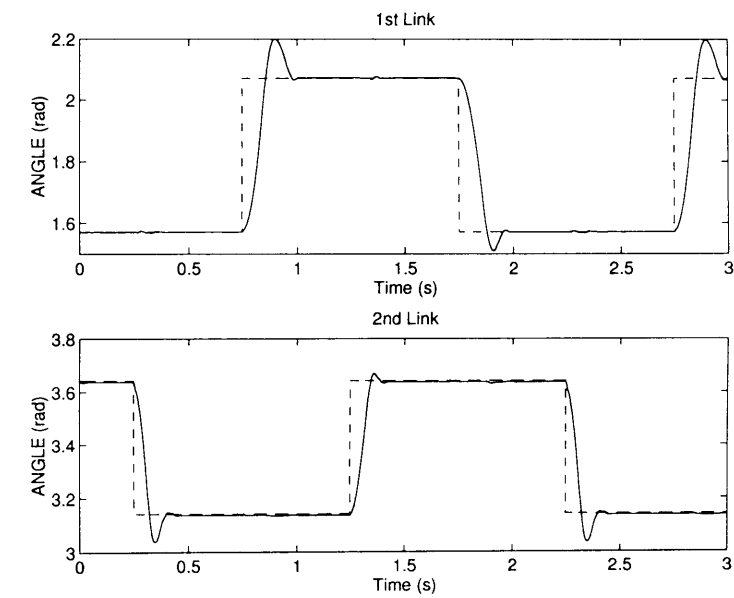
(b) PD Computed-Torque Control (60[g] load)

Figure 5.16: Step Response: H_∞ Control and PD Computed-Torque Control (60[g] load)

5.3 μ-Synthesis of Robot Manipulators Using Linear Parameter Varying Representation

In this section, we present a robust control for a flexible-joint robot manipulator using linear parameter varying representation. The robot manipulator dynamics can be brought to a quasi linear parameter varying (LPV) form by a state transformation. An LPV system is defined as a linear system whose dynamics depend on an exogenous variable which can be measured upon system operation. In this case, the scheduling variables are the joint angles q. which are state variables. Using a quasi-LPV form, we design a robust controller by μ-synthesis to achieve robust performance specification.

5.3.1 Introduction

Gain scheduling methodology has proven to be a successful design method in main engineering application. This idea is to construct a global feedback control system for a time-varying and/or nonlinear plant from a collection of local 'linear' 'time-invariant' designs [66][67][3][60] [83].

The gain scheduled design is novel in that it does not involve linearizations about trim conditions of the plant dynamics. Rather, the plant dynamics are brought to a linear parameter varying (LPV) form via a state transformation.

In this section, we present a LPV approach [66] [67] to a gain scheduled flexible-joint robot manipulator design. The robot manipulator control problem under consideration is gravity force cancellation. In standard gain scheduling, the design plants consist of a collection of linearizations about equilibrium conditions indexed by the scheduling variable, in this case the link angle, q. In the present approach, the design plants also consist of a family of linear plants indexed by the joint angle. A key difference between the present approach and standard gain scheduling is that this family is not the result of linearizations. Rather, it is derived via a state-transformation of the original plant dynamics. Since no linearization is involved, the approach is not limited by the local nature of standard gain scheduled designs. Since gain scheduling generally encounters families of linear plants indexed by a scheduling variable, Shamma [66][67] defined to such a family as a Linear Parameter Varying (LPV) plants. LPV plants differ from linear time-varying plants in that the time-variations (i.e., the scheduling variable) is unknown from the first but may be measured/estimated upon operation of the feedback system. Such a family is called

LPV in case the scheduling variable is actually endogenous to the state dynamics. In this case, the scheduling variable is the joint angle. This is actually an endogenous variable. Once in a LPV form, a robust controller using μ-synthesis is designed to achieve robust performance condition.

The remainder of this section is organized as follows. First, we derive the LPV form of the nonlinear flexible-link robot manipulator. Next, we design a linear robust controller based on μ-synthesis. Then the simulation results for the flexible-link robot manipulator system are presented. Finally, some concluding remarks are given.

5.3.2 Robot Dynamics

Flexible Joint Robot

The plant that is a 2-DOF flexible joint robot manipulator is shown in Fig. 5.17.
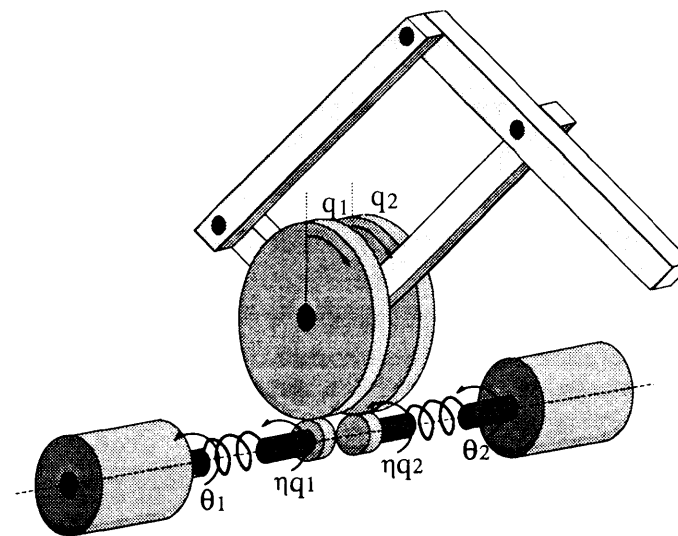
Figure 5.17: 2-DOF Flexible Joint Robot Manipulator

This system is constructed with two DC motors and a parallel link robot manipulator. Each joint is actuated by an 11 watt DC motor through a reduction gear whose ratio is 1:8. This manipulator has four incremental encoders, two of them which measure link angle, are used for the feedback control, and the other two encoders are employed to measure only joint angles. The total mass of this robot manipulator system is about only 2.0 [kg]. Link flexibility can be changed according to spring at joints [56].

Modeling

The dynamic model of the DC motors and joints are described as following equations,

$$J_{\theta 1}\ddot{\theta}_1 + \frac{a_m K^2}{R}\dot{\theta}_1 + k(\theta_1 - \eta q_1) = \frac{a_m K}{R}v_1,$$

$$J_{\theta 2}\ddot{\theta}_2 + \frac{a_m K^2}{R}\dot{\theta}_2 + k(\theta_2 - \eta q_2) = \frac{a_m K}{R}v_2, \qquad (5.64)$$

where $J_{\theta i}$ is inertia of DC motor, a_m is amplifier gain, K is back electromotive force (emf), k is spring constant, η is gear ratio, θ_i is motor angle, and q_i is link angle ($i = 1,\ 2$).

Furthermore, the dynamics of the parallel link robot manipulator is written as follows[57].

$$\begin{bmatrix} M_{11} & M_{12}\cos(q_2-q_1) \\ M_{12}\cos(q_2-q_1) & M_{22} \end{bmatrix}\begin{bmatrix} \ddot{q}_1 \\ \ddot{q}_2 \end{bmatrix}$$
$$+ \begin{bmatrix} f_1 & -M_{12}\dot{q}_2\sin(q_2-q_1) \\ M_{12}\dot{q}_1\sin(q_2-q_1) & f_2 \end{bmatrix}\begin{bmatrix} \dot{q}_1 \\ \dot{q}_2 \end{bmatrix}$$
$$+ \begin{bmatrix} V_1\sin q_1 \\ V_2\sin q_2 \end{bmatrix} = \begin{bmatrix} \eta k(\theta_1 - \eta q_1) \\ \eta k(\theta_2 - \eta q_2) \end{bmatrix}. \qquad (5.65)$$

Model parameter values are listed in Table 5.4. Hence the dynamics of this robot manipulator with actuator and flexible-joint is expressed by eq.(5.64) and (5.65).

Table 5.4: Parameter of the experimental system

Parameter	Symbols	Value
Motor Inertia [Nm/sec^2]	$J_{\theta 1},\ J_{\theta 2}$	2.25×10^{-6}
Amplifier Gain	a_m	2.0
EMF constant [V/rad·s]	K	3.4×10^{-2}
Resistance [Ω]	R	7.9
Gear ratio	η	8.0
spring constant [kgm/rad]	k	1.74
Inertia element [N·s^2/rad^2]	M_{11}	3.77×10^{-3}
	M_{12}	-2.30×10^{-5}
	M_{22}	2.86×10^{-3}
Gravity element [N]	V_1	8.99×10^{-2}
	V_2	2.08×10^{-2}
Friction element [N·s/rad]	$f_1,\ f_2$	9.37×10^{-3}

LPV Representation

If we assume a priori bounds on the angular velocities of the links,

$$|\dot{q}_1| < \nu_1, \qquad |\dot{q}_2| < \nu_2. \qquad (5.66)$$

From (5.64), (5.65), and (5.66), the following state-space model is derived.

$$\frac{d}{dt}\begin{bmatrix} z \\ w \end{bmatrix} = f(z) + A(z)\begin{bmatrix} z \\ w \end{bmatrix} + B(z)u. \qquad (5.67)$$

where

$$z = [\,q_1,\ q_2\,]^T, \quad w = [\,\theta_1,\ \theta_2,\ \dot{q}_1,\ \dot{q}_2,\ \dot{\theta}_1,\ \dot{\theta}_2\,]^T,$$

$$u = [\,v_1,\ v_2\,]^T,$$

$$f(z) = \begin{bmatrix} 0 \\ 0 \\ 0 \\ 0 \\ m_{11}(z)V_1\sin q_1 + m_{12}(z)V_2\sin q_2 \\ m_{12}(z)V_1\sin q_1 + m_{22}(z)V_2\sin q_2 \\ 0 \\ 0 \end{bmatrix},$$

$$A(z) = \begin{bmatrix} 0 & 0 & 0 & 0 & 1 & 0 & 0 & 0 \\ 0 & 0 & 0 & 0 & 0 & 1 & 0 & 0 \\ 0 & 0 & 0 & 0 & 0 & 0 & 1 & 0 \\ 0 & 0 & 0 & 0 & 0 & 0 & 0 & 1 \\ -m_{11}\eta^2 k & -m_{12}\eta^2 k & m_{11}\eta k & m_{12}\eta k & \hat{m}_{11} & \hat{m}_{12} & 0 & 0 \\ -m_{12}\eta^2 k & -m_{22}\eta^2 k & m_{12}\eta k & m_{22}\eta k & \hat{m}_{21} & \hat{m}_{22} & 0 & 0 \\ \frac{\eta^2 k}{J_1} & 0 & -\frac{k}{J_1} & 0 & 0 & 0 & -\frac{a_m}{J_1 R} & 0 \\ 0 & \frac{\eta^2 k}{J_2} & 0 & -\frac{k}{J_2} & 0 & 0 & 0 & -\frac{a_m}{J_2 R} \end{bmatrix},$$

$$B(z) = \begin{bmatrix} 0 & 0 & 0 & 0 & 0 & \frac{a_m K}{J_1 R} & 0 \\ 0 & 0 & 0 & 0 & 0 & 0 & \frac{a_m K}{J_2 R} \end{bmatrix}^T,$$

$$\hat{m}_{11}(z) = -m_{12}(z)M_{12}\nu_1\sin(q_2-q_1) - m_{11}F_1,$$

$$\hat{m}_{12}(z) = -m_{11}(z)M_{12}\nu_2\sin(q_2-q_1) - m_{12}F_2,$$

$$\hat{m}_{21}(z) = -m_{22}(z)M_{12}\nu_1\sin(q_2-q_1) - m_{12}F_1,$$

$$\hat{m}_{22}(z) = -m_{12}(z)M_{12}\nu_2\sin(q_2-q_1) - m_{22}F_2,$$

$$m_{11}(z) = M_{22}/\{M_{11}M_{22} - M_{12}^2 \cos^2(q_2 - q_1)\},$$

$$m_{12}(z) = -M_{12}\cos(q_2 - q_1)/\{M_{11}M_{22} - M_{12}^2 \cos^2(q_2 - q_1)\},$$

$$m_{22}(z) = M_{11}/\{M_{11}M_{22} - M_{12}^2 \cos^2(q_2 - q_1)\}.$$

In equation (5.67), $z(t)$ is the controlled output, and the nonlinearities depend only on $z(t)$. Such systems are sometimes called "output-nonlinear" systems.

We assume that there exist continuously differentiable functions $w_{eq}(z)$ and $u_{eq}(z)$ such that

$$0 = f(z) + A(z)\begin{bmatrix} z \\ w_{eq} \end{bmatrix} + B(z)u_{eq}(z). \tag{5.68}$$

In other words, we have a family of equilibrium states parameterized by the controlled output $z(t)$.

Further, we can easily find the equilibrium states as

$$w_{eq}(z) = \begin{bmatrix} \eta q_1 - \frac{V_1}{\eta k}\sin q_1 \\ \eta q_2 - \frac{V_2}{\eta k}\sin q_2 \\ 0 \\ 0 \\ 0 \\ 0 \\ \frac{RV_1}{\eta a_m K}\sin q_1 \\ \frac{RV_2}{\eta a_m K}\sin q_2 \end{bmatrix}, \qquad u_{eq} = \begin{bmatrix} 0 \\ 0 \end{bmatrix}.$$

Next, we divide $A(z)$, $B(z)$ to conform with $[z \;\; w]^T$ as

$$A(z) = \begin{bmatrix} A_{11}(z) & A_{12}(z) \\ A_{21}(z) & A_{22}(z) \end{bmatrix}, \quad B(z) = \begin{bmatrix} B_1(z) \\ B_2(z) \end{bmatrix}, \tag{5.69}$$

From (5.67), (5.68) and (5.69), it is easy to show that the state dynamics may be written as

$$\frac{d}{dt}\begin{bmatrix} z \\ w \end{bmatrix} = \begin{bmatrix} 0 & A_{12}(z) \\ 0 & A_{22}(z) \end{bmatrix}\begin{bmatrix} z \\ w - w_{eq} \end{bmatrix} + \begin{bmatrix} B_1(z) \\ B_2(z) \end{bmatrix}u. \tag{5.70}$$

Furthermore it is transformed as

$$\frac{d}{dt}\begin{bmatrix} z \\ w - w_{eq} \end{bmatrix} = \begin{bmatrix} 0 & A_{12}(z) \\ 0 & A_{22}(z) - Dw_{eq}A_{12}(z) \end{bmatrix}\begin{bmatrix} z \\ w - w_{eq} \end{bmatrix} + \begin{bmatrix} B_1(z) \\ B_2(z) - Dw_{eq}B_1(z) \end{bmatrix}u, \tag{5.71}$$

where $Dw_{eq} = \partial w_{eq}/\partial z$.

We have obtained the above linear parameter varying representation (LPV) model, with the variable $z(t)$ as the "exogenous" parameter.

5.3.3 Control System Design

Problem Setup

In this section, we design the control system by using the obtained LPV model representation. Now we consider the block structure shown in Fig.5.18, where the block P_{des} shows the LPV design plant.
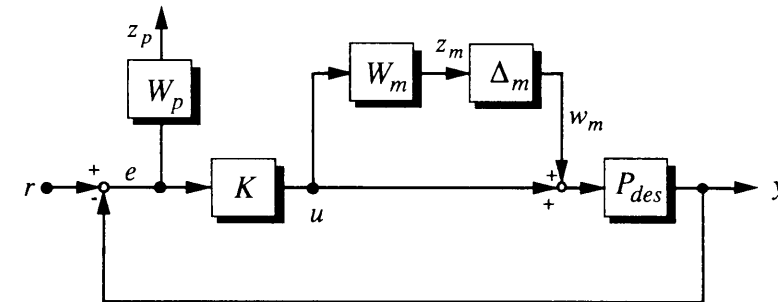

Figure 5.18: Control Problem

The design specification for the robustness and the performance is defined as.

- **Robust stability specification**

  The block Δ_m shows the input uncertainty of the plant (motor and joint), especially the perturbation of the spring constant of the joint. Δ_m is the linear time invariant multiplicative uncertainty, at the plant input and the function W_m is its weighting. Hence the robust stability condition for Δ_m is $||T_{W_m Z_m}||_\infty < 1$, where $T_{W_m Z_m}$ is the transfer function $W_m \to Z_m$.

- **Performance specification**

  The performance specification is to keep the influence below from the reference r to the error e. This requirement should be replaced to the problem which find the controller K to achieve $||W_p T_{re}||_\infty < 1$, where W_p is a weighting function, and T_{re} is the transfer function $r \to e$

The above design specification is fitted in the μ-synthesis framework [74].

At first, we introduce the fictitious performance uncertainty Δ_p, and define the linear time-invariant block structure $\boldsymbol{\Delta}$ with Δ_p and Δ_m as follows.

$$\boldsymbol{\Delta} := \left\{ \begin{bmatrix} \Delta_p & 0 \\ 0 & \Delta_m \end{bmatrix} : \Delta_p, \Delta_m \in C^{2\times2}, \;\; ||\Delta_p||_\infty \le 1, \;\; ||\Delta_m||_\infty \le 1 \right\}. \tag{5.72}$$

Hence the control problem is to find the controller K which satisfy the following structured singular value test, where P_{gen} is the generalized plant which is constructed with P_{des} and the weighting functions, W_p and W_m.

$$\sup_{\omega \in \mathbf{R}} \mu_{\underline{\Delta}} \left(\mathcal{F}_l \left(P_{gen}, K \right) \left(j\omega \right) \right) < 1. \tag{5.73}$$

Design

In this section, we do not schedule the controller gain on the parameter z, and we fix the z as $z_s := [\ \frac{\pi}{2}\ \ 0\ ]^T$, and design the fixed μ controller. Here our approach taken here is so-called $D - K$ iteration approach, which is to find the controller K to satisfy

$$\sup_{\omega \in \mathbf{R}} \mu_{\underline{\Delta}} \left(D \mathcal{F}_l \left(P_{gen}, K \right) D^{-1} \left(j\omega \right) \right) < 1, \tag{5.74}$$

where D is a scaling matrix.

For the weighting functions, we selected the below functions according to the several simulation results.

$$W_m = 2.0 \times 10^{-1} \times \frac{s+1}{s+10} \begin{bmatrix} 1 & 0 \\ 0 & 1 \end{bmatrix} \tag{5.75}$$

$$W_p = 3.0 \times \frac{s+10}{s+0.1} \begin{bmatrix} 1 & 0 \\ 0 & 1 \end{bmatrix} \tag{5.76}$$

A μ-synthesis design procedure [74] was performed with this formulation at the set point $z_s := [\ \frac{\pi}{2}\ \ 0\ ]^T$. That is the z-dependent coefficient matrices of the LPV plant P_{des} were evaluated at $z_s := [\ \frac{\pi}{2}\ \ 0\ ]^T$ for the design. The first pass led to a frozen z robust performance level of 1.09. After two iterations, this value was reduced to 0.8. For the scaling matrix D, we selected the following static matrix

$$D = \mathrm{diag}[-2.68 \times 10^{-2}, 2.97 \times 10^0, 2.05 \times 10^{-2}, I_{2 \times 2}] \tag{5.77}$$

The obtained final controller $K(s)$ is as below.

$$K(s) = \begin{bmatrix} K_{11}(s) & K_{12}(s) \\ K_{21}(s) & K_{22}(s) \end{bmatrix} \tag{5.78}$$

The frequency response of the controller K is shown in Fig. 5.19, where $K_{11}(s)$ and $K_{22}(s)$ are indicated by the solid line and the dashed line, respectively. $K_{12}(s)$ and $K_{21}(s)$ are relatively small because of the reduction gears.

Now gain scheduled design procedure would typically involve repeating of design at the fixed-q set points and its interpolation. However, it turns out the obtained controller delivered robust performance for all $\{18 \times 18\}$ (q_1, q_2) sets. Thus, no controller gain-scheduling was employed.
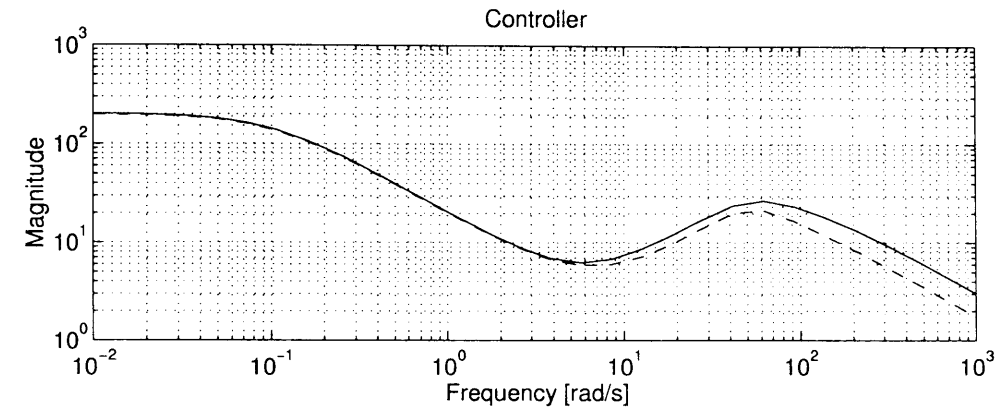
Figure 5.19: Frequency Response of the Controller K

5.3.4 Simulation Results

With the obtained final controller $K(s)$, we realize the control law on the simulator, SIMULINK, and evaluate the effect of this proposed approach. For the comparison, we add the result with the PI controller.

Simulation is done with the following conditions.

- Time response with step reference.

- Response of the first link.

- The reference angle is 90 degree(0.785[rad]).

- Solid line: μ controller, dashed line: PI controller.

The result is shown in Fig. 5.20. It can be shown that response indicates overshooted which is caused by the spring, but it is quickly got under control.

Figure 5.20: Simulation Results of the Step Response

5.3.5   Conclusion

In this section, we apply a linear parameter varying approach to a flexible joint robot control. At first, we introduce the flexible joint robot, and after that derive the LPV form of the nonlinear flex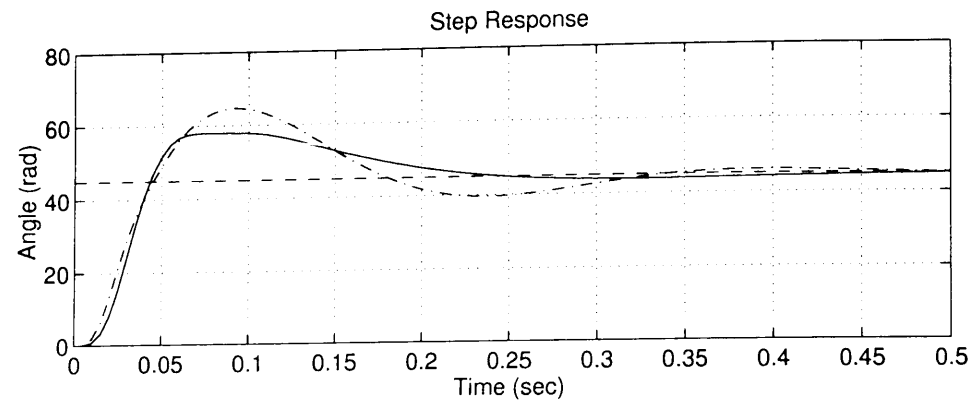ible-link robot manipulator. Next, we review background material on LPV systems, gain scheduling control and μ-synthesis. Then we presented the design, simulation results for the flexible-link robot manipulator system.

5.4   Consideration and Investigation for Approaches

All three control methodologies showed the better robustness and performance than conventional PD or computed torque method. Each method has its merits and demerits, and summary is written as follows.

- μ-synthesis with exact linearization

    - The evaluation of the uncertainties: E and H are conservative.

    - The controller employs inverse dynamic computation, a sampling period of this approach is long. This long sampling period deteriorate the control performance.

    - The generalized plant is relatively simple and control system design is easy.

- constant scaled H_∞ control considering structured uncertainties

    - The evaluation of the uncertainties contains less conservativeness because uncertainties are described as structured.

    - The controller does not employ inverse dynamic computation, computational burden for the controller is only matrix vector multiplications. The sampling period of this approach is shorter than the other nonlinear control schemes.

    - The control input is continuous.

    - The generalized plant is very complex and application of this approach to 6-DOF manipulator is not easy.

- linear parameter varying representation approach

    - Controller implementation contains nonlinear calculation but the total burden is not so heavy.

    - Feedback gain is regulated according to the link angle, hence the performance against arm position is excellent.

Chapter 6

Conclusions

In this thesis, I discussed robust H_∞/μ control and uncertainty description of mechatronic systems including robot manipulators.

The contribution of this thesis is as follows.

- We made a set of plant model and quantify the model uncertainties, and clarified the limit of allowable class of perturbation for robust stability and performance.

- We applied this robust H_∞/μ control theory to robot manipulators in order to show the effectiveness of H_∞/μ control law for nonlinear robot manipulators. Our approaches taken here were as follows.

    - μ-synthesis with exact linearization

    - constant scaled H_∞ control considering structured uncertainties

    - μ-synthesis using linear parameter varying representation

- We developed the H_∞/μ control technique and applied it to real mechanical systems, then evaluated the performance of the control theme and expressive ability of LFT against various forms of uncertainties. And we showed that H_∞/μ control has a good framework to treat uncertainties, in order to guarantee robust stability and robust performance by using magnetic bearing, a pantograph system with linear DC motor, and robot manipulator

Chapter 2

Chapter 2 referred a general robust control problem. In this chapter, at first, framework of the robust control was described, especially about modeling, uncertainty, and uncertainty

descriptions. Then H_∞ control problem/theory, and μ-analysis and synthesis approach was introduced.

Chapter 3

In chapter 3, robust control of magnetic suspension systems was described.

Section 3.1

In this section, we experimentally evaluated a controller designed by μ-synthesis methodology with an electromagnetic suspension system. We have obtained a nominal mathematical model as well as a set of plant models in which the real system is assumed to reside. With this set of the models we designed the control system to achieve robust performance objective utilizing μ-synthesis method. Firstly, four types of different model structures were derived based on the several idealizing assumptions for the real system. Secondly, for every model, the nominal value as well as the possible maximum and minimum values of each model parameter was determined by measurements and/or experiments. Thirdly, a nominal model was naturally chosen. This model has the simplest model structure of all four models and makes use of nominal parameter values. Then, model perturbations were defined to account for additive unstructured uncertainties from such as neglected nonlinearities and model parameter errors. Fourthly, we defined a family of plant models where the unstructured additive perturbation was employed. The method to model the plant as belonging to a family or set plays a key role for systematic robust control design. Fifthly, we setup robust performance objective as a structured singular value test. Next, for the design, the $D - K$ iteration approach was employed. Finally, the experimental results showed that the closed-loop system with the μ-controller achieves not only nominal performance and robust stability, but in addition robust performance.

Section 3.2

In this section, we proposed the gain scheduled H_∞ robust control scheme with the free parameter for a magnetic bearing in order to eliminate the unbalance vibration. We treated the changing unbalance vibration caused by varying rotational speed as the known frequency-varying disturbance, and adjusted the controller gain according to the rotational speed of the rotor using the free parameter Φ of the H_∞ controller. The obtained controller K has high gain at the operating frequency. First, the dynamics of the AMB system was

considered and a nominal mathematical model for the system was derived. Next, the conditions for the existence of controllers were derived, and, we designed the gain scheduled H_∞ robust controllers using LSDP. It rejected the sinusoidal disturbance of the varying rotor speed. Finally the simulations and experimental results showed the effectiveness of this proposed method.

Chapter 4

In this chapter, we improved the control performance of active pantograph system which has very oscillating property, at the resonance frequency by applying μ-synthesis approach. We considered parametric uncertainty and uncertainty caused by unmodeled dynamics, and measure their quantities, and for these uncertainties, we setup the robust performance problem. And then, we solved the above problem, designed a robust controller. Finally, we showed several experimental results, and indicated the effectiveness of proposed control system design methodology by comparing conventional H_∞ controller with time and frequency responses.

Chapter 5

In chapter 5, robust control of robot manipulators was discussed.

Section 5.1

This section has presented that performance of controllers depend on their sampling rates experimentally. We have indicated that if time delay for implementation get over a threshold value $T_{\max}$, the design specification of the controller is not satisfied. This represents that high-speed processors are indispensable, and control system design should be considered time delay for the achievement of performance specification. For the control system design, we utilized μ-synthesis methodology and carried out experiments with a robot manipulator using DSP. Firstly, we considered a dynamics of the robot manipulator, and derived a linear model as well as the uncertainties for the model. We employed the computed-torque method to obtain a simple linear model for manipulators.Secondly, we constructed the generalized plant which is considered the above uncertainties, and set robust performance objectives as a structured singular value test. We designed control systems by $D - K$ iteration approach. Three controllers: T_a, T_b, and T_c are obtained, which are designed in consideration of time delay. Next, continuous controller K_2 designed without considering

time delay was discretized to Kd_a, Kd_b, and Kd_c with the sampling rate of T_a, T_b, and T_c, respectively. After that, we carried out a lot of experiments using a DSP. Experimental results show that controller K_c and Kd_c which have long sampling period are not satisfied robust performance. This showed that high-speed processors can bring out the high performance in the designed controllers. In other words, robust performance can be realized owing to the latest high-speed digital signal processors.

Section 5.2

This section proposed a linear robust control scheme for the robotic trajectory tracking based on the H_∞ control theory. We demonstrated the robustness of the proposed scheme by experiments on a parallel link robot manipulator. Taking the actuator dynamics into account, the nominal linear dynamic model of the manipulator was derived. The coupling between joints and the gravity forces were treated as the real structured uncertainties. These uncertainties are nonlinear, but bounded by known constants, hence the constant scaled H_∞ control scheme was employed to achieve robust performance specifications. The controller was designed with consideration of the perturbation of link parameters, which was caused by loads putted on the end of the hand. The experimental results showed remarkable robustness of the proposed controller.

Section 5.3

In this section, we apply a linear parameter varying approach to a flexible joint robot control. At first, we introduce the flexible joint robot, and after that derive the LPV form of the nonlinear flexible-link robot manipulator. In section 5.3.3, we review background material on LPV systems, gain scheduling control and μ-synthesis. Section 5.3.4 presents the design, simulation results for the flexible-link robot manipulator system.

In this thesis, I discussed the latest advanced robust control theory and uncertainty description for mechatronic systems.

H_∞/μ and linear fractional transformation has a good expressive ability of uncertainty. Guarantee of the robust stability depends on small gain theorem and Nyquist stability criterion. The small gain theorem is very powerful, and useful in a variety of ways. Conservativeness is the only demerit.

In this paper, I did not treat the uncertainty caused by unmodeled nonlinear dynamics. This is the most challenging issue in the robust control theory. If I could, I would like to contribute to solve this problem theoretically.

To conclude, I would like to hope that Robust Control Theory and Mechatronics will develop infinitely(∞)!!

Bibliography

[1] P. Allaire, Ed., " *Magnetic Bearings,*" *Proc. Third Int. Symp. Magnetic Bearings,* Alexandria, Virginia, 1992.

[2] P. Apkarian, P. Gahinet, G. Becker, " Self-Scheduled H_∞ Control of Linear Parameter-Varying Systems," *Proc. of American Control Conference,* pp. 856-860, 1994.

[3] P. Apkarian, P. Gahinet and G. Becker, "Self-scheduled $\mathcal{H}_\infty$ Control of Linear Parameter-varying Systems: a Design Example," *Automatica,* vol. 31, no. 9, pp. 1251-1261, 1995.

[4] S. Asai, M. Koide, K. Ohshima, and S. Fujii, " Joint Torque Sensory Feedback Control of a Manipulator Using μ-Synthesis," *Proc. of SICE'95,* pp. 403-404, 1995 (in Japanese).

[5] G. J. Balas and J. C. Doyle, " Robustness and Performance Tradeoffs in Control Design for Flexible Structures," *Proc. 29th IEEE Conference on Decision and Control,* Hawaii, 1990.

[6] G. J. Balas, J. C. Doyle, K. Glover, A. Packard and R. Smith, "*μ-Analysis and Synthesis Toolbox User's Guide,*" Musyn Inc. and The Math Works Inc., 1991.

[7] G. J. Balas, P. Young and J. C. Doyle, " The Process of Control Design for the NASA Langley Minimast Structure," *Proc. American Control Conference,* pp. 562-567, Boston, 1991.

[8] C. Checkoway, K. Kirk, D. Sullivan and M. Townsend, " *SIMULINK User's Guide,*" The Math Works, Inc., 1992.

[9] R. F. Cotellessa, Ed., "*Robust Control,*" *IEEE Press selected reprint series, IEEE order number: PC02204,* 1987.

[10] J. J. Craig, " *Introduction to robotics: mechanics and control,*" Addison Wesley Publishing Company, 2nd Ed., 1989.

[11] J. C. Doyle, B. A. Francis, and A. R. Tannenbaum, " *Feedback Control Theory,*" Macmillan Publishing Company, 1992.

[12] J. C. Doyle, K. Glover, P. P. Khagonekar and B. A. Francis, " State-Space Solutions to Standard H_2 and H_∞ Control Problems," *IEEE Trans. on Automatic Control,* vol. 34, no. 8, pp. 831-847, 1989.

[13] J. C. Doyle, A. Packard, and K. Zhou., " Review of LFTs, LMIs and μ," *Proc. 30th IEEE Conference on Decision and Control,* Brighton, England, 1991.

[14] J. C. Doyle, B. A. Francis, and A. R. Tannenbaum, " *Feedback Control Theory,*" Macmillan, 1992.

[15] dSPACE, " *DSP-CITpro Hardware manual,*" dSPACE digital signal processing and control engineering GmbH., An der Schonen Aussicht 2. D-4790, 1989.

[16] B. A. Francis, " *A Course in H_∞ Theory,*" *Lecture Notes in Control and Information Sciences,* vol. 88, Springer-Verlag, 1986.

[17] M. Fujita, K. Hatake and F. Matsumura, "Loop Shaping Based H^∞ Robust Control of a Horizontal Shaft Magnetic Bearing," *Proc. 31st SICE Annual Conference,* pp. 941-944, Kumamoto, Japan, 1992.

[18] M. Fujita, K. Hatake and F. Matsumura, " Loop Shaping Based Robust Control of a Magnetic Bearing," *IEEE Control Systems Magazine,* vol. 13, no. 4, pp. 57-65, Aug., 1993.

[19] M. Fujita, K. Hatake, F. Matsumura, and K. Uchida "An Experimental Evaluation and Comparison of H_∞/μ Control for a Magnetic Bearing," to be presented in *the 12th IFAC World Congress,* Sydney, Australia, 1993.

[20] M. Fujita, K. Hatake, F. Matsumura and K. Uchida, " Experiments on the Loop Shaping Based H_∞ Control of a Magnetic Bearing," *Proc. 1993 American Control Conf.,* San Francisco, California, pp. 8-12 1993.

[21] M. Fujita, M. Kubo, F. Matsumura and K. Uchida, " H_∞ Robust Control of a Simple Magnetic Suspension System with a Flexible Beam," *13th SICE Symp. on Dynamical System Theory,* pp. 77-81 1991.

[22] M. Fujita, F. Matsumura, and T. Namerikawa, " μ-Analysis and Synthesis of a Flexible Beam Magnetic Suspension System," *Proc. Third Int. Symp. Magnetic Bearings,* Virginia, pp. 495-504, 1992.

[23] M. Fujita, T. Namerikawa, F. Matsumura and K. Uchida, " μ-Synthesis of an Electromagnetic Suspension System," *Proc. 31st IEEE Conference on Decision and Control,* Tucson, Arizona, 1992.

[24] M. Fujita, T. Namerikawa, F. Matumura and K. Uchida, " μ-Synthesis of an Electromagnetic Suspension System," *IEEE Trans. on Automatic Control,* vol. 40, no. 3, pp. 530-536 1995.

[25] K. Glover and J. C. Doyle, " State-space formulae for all stabilizing controllers that satisfy an H_∞-norm bound and relations to risk sensitivity," *Systems & Control Letters,* vol. 11, pp. 167, 1988.

[26] M. Hamada, " Progress of the Shinkansen," *Nikkei Mechanical,* vol. 375, no. 22, pp. 1412-1419, 1992 (in Japanese).

[27] M. Kawabata, K. Hashimoto, and H. Kimura, " H_∞ Control of Robot with Linearized Model," *Trans. of JSME,* vol. 59, no. 566, pp. 3151-3156, 1993 (in Japanese).

[28] H. Hanselmann, " Implementation of Digital Controllers: A Survey," *Automatica,* vol. 23, no. 1, pp. 7-32, 1987.

[29] R. A. Hyde and K. Glover, " The Application of Scheduled H_∞ Controllers to a VSTOL Aircraft," *IEEE Transactions on Automatic Control,* vol. 38, no. 7, pp. 1021-1039, 1993.

[30] R. A. Hyde, K. Glover, and G. T. Shanks, " VSTOL first flight of an H_∞ control law," *IEE Computing and Control Engineering Journal,* vol. 6, no. 1, pp. 11-16, 1995.

[31] R. A. Hyde, " H_∞ Aerospace control: A VSTOL Application," Advances in Industrial Control Series, Springer-Verlag, 1995.

[32] T. Higuchi, Ed., "*Magnetic Bearings*," *Proc. Second Int. Symp. Magnetic Bearings*, Tokyo, Japan, 1990.

[33] T. Higuchi, T. Mizuno, and T. Tsukamoto, " Digital control for magnetic bearing with automatic balancing," *Proc. of 2nd International Symposium on Magnetic Bearings*, Tokyo, July, 1990.

[34] M. Hirata, K. Z. Liu, T. Mita, " Active Vibration Control of a 2-mass Spring System Using μ-Synthesis," *Trans. of IEE Japan*, vol. 114-D, no. 5, pp. 512-519 1994 (in Japanese).

[35] C. H. Houpis and G. B. Lamont, " *Digital Control Systems: theory, hardware, software,*" McGraw Hill, pp. 611-614, 1985.

[36] R. R. Humphris, R. D. Kelm, D. W. Lewis and P. E. Allaire, "Effect of control algorithms on magnetic journal bearing properties," *J. Eng. Gas Turbines Power*, vol. 108, no. 10, 1986.

[37] Y. Kano, " Fundamental of Linear DC Motor," *Handbook of Linear Motor Applications,* Kogyo Chosakai Pub, pp. 146, 1986 (in Japanese).

[38] Y. Kawazoe, A. Mochizuki, " Performance of Rolling Stock and Power Collector," *J. of IEE Japan B*, vol. 102, no. 10, 885, 1982 (in Japanese).

[39] H. Kimura " From LQG to H_∞," *J. of SICE*, vol. 29, no. 111, pp. 111-119 1990 (in Japanese).

[40] C. R. Knospe, " Robustness of unbalance response controllers," *Proc. of 3rd International Symposium on Magnetic Bearings,* Virginia, July, 1992.

[41] J.M. Maciejowski, *Multivariable Feedback Design* , Addison-Wesley Pub. Com. Inc., 1993.

[42] K. Manabe, M. Ikeda, Y. Noguchi, I. Sakai, " Development of a low noise pantograph," *Proc. of WCRR'94*, pp. 1395, 1994.

[43] K. Manabe, " A Study on Periodic Contact Breaks at Every Hanger Space," *RTRI Report*, vol. 6, no. 9, pp. 33-42 1992 (in Japanese).

[44] D. McFarlane and K. Glover, " Robust Controller Design Using Normalized Coprime Factor Plant Descriptions," *Lecture Notes in Control and Information Sciences*, vol. 138, Springer-Verlag, 1990.

[45] T. Mizuno, T. Higuchi, " Compensation for Unbalance in Magnetic Bearing Systems," *Trans. of SICE*, vol. 20, no. 12, pp. 23-29, 1984 (in Japanese).

[46] F. Matsumura, M. Fujita and K. Hatake, " Output Regulation in Magnetic Bearing Systems by a Dynamic Output Feedback Controller," *Trans. IEE of Japan*, vol. 112-C, no. 10, pp. 977-983, 1992 (in Japanese).

[47] F. Matsumura, M. Fujita, and K. Okawa, " Modeling and Control of magnetic bearing systems achieving a rotation around the axis of inertia," *Proc. of 2nd International Symposium on Magnetic Bearings,* Tokyo, July, 1990.

[48] F. Matsumura, S. Isobe, K. Hagiwara, "Force Control of a Linear DC Motor Using H_∞ Control," *Proc. of IEE Japan*, LD-94-74, pp. 1-8, 1994 (in Japanese).

[49] F. Matsumura, H. Kobayashi and Y. Akiyama, " Fundamental Equation of Horizontal Shaft Magnetic Bearing and its Control System Design," *Trans. IEE of Japan*, vol. 101-C, no. 6, pp. 137-144, 1981 (in Japanese).

[50] F. Matsumura, Y. Okada, M. Fujita and T. Namerikawa, Ed., *Proc. of the Fifth Int. Symp. on Magnetic Bearings*, Kanazawa, Japan, August 1996.

[51] F. Matsumura, Y. Suzuki and S. Isobe, " Force Control in Oscillatory System Using Linear DC Motor," *Proc. of IEE Japan*, LD-93-81, pp. 9-16, 1993 (in Japanese).

[52] F. Matsumura and S. Tachimori, " Magnetic Suspension System Suitable for Wide Range Operation," *Trans. IEE of Japan*, vol. 99-B, pp. 25-32, 1978 (in Japanese).

[53] F. Matsumura and S. Yamada, " A Control Method of Suspension Control System by Magnetic Attractive Force," *Trans. IEE of Japan*, vol. 94-B, pp. 567-574, 1974 (in Japanese).

[54] A. M. Mohamed, F. P. Emad, " Conical Magnetic Bearing with Radial and Thrust Control," *IEEE Trans. on Automatic Control*, vol. 37, no. 12, pp. 1859-1868, Dec., 1992.

[55] A. M. Mohamed, I. J. Busch-Vishniac, " Imbalance Compensation and Automation Balancing in Magnetic Bearing Systems Using the Q-Parameterization Theory," *IEEE Trans. on Control Systems Technology,* vol. 3, no. 2, pp. 202-211, June, 1995.

[56] T. Namerikawa, M. Fujita, and F. Matsumura " Robust Trajectory Following for an Uncertain Robot Manipulator Using H_∞ Synthesis," *Proc. of ECC,* vol. 4, pp. 3474-3478, 1995.

[57] T. Namerikawa, S. Isobe, and F. Matsumura, " H_∞ Control for an Experimental System of the Panograph with a Linear DC Motor," *Trans. of IEE Japan,* vol. 115-D, no. 11, pp. 1412-1419, 1995 (in Japanese).

[58] T. Namerikawa, M. Fujita, and F. Matsumura, " Robust H_∞ Control for a Parallel Link Robot Manipulator," *Trans. of IEE Japan,* vol. 116-D, no. 2, pp. 207-215, 1996 (in Japanese).

[59] R. A. Nichols, R. T. Reichert, W. J. Rugh, " Gain Scheduling for H_∞ Controllers: A Flight Control Example," *IEEE Transactions on Control Systems Technology,* vol. 1, no. 2, pp. 69-79, 1993.

[60] A. Packard, " Gain scheduling via linear fractional transformations," *System & Control Letters,* vol. 22, no. 2, pp. 79-92, 1994.

[61] A. Packard and J. Doyle, " The Complex Structured Singular Value," *Automatica,* vol. 29, no. 1, pp. 71-109, 1993.

[62] M. Saeki, " Optimal Constant Scaling Matrix for H_∞ Control and μ-Synthesis -State Feedback Case-," *Proc. of the 31st Conference on Decision and Control,* pp. 243-248 1992.

[63] Sakawa, " Modeling and Control of Flexible Manipulators," *Journal of RSJ,* vol. 12, no. 2, pp. 172-177, 1994 (in Japanese).

[64] J. Sefton and K. Glover, " Pole-zero cancellations in the general H_∞ problem with reference to a two block design," *IBID.,* vol. 14, pp. 295 1990.

[65] B. Shafai, S. Beale, P. LaRocc and E. Cusson, " Magnetic Bearing Control Systems and Adaptive Forced Balancing," *IEEE Control Systems Magazine,* vol. 14, no. 2, pp. 4-13, April, 1994.

[66] J. S. Shamma and M. Athans, " Gain Scheduling: Potential Hazards and Possible Remedies," *IEEE Control Systems Magazine,* vol. 12, no. 3, pp. 101-107, 1992.

[67] J. S. Shamma and James R. Cloutier, " A Linear Parameter Varying Approach to Gain Scheduled Missile Autopilot Design," *Proc. of the 13th ACC,* vol. 2, no. 4, pp. 101-107, June 1992.

[68] K. Shibukawa, T. Tsubakiji and H. Kimura, " Robust Control of Magnetically Suspended System," *Proc. 13st SICE Dynamical System Theory,* pp. 397-400, Tokyo, Japan, 1990 (in Japanese).

[69] P. K. Sinha, " *Electromagnetic Suspension: Dynamics and Control,*" IEE, Peter Peregrinus, London, 1987.

[70] P. K. Sinha, G. Pech and H. A. Abbassi, " Digital Control of an Electromagnetic Suspension System Using the TMS-32020 Signal Processor," *Automatica,* vol. 27, no. 6, pp. 1051-1054 1991.

[71] G. Schweitzer, Ed., "*Magnetic Bearings,*" *Proc. First Int. Symp. Magnetic Bearings,* Zurich, Switzerland, Springer-Verlag, 1988.

[72] M. W. Spong and M. Vidyasagar, " Robot Dynamics and Control," *John Wiley and Sons, Inc.,* 1989.

[73] M. W. Spong and M. Vidyasagar, " Robust Linear Compensator Design for Nonlinear Robotic Control," *IEEE J. Robotics and Automation,* vol. RA-3, no. 4, pp. 345-351, Aug. 1987.

[74] G. Stein and J. C. Doyle, " Beyond Singular Values and Loop Shapes," *J. Guidance,* vol. 14, no. 1, pp. 5-16, 1991.

[75] M. Steinbuch, G. Schootstra and O. H. Bosgra, " Robust Control of a Compact Disc Player," *Proc. IEEE Conference on Decision and Control,* pp. 2596-2600, Tucson, Arizona, 1992.

[76] T. Sugie, M. Fujita and S. Hara, " Multiobjective Controller Design with the Guaranteed H_∞ Control Performance," *Proc. of 12th IFAC World Congress,,* vol. 4, pp. 43-46, 1993.

[77] T. Sugie and S. Hara, " H_∞ - suboptimal control problem with boundary constraints," *Systems & Control Letters*, vol. 13, pp. 93-99, 1989.

[78] T. Sugie and M. Kawanishi, " Analysis and Design of Magnetic Levitation Systems Considering Physical Parameter Perturbations," Trans. of ISCIE, vol. 8, no. 2, pp. 70-79 1995 (in Japanese).

[79] T. Sugie and M. Kawanishi, " μ Analysis Based on An Exact Description of Physical Parameter Variations," Trans. of SICE, vol. 31, no. 12, pp. 1936-1944 1995 (in Japanese).

[80] J. Tani, Ed., *"Dynamics of the Apparatus Related to Electromagnetic Forces," JSME and Corona Publishing Co., Ltd.,* 1990 (in Japanese).

[81] O. Tsukamoto, Y. Tsuchiya, S. Yamamura, " Servo-Controlled Power Collector," Trans. of IEE Japan, vol. 96, no. 6, pp. 267-273, 1976 (in Japanese).

[82] K. Uchida and M. Fujita, " On the Central Controller: Characterizations via Differential Games and LEQG Control Problems," System & Control Letters, vol. 13, no. 1, pp. 9 1989.

[83] R. Watanabe, K. Uchida, M. Fujita and E. Shimemura " H_∞ Control of Linear Systems with Scheduling Parameter," *Trans. of SICE*, vol. 31, no. 4, pp. 481-488, 1995 (in Japanese).

[84] R. D. Williams, F. J. Keith and P. E. Allaire, " Digital Control of Active Magnetic Bearings," *IEEE, Trans. Industrial Electronics,* vol. 37, no. 1, 1990.

[85] Y. Yamada, T. Koseki, and S. Sone, " Investigation on Active Pantograph controlled using State Observer," Proc. IEE Japan Annual Conference, vol. 5, pp. 401, 1995 (in Japanese).

[86] G. Zames, " Feedback and optimal control sensitivity: Model refernce transformations. Multiplicative seminorms and approximate inverses," *IEEE, Trans. Automatic Control,* vol. 26, pp. 585-601, 1981.

[87] K. Zhou, J. C. Doyle, and K. Glover, " Robust and Optimal Control," Prentice Hall, 1996.

Publications

[1] M. Fujita, F. Matsumura and T. Namerikawa, "μ-Analysis and Synthesis of a Flexible Beam Magnetic Suspension System ," *Proc. of the 3rd International Symposium on Magnetic Bearings*, pp. 495–504 , 1992.

[2] M. Fujita, T. Namerikawa, F. Matsumura, and K. Uchida, "μ-Synthesis of an Electromagnetic Suspension System," *Proc. of IEEE Conference on Decision and Control*, pp. 2574–2579, 1992.

[3] M. Fujita and T. Namerikawa, "Robust Control of Magnetic Suspension Systems," *Science of Machine*, Yokendo Ltd, vol. 46, no. 3, pp. 339–347, 1994 (in Japanese).

[4] T. Namerikawa, M. Fujita, and F. Matsumura, "Robust Position Control and its Implementation for a Robot Manipulator using μ-Synthesis ," *Proc. of the 3rd International Workshop on Advanced Motion Control*, pp. 545–554, 1994.

[5] M. Fujita, T. Namerikawa, and K. Uchida, "Digital Implementation of Robust μ-Control for a Robot Manipulator ," *Proc. of the American Control Conference*, pp. 2450–2454, 1994.

[6] M. Fujita, T. Namerikawa, F. Matsumura, and K. Uchida, "μ-Synthesis of an Electromagnetic Suspension System ," *IEEE Transactions on Automatic Control*, vol. 40, no. 3, pp. 530–536, 1995.

[7] T. Namerikawa, M. Fujita, and F. Matsumura, "Application of Gain Scheduled H_∞ Robust Controllers to a Magnetic Bearing," *Proc. of the International Power Electronics Conference*, pp. 1340–1345, 1995.

[8] T. Namerikawa, M. Fujita, and F. Matsumura, "Robust Trajectory Following for an Uncertain Robot Manipulator Using H_∞ Synthesis," *Proc. of 3rd European Control Conference*, vol. 4, pp. 3474–3479, 1995.

[9] T. Namerikawa, S. Isobe, and F. Matsumura, "H_∞ Control for an Experimental System of the Pantograph with a Linear DC Motor," *Trans. of IEE Japan,* vol. 115-D, no. 11, pp. 1412–1419, 1995 (in Japanese).

[10] T. Namerikawa, M. Fujita, and F. Matsumura, "Robust H_∞ Control for a Parallel Link Robot Manipulator," *Trans. of IEE Japan,* vol. 116-D, no. 2, pp. 207–215, 1996 (in Japanese).

[11] T. Namerikawa, M. Fujita, and F. Matsumura, "A Linear Parameter Varying Approach to a Gain Scheduled Flexible Joint Robot ," *Proc. of the 4th International Workshop on Advanced Motion Control,* pp. 653–656, 1996.

[12] T. Namerikawa, K. Hagiwara, M. Fujita, and F. Matsumura, "Experimental Evaluation of the Gain-Scheduled H_∞ Robust Controllers to a Magnetic Bearing," *Proc. of the 5th International Symposium on Magnetic Bearings,* pp. 137–142, 1996.

[13] F. Matsumura, T. Namerikawa, K. Hagiwara, and M. Fujita, "Application of Gain Scheduled H_∞ Robust Controllers to a Magnetic Bearing," *IEEE Transactions on Control Systems Technology,* vol. 4, no. 5, pp. 484–493, 1996.

[14] T. Namerikawa, M. Fujita, and F. Matsumura, "Robust Control of a Robot Manipulator using a Linear Parameter Varying Representation," *Proc. of IEEE International Conference on Industrial Technology,* pp. 489–492, 1996.

[15] T. Namerikawa, M. Fujita, and F. Matsumura, "H_∞ Control of a Robot Manipulator using a Linear Parameter Varying Representation," *Proc. of the American Control Conference,* Albuquerque, New Mexico, June, 1997 (to appear).

[16] T. Namerikawa, S. Goto, and F. Matsumura, "Robust Force Control of a Pantograph System by considering Model Parameter Perturbation," *Proc. of 1997 IEEE/ASME Int. Conf. on Advanced Intelligent Mechatronics,* Waseda, June, 1997 (to appear).

[17] T. Namerikawa, M. Fujita, and F. Matsumura, "Robust H_∞ Control of a flexible-joint Robot Manipulator using a Linear Parameter Varying Approach," *Proc. of the 2nd Asian Control Conference,* Seoul, July, 1997 (to appear).